

DELFT UNIVERSITY OF TECHNOLOGY

MSc THESIS

**Numerical modeling of wave-current
interaction with the use of a two way coupled
system**

Author:
Guido CATS

Graduation committee:
Prof. dr. ir. UIJTTEWAAL, W.S.J.
Dr. ir. VAN VLEDDER, G, PH.
Dr. ir. ZIJLEMA, M.
Dr. ir. DE SCHIPPER, M.A.
Drs. ADEMA, J.

August 18, 2014



This page is intentionally left blank

This page is intentionally left blank

This page is intentionally left blank

Summary

The Dutch Flood Defense Act prescribes the assessment of the safety level of Dutch primary sea and flood defenses every six years. To assess if the required level of security of the sea and flood defenses is guaranteed, first the Hydraulic Boundary Conditions (HBC) which the sea and flood defenses are exposed to, have to be determined.

At the eastern Wadden Sea, nonlinear wave-current interaction is important in the determination of wave fields and the wave set-up contributions to the surge elevation. The Hydraulic Boundary Conditions of the primary sea and flood defenses adjacent to the Wadden Sea are therefore determined with the use of a two-way coupled modeling system, existing of the circulation model Delft3D-FLOW and the wind wave model SWAN, to account for wave-current interaction.

An inextricable consequence of modeling is the introduction of errors and the aim always should be to minimize these errors. The goal of this study is to improve the understanding of the two-way coupled modeling system and to increase the knowledge on the reliability of the result.

A literature survey is performed with the goal to improve the understanding of the two-way coupled modeling system and to identify the largest sources of uncertainty. The relative importance of all sorts of physical processes is highly dependent on the set-up of the model schematization and the location.

The effect on the result due to the applied coupling interval, wind drag parameterization in both Delft3D-FLOW and SWAN and different depth-induced wave breaking parameterizations is investigated at the eastern Wadden Sea, for the storm of 9 November 2007. Results showed that increasing the coupling interval mainly influenced the predicted water level, while the wave conditions were hardly influenced. The advice is to not increase the coupling interval to larger intervals than 30 minutes during storm conditions. The *fit* wind drag parameterization ([Zijlema et al., 2012](#)), is compared with [Wu \(1982\)](#) in SWAN and [Charnock \(1955\)](#) in Delft3D-FLOW. The largest differences are observed due to different wind drag parameterization in Delft3D-FLOW, though the effect of wind drag parameterization in SWAN possibly also might have an effect at higher wind speeds. The effect of applying the depth-induced wave breaking by [Salmon et al. \(2013\)](#) is investigated by comparing the results with the results generated when [Battjes and Janssen \(1978\)](#) is applied. Differences in wave set-up were in the order of 8 cm, while wave conditions showed better agreement with measurements in case of [Battjes and Janssen \(1978\)](#), compared with [Salmon et al. \(2013\)](#), with exception of low-frequency wave energy.

This page is intentionally left blank

This page is intentionally left blank

Acknowledgments

This thesis concludes my master study Hydraulic Engineering specialization 'Environmental Fluid Mechanics' at the faculty of Civil Engineering at the Delft University of Technology. The thesis was conducted at Arcadis, Zwolle. After the past eleven months, I think a few words of gratitude are in place.

I would like to thank my graduation committee for their time, feedback and supervision: Prof. dr. ir. Wim Uijttewaal for his critical, but positive feedback; Dr. ir. Marcel Zijlema for all comments; Dr. ir. Matthieu de Schipper for his sincere interest during the project; Dr. ir. Gerbrant van Vledder for providing me with good advice and always being supportive; Drs. Jeroen Adema, who was always helpful and always made time for me, for both report and modeling related question.

In addition to this, I would like Arcadis for the opportunity they gave me and the office facility they offered me to write my MSc Thesis. Thereby, I would like to thank all colleagues at Arcadis Zwolle, for the readiness to help and the fun conversations we had.

Amsterdam, August 2014

Guido Cats

Contents

1	Introduction	1
1.1	Background	1
1.1.1	Hydraulic Boundary Conditions	1
1.1.2	Two-way coupled model	2
1.1.3	Numerical modeling at the Wadden Sea	3
1.2	Goals	4
1.3	Approach	5
2	Literature study	6
2.1	Introduction	6
2.2	Literature study	6
2.3	Conclusion	10
3	Circulation models	12
3.1	Introduction	12
3.2	Method	12
3.3	Governing equations	12
3.3.1	Shallow-water equations	12
3.4	Wave-current interaction related modifications	15
3.4.1	Current	15
3.4.2	Surface stress	16
3.4.3	Wave force	17
3.4.4	Streaming	19
3.4.5	Bed boundary conditions	20
3.4.6	Turbulence	24
3.5	Conclusion	27
4	SWAN	28
4.1	Introduction	28
4.2	Physics in SWAN	28
4.2.1	Action balance equation	28
4.2.2	Wind	29
4.2.3	Bottom friction	31
4.2.4	Depth-induced wave breaking	32
5	Conclusion Literature Survey	34

6	Introduction numerical modeling	36
6.1	Introduction	36
6.2	Numerical modeling	36
6.2.1	Introduction	36
6.2.2	Delft3D-FLOW - SWAN model	37
6.2.3	Demand on locations	37
6.2.4	Eastern Wadden Sea	37
6.3	Choice of subjects	37
6.4	Research questions	38
6.4.1	Coupling interval	38
6.4.2	Wind drag	39
6.4.3	Depth-induced wave breaking	39
7	Idealized case	41
7.1	Introduction	41
7.2	Method	41
7.2.1	Analytical solution	41
7.3	Model set-up	42
7.3.1	Grid and bathymetry	42
7.3.2	Model set-up Delft3D-FLOW	43
7.3.3	Model set-up SWAN	44
7.4	Results	44
7.5	Analysis	45
7.6	Conclusion	46
8	Coupling interval	47
8.1	Introduction	47
8.2	Method	47
8.3	Model set-up Eastern Wadden Sea	48
8.3.1	Grid	48
8.3.2	Bathymetry	48
8.3.3	Delft3D-FLOW boundary conditions	50
8.3.4	Wave boundary conditions	50
8.3.5	Wind	51
8.3.6	Model settings	52
8.4	Results	53
8.4.1	Visual interpretation water level	53
8.4.2	Statistical analysis water level	55
8.4.3	Visual interpretation wave conditions	57
8.4.4	Statistical analysis wave conditions	59
8.4.5	Analysis	63
8.5	Conclusions	64
9	Wind drag	66
9.1	Introduction	66
9.2	Method	67
9.3	Assessment of S_{in}	68
9.4	Idealized case	70

9.4.1	Results idealized case	70
9.5	Wadden Sea case	72
9.5.1	Visual interpretation water level	72
9.5.2	Statistical analysis water level	73
9.5.3	Visual interpretation wave conditions	74
9.5.4	Statistical analysis wave conditions	74
9.6	Conclusion	74
10	Depth-induced wave breaking	77
10.1	Introduction	77
10.2	Method	77
10.3	Model settings	77
10.3.1	Depth-induced wave breaking	78
10.4	Results	78
10.4.1	Visual interpretation water level	78
10.4.2	Statistical analysis water level	80
10.4.3	Visual interpretation wave conditions	81
10.4.4	Statistical analysis wave conditions	82
10.5	Analysis	84
10.6	Conclusion	86
11	Conclusions	87
11.1	Introduction	87
11.2	Literature survey	87
11.3	Numerical modeling	88
11.4	Conclusions regarding the set goals	90
12	Recommendations	91
13	Bibliography	93
A	Matlab codes	A-1
A.1	Introduction	A-1
A.2	Depth-induced wave breaking	A-1
B	Input files	B-1
B.1	Introduction	B-1
B.2	Delft3D-FLOW	B-2
B.3	SWAN	B-5
B.4	Coupling procedure	B-8

Chapter 1

Introduction

1.1 Background

1.1.1 Hydraulic Boundary Conditions

The Dutch Flood Defense Act prescribes the assessment of the safety level of Dutch primary sea and flood defenses every six years. To assess if the required level of security of the sea and flood defenses is guaranteed, first the Hydraulic Boundary Conditions (HBC) which the sea and flood defenses are exposed to, have to be determined.

The hydraulic boundary conditions of the primary sea and flood defenses adjacent to the Wadden Sea are determined with the use of a two-way coupled modeling system. The two-way coupled modeling system exists of the circulation model Delft3D-FLOW and the wave model SWAN (*Booij et al., 1999*). The system is driven by the tidal constituents and wave boundary conditions at the open boundaries of the model and wind at the entire domain of the model. An important outcome of the model is the predicted water level, which is influenced by the presence of waves. The radiation stress is defined as the excess flow of momentum due to the presence of waves (*Longuet-Higgins and Stewart, 1962, 1964*). The gradient of the radiation stress can result in either wave setup or wave set-down of the water level in shallow water regions, which can have a significant contribution to the total storm surge elevation (*Dean and Bender, 2006*).

Though making an error is an inextricably consequence of using a model, the aim always should be to minimize the error made. In case of a coupled system, the total error made exists of errors made due to wrong or incomplete physics, numerical introduced errors and errors made due to incorrectness of the forcing of the system.

The error made due to wrong or incomplete physics can be further divided into an error made in different parameterizations of physical processes and including, or leaving out, physical processes. Numerical introduced errors can be split up in errors introduced due to numerical solving schemes, choices made in running SWAN in stationary or instationary mode, choices made with respect to the numerical grid and in case of a coupled system, also out of the frequency interval of coupling. The error made due to incorrect forcing exists of an error made in the representation of the wind and on the boundaries of the model the error exists of a wrong representation of the tidal constituents, set-up and waves.

Currently it is unknown what the magnitude of the errors are and what is responsible for the largest error. This leaves an uncertainty on the reliability of the result generated by the model. This clearly is undesirable when the result is used as an input parameter for the assessment of the safety level of Dutch primary sea and flood defenses.

1.1.2 Two-way coupled model

The two-way coupled model used to determine the hydraulic boundary conditions (Subsection 1.1.1) will be discussed in this subsection with the use of Figure 1.1.

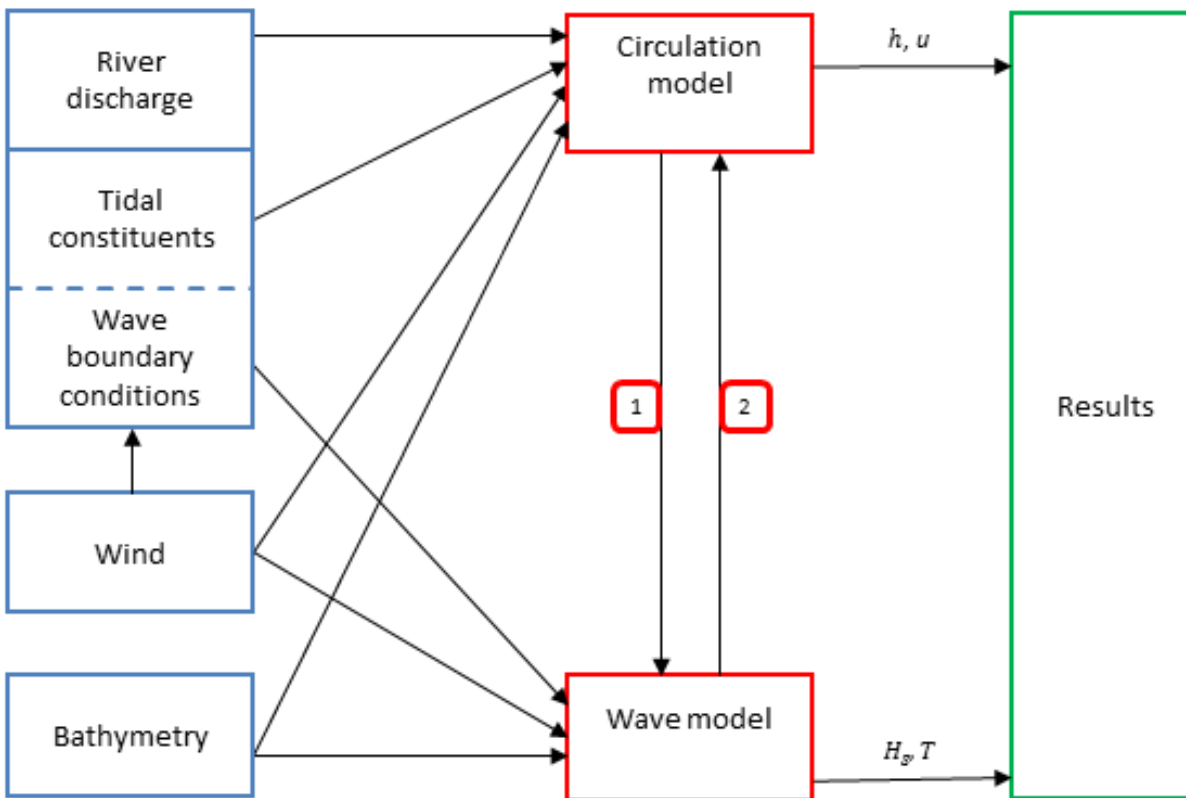


Figure 1.1: Schematized overview of model

Figure 1.1 gives a schematic view on the interaction between the wave model and the circulation model in an estuary similar to the Wadden Sea. The blue boxes indicate the input of the model.

The river discharge, tidal constituents and wave boundary conditions form together the open boundary conditions of the modeling system. The river discharge and the tidal constituents are the open boundary conditions of the circulation model, while the wave model uses wave boundary conditions that describe the wave spectrum.

The wind influences both the current and the development of waves. Thereby it also influences the set-up at the boundary of the domain. The wind-wave-current interaction is a one-way coupling. This means that the wind in the model is not influenced by wave- or current conditions.

Morphodynamics are not included in this study, which means the bathymetry does not evolve in time.

The red boxes indicate the circulation model and the wave model. The numbers 1 and 2 describe the information sent from the circulation model to the wave model and vice versa. The information indicated with number 1 consists of time and place dependent water depth $h(x, y, t)$ and the depth-averaged velocity field $\bar{u}(x, y, t)$. The wave model sends the circulation model information, indicated with number 2, on wave characteristics, wave induced force and dissipation rate. This information is used in the computations by the circulation model. The circulation model modifies or adds equations to account for physical processes to account for wave-current interaction. Which physical processes are modified or added is dependent on which circulation model is used. The wave model uses the current and water depth calculated by the circulation model. The interval rate of information exchange between the modes is adjustable.

1.1.3 Numerical modeling at the Wadden Sea

The hydraulic boundary conditions at the Wadden Sea are currently determined with the numerical wave model SWAN and the numerical circulation model Delft3D-FLOW. The performance of numerical models at the Wadden Sea has been tested in several studies summed up in this subsection.

The Wadden Sea is a geographical complex area and the reliability of SWAN has been tested by WL—Delft Hydraulics in numerous studies in the past. Hindcasts have been performed for the Nordemeyer Zeegat and Ameland Zeegat ([WL, 2006](#)), for the inlet system of Ameland and Norderney and Lunenburg Bay ([WL, 2007a](#)) and the Eastern Wadden-Sea and Eems-Dollard estuary ([Alkyon, 2009](#)). Thereby a sensitivity analysis was performed for the Ameland Zeegat ([WL, 2007b](#)), a study was done to investigate the performance of wave-current interaction in SWAN ([WL, 2007c](#)) and an uncertainty analysis of the hydraulic boundary conditions in the Wadden Sea was performed ([WL, 2008](#)).

In [WL \(2007b\)](#) the sensitivity of the outcome of SWAN to variations in model input and model settings was investigated for both observed as hypothetical storms at the Frisian coast behind the Ameland Zeegat. The sensitivity due to model input consists of variation in offshore boundary conditions, variations in water level and variations in wind speed, direction and spatial variability. The sensitivity due to model settings was performed with the use of limiting the amount of wind energy transfer to young waves. The water level and current fields used in this study are simulated with WAQUA and were interpolated to the non-uniform SWAN computational field. The most important conclusions are that wave growth in the entire Wadden Sea is depth limited and the largest model responses observed are due to variation in water depth and the inclusion of wave-current interaction. Also, conditions at the primary sea defenses are highly determined by local wave generation. Wave directions at the primary sea defenses are very sensitive to wind direction and a high accuracy of wind direction is therefore recommended.

The aim of the study in [WL \(2007c\)](#) is to investigate the performance of wave-current modeling in SWAN. The goal was to assess whether the modeling of wave-current interaction is improved by the use of depth varying current fields and to assess the performance of SWAN to the modeling in case of wave dissipation in opposing currents. Analytical solutions, laboratory cases and field observations were used in this study to assess the performance of SWAN. The most important conclusion with respect to the field case is SWAN strongly overestimates wave heights in its standard setting, when

strong opposing currents are present, while the modeling of frequency shifts in the spectrum agree with observations. This implies a problem with the dissipation of wave energy in the model.

WL (2008) investigated the uncertainty with the use of a Monte-Carlo simulation. The goal was to estimate the level of uncertainty of the Hydraulic Boundary Conditions and the contribution of the uncertainty to input parameters of SWAN and the HYDRA-K model. The HYDRA-K model assesses the failure mechanisms of the primary sea defenses. The water level used in the SWAN computations is fixed at the coast and due to wind set-up the water is tilted in offshore direction. The influence of breaking waves on water level is neglected in this study. The study showed the contribution of uncertainties of near shore wave heights and wave period is mostly due to uncertainty of model parameters. The contribution of model input is relatively small. Hence, the uncertainty of model input for wind is only investigated by means of wind direction. The wind speed and variations in water level are not included in this study.

In *Alkyon* (2009) a hindcast was performed for the Eastern Wadden Sea and Eems-Dollard estuary with a two-way coupled system for a storm on 9 November 2007. The circulation model used was Delft3D-FLOW and SWAN as the wave model. The study showed currents affect wave conditions significantly, but the results did not improve compared with a stand-alone SWAN computation at the location of the measurement buoys. Hence, water level predictions did improve when including the wave-induced forcing. Therefore it was expected that the prediction of wave conditions would improve at locations where depth-effects play a significant role. The study also made a comparison between the wind velocity measurements and HIRLAM wind fields. Bi-linear interpolation per wind component was used to derive the HIRLAM wind speed at the location of the measurements. The wind speed from HIRLAM appeared to be structurally almost 4 *m/s* higher at measurement station West-Terschelling, while at station Texelhors the wind speed from HIRLAM appeared to be 20% lower during peak velocities. It was concluded that HIRLAM overestimates wind speeds for Westerly and South-Westerly winds due to land effects. Thereby changes in direction are more gradually in HIRLAM compared with the measurements. The study used both the HIRLAM wind field and a uniform wind field based on the measurements at Huibertgat and concluded that the uniform wind speed at Huibertgat gave the best result to drive the flow model.

Recently, the above described model for the Nordemeyer Zeegat and Ameland Zeegat (*WL*, 2006) is re-evaluated in *Westhuysen et al.* (2012) with three improvements in SWAN. These improvements render a new breaker formulation that solves the under-prediction of wave heights is used, the wave-age effect on waves generated in ambient current is improved and the bottom friction dissipation was reduced in the tidal inlets to improve the variance density of lower-frequency wind waves penetrating through these inlets into the Wadden Sea. These improvements have led to more accurate predictions of H_{m0} , $T_{m-1,0}$ and T_{m01} compared with the study of 2006.

1.2 Goals

The goals of this research are:

- To improve the understanding of a two-way coupled system
- To increase the knowledge on the reliability of the result of the two-way coupled system
- To identify the largest sources of uncertainty
- To advise on the direction on further improvement of the two-way coupled system

1.3 Approach

To improve the understanding of a two-way coupled system a literature survey is performed. The literature survey exists of a literature study, the description of the wave model SWAN and the description the most widely used circulation models. The literature study has the goal to identify what currently the state-of-the-art wave-current interaction features are and what the largest uncertainty is. Thereby the physical processes in the wind-wave model SWAN and numerous circulation models are discussed. An extensive comparison between the physics in the circulation models has to point out which processes differ from each other. Finally, an conclusion of the literature survey will be provided.

At the start of the second part a set of hypotheses will be formulated with the use of the conclusions from the literature survey. The hypotheses will be tested with the use of the numerical circulation model Delft3D-FLOW and the wave model SWAN. Dependent on the formulation of the individual hypotheses an idealized schematic situation or a field case will be used.

Chapter 2

Literature study

2.1 Introduction

Many studies have focused on wave-current interaction driven systems with a large variety of circulation models and wave models. Section 2.2 discusses studies that involve the topic of wave current interaction and will sum up their conclusions and recommendations. This literature study has to point out what the determining processes are in the modeling of wave-current interaction.

2.2 Literature study

The importance of the inclusion of wave-current interaction in semi-enclosed basins is stressed by [Benetazzo et al. \(2013\)](#) after performing two hindcasts at the North-Adriatic Sea. The oceanic circulation model ROMS (Regional Oceanic Modeling System; [Shchepetkin and McWilliams \(2005\)](#)) is used in combination with SWAN (Simulating Waves Nearshore; [Booij et al. \(1999\)](#)) to model the effect on waves at the semi-enclosed Gulf of Venice. Especially the significant wave height is affected by currents under storm conditions. The wind speed is modified by using the relative wind speed compared with respect to the current. [Warner et al. \(2008a\)](#) compares the ROMS-SWAN model with a Coupled Ocean Atmosphere Prediction System (COAMPS).

[Funakoshi et al. \(2008\)](#) uses both a one-way and a two-way coupling procedure with the circulation model ADCIRC (ADvanced CIRCulation model; [Luettich and Westerink \(2004\)](#)) and wave model SWAN to perform a hindcast on the Hurricane Floyd in Florida, United States. The one-way coupling procedure holds that the radiation stress is provided to ADCIRC by SWAN. The former is also the case in the two-way coupling procedure with the addition of currents and water level from ADCIRC to SWAN. They conclude that the two-way coupling procedure did not improve the results significantly, compared with the one-way coupling procedure. Both the wind drag formulation and the interval of coupling are investigated by performing sensitivity analyses. They conclude that the scientific understanding of the transfer of momentum from the wind to the water surface is not sufficient and suggest a spatial and temporal variance in the formulation of the wind drag. The interval of coupling was arbitrarily chosen with interval of 1h, 2h and 4h, while they earlier state that the exchange rate of information should be dependent on the temporal variability of the interacting processes. It is concluded that model results are insensitive for the exchange rate at

this particular location and the advise is to chose the interval at such a rate that the computational time is limited to a minimum. A reference to the temporal variability of the interacting processes is not made. [Dietrich et al. \(2011a\)](#) describes the hindcast of the hurricanes Katrina and Rita. The coupling between ADCIRC and SWAN is extensively described. [Dietrich et al. \(2012\)](#) tested the performance of the hindcasts of Hurricanes Katrina and Rita (2005) and Gustav and Ike (2008). It was concluded that the performance of the coupled model was a faithful match compared with measurements for water level and wave conditions. The coupled model produces hindcasts in 10 min/day on a Lonestar 8,192 cores computer, which seems to be fast enough to use the system for forecasting hurricanes by emergency managers in the Mexican Gulf.

The inundation of Charleston Harbor, South Carolina during hurricane Hugo (1989) were investigated by [Xie et al. \(2008\)](#). The models used are POM for flow modeling and SWAN for wave modeling and are dynamically coupled in a two-way coupling framework. It is investigated which processes within the coupling are important by including or excluding wave induced surface stress, wave induced bottom stress and radiation stress. It was shown that none of the above mentioned processes could be neglected and all have significant influence on peak surge and inundation area. [Tang et al. \(2007\)](#) used POM and WAVEWATCH-III to investigate the effect of surface waves on surface currents. The Stokes drift appeared to be the dominant wave effect, with a contribution of 35% on the current. They also showed that the transfer of momentum from wind to current reduces when waves are taken into account.

A POLCOMS-WAM coupled model was used for an 11-year hindcast of the eastern Irish Sea ([Brown et al., 2011](#)). It was shown that the use of the coupled model performs good, and sometimes very good, at predicting water level, tides and wave conditions. [Bolanos-Sanchez et al. \(2009\)](#) studied the North West Mediterranean Sea, in particular the Catalan coast, with the use of a 3D POLCOMS-WAM wave-current interaction model. The effect of Stokes drift and radiation stress on current are included in the model. The effect of current on wave modification and on significant wave height and mean period is limited in this area, while the effect of wave induced currents is considerably, as it is in the same order of magnitude as the ambient current in this area, having an effect of about 25% on the total current. [Bolaños et al. \(2011\)](#) discusses the implementation of a 3D POLCOMS model in the Dee Estuary, Liverpool Bay (UK). POLCOMS is coupled with WAM and the effect of barotropic- and baroclinic processes is included. Processes that are enhanced due to wave-current interaction are wave refraction, bottom friction due to waves and current, wind drag due to waves, Stokes drift, radiation stress and Doppler shift. [Bolanos et al. \(2011\)](#) investigates the performance of the POLCOMS-WAM model at the Mediterranean Sea. Radiation stress is not included in this study, because the effect is suspected to be too limited for the spatial resolution used, but Stokes drift is included. The wind stress is modified to account for waves, according the theory of [Janssen \(1991\)](#) and [Janssen et al. \(2004\)](#). In this area, the modified wind stress appeared to be the most determining factor. After many have questioned the reliability of the 3D radiation stress, 2D radiation stress was implemented in the POLCOMS-WAM model by [Brown et al. \(2013\)](#) in the Irish Sea model and the nested Liverpool Bay model. The Liverpool Bay model boundary is forced with tide-surge conditions every 30 *m* and 2D spectral wave conditions are updated with an interval of 1 *h*, derived with the Irish Sea model. The wind velocity and pressure fields have a temporal resolution of 1 *h* at both the Irish Sea and Liverpool Bay model. The coupling interval is respectively 200 *s* and 30 *s*. It was found the model produces accurately the water levels and vertical variation of the current.

Sensitivity due to input conditions in the Gulf of Mexico was studied with the use of a two-way coupled system of Delft3D-FLOW and SWAN ([Edwards et al., 2009](#)). The sensitivity analysis in-

volves eight cases, with various combinations of two different bathymetry, the inclusion or exclusion of wind and regional or assimilated wave boundary conditions. Changes in bathymetry hardly had any effect on wave and circulation conditions. The model is sensitive for variation in wave boundary conditions at isolated areas. A more extensive study has to be performed to quantify this. The wind effects could not be investigated properly, as the model showed instability due to quadruplet wave-wave interactions in third generation mode.

The importance of wind direction and wind speed with respect to the current direction is stressed in *Fan et al. (2009)*. Four models are coupled, a tropical storm model (TS), the ocean model POM, the wave model WAVEWATCH III and a wave boundary layer model (WBLM). The WBLM model estimates the momentum flux of air, which is dependent on the sea-state. It was found that that the wave field was affected by taking wind-wave-current interaction into account. The maximum of the significant wave height was reduced significantly and the location shifted with a distance of several kilometers.

Mellor (2003) describes surface wave equations appropriate to three-dimensional ocean models. Expressions of the radiation stress in the vertical (3D) and a definition of the Doppler velocity for a vertically dependent current field are obtained. In this way the interaction between surface gravity waves and underlying currents is taken into account. Some consequences of the derived equations on the three-dimensional, interacting current and surface gravity wave equations are assessed later in *Mellor (2005)*. Energy transfer, wave energy, and turbulent energy are subject of investigation. A comparison with wave-current formulations of *Craik and Leibovich (1976)*, *Leibovich (1980)* and *McWilliams and Restrepo (1999)* is made. The correctness of the formulation of the 3D radiation stress has been questioned and has lead to reciprocal critics by *Xia et al. (2004)*, *Arduin et al. (2008a,b)*, *Bennis and Arduin (2011)*, *Bennis et al. (2011)*, *Mellor et al. (2008)* and *Mellor (2011a,b,c, 2013)*. The three-dimensional, continuity and momentum equations with the inclusion of a vertically distributed, wave radiation stress term were used. Especially when incident waves entering a beach with essentially zero turbulence momentum mixing showed problems. The balance between radiation stress and elevation does not apply anymore and velocities became very large.

Lane et al. (2007) compares radiation stress and vortex force representation. Both the radiation stress and vortex force representation encompass the same effects on currents: quasi-static set-up, infragravity wave forcing, Stokes drift and vortex force or comparable momentum effects. The vortex force representation decomposes the physics into a vortex force and a Bernoulli head, in which the Bernoulli head represents the wave set-up, while the vortex force represents a combination of the wave vorticity and wave velocity. The radiation stress cannot make such a clear physical decomposition.

The influence of tides on mean wave characteristics is appointed in *Moon (2005)*, with the use of the wave model WAVEWATCH II and the ocean model POM on the Yellow and eastern China Sea. The effects of tides on wave setup at the Korean Sea with the use of a coupled model, called SuWAT is studied in *Kim et al. (2008)*. This model exist of a Surge, WAVE and Tide mode, of which the WAVE model is SWAN. One found that surges decrease at high tide and increase during low tide, while the opposite holds for wave growth.

The formulation of wind drag is currently subject of research, especially under hurricane conditions. In most cases the wind drag coefficient is only dependent on the wind speed. Many models use parameterization of the wind drag coefficient that are based on field studies with relative low wind speeds and the wind drag coefficient is extrapolated for higher wind speeds (*Garratt, 1977*;

Charnock, 1955; *Wu*, 1982, e.g.). The occurrence of Hurricane Katrina (2005) resulted in an enormous increase of measurements in the Gulf of Mexico, which is useful for the validation of hindcasts of other hurricanes. It appears that the wind drag coefficient is over-estimated at high wind speeds. (*Dietrich et al.*, 2011a) describes that both the wind drag parameter in ADCIRC (*Garratt*, 1977) and SWAN (*Wu*, 1982) are capped off at a value of $C_D = 0.0035$. (*Donelan et al.*, 2004) proposes a parameterization that depends on the geometric roughness of the sea surface and on the speed of the waves relative to the wind speed. *Powell et al.* (2003) shows that at wind speeds larger than 50 m/s the hurricane's kinetic energy would decrease, because it loses more energy to sea surface stress, than it reasonably can be supplied by oceanic heat sources. *Bye and Jenkins* (2006) proposes an adjusted wind drag parameterization, based on the existence of spray, which causes that the transfer of momentum to the sea surface is capped at a wind speed of 40 m/s. *Dietrich et al.* (2011b) describes the validation of a hindcast for Hurricane Gustav (2008) in the Gulf of Mexico. The modeling of waves is done in three models: in deep water WAM is used, near shore the steady-state model STWAVE on the one hand and SWAN on the other hand are used. These models are used in combination with the circulation model ADCIRC. The wind drag coefficient is dependent on the radial distance and location of the eye of the hurricane. *Bye et al.* (2010) continues with an adjusted formulation of the α parameter in the Charnock wind drag parameterization, applicable during high wind speed conditions and is in general record with observations. *Zijlema et al.* (2012) defines a new parameterization of the wind drag coefficient, based on a fit through many observations from numerous studies. They found that the wind drag parameter, in contrary to the wind drag formulation by *Charnock* (1955) and *Wu* (1982), decreases at wind speeds higher than approximately $\sim 30 \text{ m s}^{-1}$.

The depth-induced wave breaking parameterization by *Battjes and Janssen* (1978) and *Battjes and Stive* (1985) forms the basis of many studies and parameterizations on this topic. *Battjes and Janssen* (1978) suggest a value of the breaker parameter γ of 0.78 and the Battjes-Janssen a proportionality factor of $\alpha = 1.0$. The breaker parameter provides the relation between the total water depth d and the maximum wave height H_{max} by $H_{max} = \gamma d$. *Battjes and Stive* (1985) reanalyzed laboratory and field observations and suggested the values $\alpha = 1.0$ and $0.6 \leq \gamma \leq 0.83$ with an average of $\gamma = 0.73$. *Kaminsky and Kraus* (1993) found values between $0.6 \leq \gamma \leq 1.59$ with an average value of $\gamma = 0.79$. Later *Ruessink et al.* (2003) found that γ is dependent on the product of the wave number k and the water depth h , but could not find a physical explanation for this. *Thornton and Guza* (1983) show that the wave heights in the surf zone remain Rayleigh distributed after breaking in contradiction to *Battjes and Janssen* (1978). *Apotsos et al.* (2008) investigate several parameterizations and concludes that tuning γ for each individual model gives the best results. *Westhuysen* (2010) introduces a biphasic breaker model with the aim to improve the performance of SWAN in situations of finite-depth growth. The model seems an improvement on the still widely used formulation by *Battjes and Janssen* (1978). The results are comparable with the model by *Ruessink et al.* (2003), but does not suffer lack on physical explanation. *Salmon and Holthuijsen* (2010) continue on this subject and found a scaling that depends on the normalized water depth kd on the one hand and bottom slope on the other hand. After calibration and validation on many laboratory flume cases and in the field, the root-mean square error in significant wave height compared with the bore-model by *Battjes and Janssen* (1978) decreased significantly for flat bottoms (lakes and reefs), while it did not for gently sloping bottoms.

Whitecapping is usually modeled with the use of *Komen et al.* (1984). *Westhuysen et al.* (2007) investigate a revised dissipation formulation of whitecapping in SWAN, based on *Alves and Banner* (2003). In this study computed wave spectra agree better with observed wave spectra, compared with the parameterization by *Komen et al.* (1984). *Rogers et al.* (2012) conclude that an adjustment

of the parameterization of *Komen et al. (1984)* is necessary. The value $\delta = 0$ is changed to $\delta = 1$ by *Rogers et al. (2012)*.

Bottom friction is a form of energy dissipation of waves. During the Joint North Sea Wave Project (JONSWAP) (*Hasselmann et al., 1973*), a parameterization with a constant of $C_{bfr} = C_{JONSWAP} = 0.038 m^2 s^{-3}$ was found for swell-waves in the North Sea. Later *Bouws and Komen (1983)* found a value of $C_{JONSWAP} = 0.067 m^2 s^{-3}$ for depth-limited wind-sea conditions in the North Sea. *Zijlema et al. (2012)* suggest, in accordance with their wind parameterization, that $C_{bfr} = 0.038 m^2 s^{-3}$ should be used for both swell-waves and wind-sea conditions. Both *Collins (1972)* and *Madsen et al. (1988)* suggest an alternative formulation of the coefficient, based on the orbital velocity near the bottom. In addition *Madsen et al. (1988)* includes a formulation that depends on bottom roughness and wave conditions.

Xu et al. (2013) have investigated depth-induced wave breaking and bottom friction during two chosen storms with SWAN at the Mackenzie Delta, Canada. The Mackenzie Delta is known for its extremely mild slopes. Not any of the bottom friction parameterizations by *Hasselmann et al. (1973)*, *Collins (1972)* and *Madsen et al. (1988)* has any preference over another (*Luo and Monbaliu, 1994*). Bottom friction dissipation at continental shelves is dependent on the bottom composition, which is non-uniform over the world. The focus of this study is to a reasonable estimate of the bottom friction parameterization at the Mackenzie Delta. The other physical process, depth-induced wave breaking, is investigated by varying the breaker index γ in the *Battjes and Janssen (1978)* parameterization. The conclusion was that a value of $C_f = 0.006$ in the *Collins (1972)* agreed best with observations for bottom friction and a value of $\gamma = 0.55$ in *Battjes and Janssen (1978)* had the best fit with observations.

2.3 Conclusion

The 3D implementation of radiation stress is heavily investigated the last decade, but consensus about the right formulation has not been reached. Therefore the 2D radiation stress is still widely implemented in both 2DH and 3D circulation models. The effect of the radiation stress on water level and currents is considered significantly during the occurrence of several hurricanes at the Gulf of Mexico (*Xie et al., 2008*).

An unambiguous way to determine the coupling interval results in many cases in little transparency with respect to the choice of the coupling interval. The coupling interval is often chosen on basis of computational time, while a choice of the coupling interval based on the correct representation of the physics would be a more scientific approach.

Both the circulation model and the wave model use a wind drag formulation to model the wind stress. *Zijlema et al. (2012)* and *Bye et al. (2010)*, for example, find parameterizations that reduce the wind drag at high wind speeds. *Funakoshi et al. (2008)* underwrites the interaction between wind and water surface lacks scientific understanding, while the importance of wind drag is stressed by *Bolanos et al. (2011)*. The combination of the independent use of wind drag formulations in both the circulation model and the wave model is questioned by *Janssen et al. (2004)* and a solution that considers the conservation of momentum is proposed.

The importance of correct representation of the wave boundary conditions at the Gulf of Mexico was stressed by *Edwards et al. (2009)*, while changes in bathymetry had hardly any influence. It has to be remarked the water depth at the Gulf of Mexico is large compared with the water depth

at for instance the Wadden Sea. The correct representation of wind fields is important, because the direction and wind speed with respect to the direction of the current are concluded to be important (*Fan et al.*, 2009). *Moon* (2005) remarks that the tide is the most influential factor in modulation mean wave characteristic in the Yellow and East China Sea. It can be concluded that many articles are written after the performance of a hindcast, which all stress the importance of either bathymetry, wind, tide and wave boundary conditions. Though this appears to be rather arbitrarily, the only conclusion that can be drawn is that these driving forces are only dependent on the model and no general conclusion can be drawn on whether any of the previously mentioned aspects is important.

Many depth-induced wave breaking parameterizations are based on *Battjes and Janssen* (1978) and this parameterization is still widely used. The variability of the suggested values of γ by *Battjes and Janssen* (1978), *Battjes and Stive* (1985) and *Kaminsky and Kraus* (1993) using the *Battjes and Janssen* (1978) parameterization demonstrate that a wide range of values could be used and models should always be calibrated and validated when using this parameterization.

Bottom friction becomes more important in shallow waters, like the Wadden Sea. The conclusion of *Zijlema et al.* (2012) after a reanalysis of *Bouws and Komen* (1983) is that the bottom friction constant for both wind-sea conditions and swell conditions should be $C_{bfr} = 0.038m^2s^{-3}$, when using *Hasselmann et al.* (1973). Other parameterizations. *Collins* (1972) and *Madsen et al.* (1988), do not perform better or worse than *Hasselmann et al.* (1973), according to *Luo and Monbaliu* (1994). The suggested value of $C_{bfr} = 0.038m^2s^{-3}$ by *Zijlema et al.* (2012) is, of course, not taken into consideration in *Luo and Monbaliu* (1994), which could have effect on which parameterizations should be preferred.

Chapter 3

Circulation models

3.1 Introduction

In Chapter 2, the most important conclusions and recommendations of numerous studies are presented with the goal to point out what the determining processes are in modeling wave-current interaction with a two-way coupled system. While there are only a few third-generation spectral wave models used, i.e. SWAN ([Booij et al., 1999](#)), WAM ([Group, 1988](#)) and WAVEWATCH III ([Tolman, 1991](#)), the variety of circulation models is larger, i.e. Delft3D-FLOW, ADCIRC, FVCOM, POLCOMS, POM and ROMS. In most cases, these studies also provide a section to show which modifications are made in the circulation model to account for wave-current interaction related processes, when the circulation model is used in combination with a wave model. This chapter will present the modifications with respect to wave-current interaction in the different circulation models, with the goal to provide technical background information on modified terms due to wave-current interaction in the circulation model and to identify whether circulation models incorporate similar physical processes.

3.2 Method

First, the governing equations of the models are presented. The circulation models Delft3D-FLOW, ADCIRC, FVCOM, POLCOMS, POM and ROMS are all based on the non-linear shallow-water equations. Thereby, Modifications in related parameterizations due to wave-current interaction are discussed subsequently. Thereby a number of circulation models applies modifications in the turbulence equations. These modifications are also discussed in this chapter.

3.3 Governing equations

3.3.1 Shallow-water equations

Though the circulation models all use different equations to solve the hydrodynamic conditions, essentially they are all based on the shallow water equations. To provide some support when looking to the modifications in the circulation model when coupled with a wave model, the governing

equations are presented first in this section. First, some important assumptions are provided, together with a variety of conventions to present the governing equations.

Water depth

The water depth is formulated with respect to a reference plane. The formulation of the total water depth is given by:

$$h = d + \zeta \quad (3.1)$$

where h is the total water depth, d is the depth below the reference plan and ζ is the free surface elevation above the reference plane.

Hydrostatic pressure assumption

The shallow-water assumption yields that vertical acceleration due to buoyancy effects or sudden variations in bottom topography is assumed to be small compared with the gravitational acceleration and is therefore not taken into account. This assumption reduces the vertical momentum equation to the hydrostatic pressure equation:

$$\frac{\partial p}{\partial z} = \rho g \quad (3.2)$$

The models assume that the density of a fluid element does not change in time. Differences in density over the depth are accounted for with an horizontal pressure term in the horizontal momentum equations (Boussinesq approximation).

Continuity equation

The continuity equation together with the horizontal momentum equations form the shallow water equation. The continuity equation is given by:

$$\frac{\partial \zeta}{\partial t} + \frac{\partial hu}{\partial x} + \frac{\partial hv}{\partial y} = 0 \quad (3.3)$$

where u and v respectively represent the velocities in x - and y -direction.

Horizontal momentum equations

Differences in depth-averaged models and 3D models cause differences in the formulation of the horizontal momentum equations. Therefore, both are presented in this section:

Depth-averaged momentum equations The horizontal depth-averaged momentum equations are presented in Equations 3.4 and 3.5:

$$\frac{\partial u}{\partial t} + u \frac{\partial u}{\partial x} - \nu_h \left(\frac{\partial^2 u}{\partial x^2} + \frac{\partial^2 u}{\partial y^2} \right) = -g \frac{\partial \zeta}{\partial x} - \frac{\tau_{b,x}}{\rho_0 h} + f v + \frac{\tau_{w,x}}{\rho_0 h} - \frac{1}{\rho_0} \frac{\partial p_{atm}}{\partial x} + F_x \quad (3.4)$$

$$\frac{\partial v}{\partial t} + v \frac{\partial v}{\partial x} - \nu_h \left(\frac{\partial^2 v}{\partial x^2} + \frac{\partial^2 v}{\partial y^2} \right) = -g \frac{\partial \zeta}{\partial y} - \frac{\tau_{b,y}}{\rho_0 h} - f u + \frac{\tau_{w,y}}{\rho_0 h} - \frac{1}{\rho_0} \frac{\partial p_{atm}}{\partial x} + F_y \quad (3.5)$$

where ν_h is the horizontal viscosity, $\tau_{b,i}$ and $\tau_{w,i}$ for $i = x, y$ respectively represent bed stress and wind shear-stress. The Coriolis parameter f is given by $f = 2\Omega \sin \theta$, where θ is the geographical latitude and Ω the angular speed of rotation of the earth. The density of water is given by ρ_0 . The atmospheric pressure is given by p_{atm} . The term F represents wave forcing.

3D horizontal momentum equations

$$\frac{Du}{Dt} = \frac{\partial}{\partial x} \left(\nu_h \frac{\partial u}{\partial x} \right) + \frac{\partial}{\partial y} \left(\nu_h \frac{\partial u}{\partial y} \right) + \frac{\partial}{\partial z} \left(\nu_v \frac{\partial u}{\partial z} \right) - g \frac{\partial \zeta}{\partial x} - \frac{1}{\rho_0} \frac{\partial p_{atm}}{\partial x} + \frac{g}{\rho_0} \int_z^\zeta \frac{\partial \rho}{\partial x} dz + f v \quad (3.6)$$

$$\frac{Dv}{Dt} = \frac{\partial}{\partial x} \left(\nu_h \frac{\partial v}{\partial x} \right) + \frac{\partial}{\partial y} \left(\nu_h \frac{\partial v}{\partial y} \right) + \frac{\partial}{\partial z} \left(\nu_v \frac{\partial v}{\partial z} \right) - g \frac{\partial \zeta}{\partial y} - \frac{1}{\rho_0} \frac{\partial p_{atm}}{\partial x} + \frac{g}{\rho_0} \int_z^\zeta \frac{\partial \rho}{\partial y} dz - f u \quad (3.7)$$

In contrary to the depth-averaged horizontal momentum equations, the bed stress and wind shear-stress are not included in the 3D horizontal momentum equations, but are imposed with the use of bed- and surface boundary conditions.

At the bed, the boundary conditions for the horizontal 3D momentum equations are given by:

$$\nu_v \frac{\partial u}{\partial z} \Big|_{z=-d} = \frac{\tau_{b,x}}{\rho_0} \quad (3.8)$$

$$\nu_v \frac{\partial v}{\partial z} \Big|_{z=-d} = \frac{\tau_{b,y}}{\rho_0} \quad (3.9)$$

where τ_b represents the bed stress included the effect of wave-current interaction. The surface boundary conditions are given by:

$$\nu_v \frac{\partial u}{\partial z} \Big|_{z=\zeta} = \frac{\tau_w}{\rho_0} \cos \phi \quad (3.10)$$

$$\nu_v \frac{\partial v}{\partial z} \Big|_{z=\zeta} = \frac{\tau_w}{\rho_0} \sin \phi \quad (3.11)$$

where τ_w is wind shear stress and ϕ is the angle between the wind vector and the x -direction.

3.4 Wave-current interaction related modifications

3.4.1 Current

The current in the depth-averaged and 3D shallow water equations is given by an Eulerian velocity, when waves are not included. POM, POLCOMS, ROMS and Delft3D-FLOW adjust their formulation of the current, to represent the effect the wave-induced driving forces. These circulation models all add Stokes drift to the Eulerian velocity, to account for the effect of waves, while ADCIRC and FVCOM do not add the Stokes drift to the Eulerian velocities. The sum of both the Eulerian velocity and Stokes drift is the GLM velocity:

$$u_{GLM} = u_e + u_s \quad (3.12)$$

$$v_{GLM} = v_e + v_s \quad (3.13)$$

where u_s and v_s are the Stokes velocities and u_e and v_e are the Eulerian velocities.

Stokes drift

Particles beneath a wave describe an orbital motion. A particle at the top of the orbit beneath a wave crest moves slightly faster in the forward direction than it does in the backward direction beneath a wave trough. The result is a net horizontal displacement in the direction of wave propagation. The average velocity of this fluid particle is known as the Stokes drift velocity.

The formulation of the Stokes drift used in the GLM-velocity in case of a depth-averaged model differs from the formulation used in case of a 3D-model. In Delft3D-FLOW, the formulation used in a depth-averaged model is derived from the wave-induced mass fluxes. The definition of the mass fluxes is given by:

$$M_x^s = \int_{-d}^{\bar{\zeta}} \rho_0 u_s dz = \frac{E}{\omega} k_x \quad (3.14)$$

$$M_y^s = \int_{-d}^{\bar{\zeta}} \rho_0 v_s dz = \frac{E}{\omega} k_y \quad (3.15)$$

where $\bar{\zeta}$ is the wave-averaged free surface elevation, k is the wave number and E is the wave energy given by:

$$E = \frac{1}{8} \rho_0 g H_{rms}^2 \quad (3.16)$$

where H_{rms} is the root-mean-square wave height, which is provided by the wave model. The depth-averaged Stokes drift is expressed as:

$$u_s = \frac{M_x^s}{\rho_0 h} \quad (3.17)$$

$$v_s = \frac{M_y^s}{\rho_0 h} \quad (3.18)$$

In Delft3D-FLOW, the Stokes drift, based on [Dabrymple and Dean \(1991\)](#), in 3D-models is given by:

$$\begin{aligned} u_s(z) &= \frac{\omega k a^2 \cosh(2kz)}{2 \sinh^2(kh)} \cos(\theta) \\ v_s(z) &= \frac{\omega k a^2 \cosh(2kz)}{2 \sinh^2(kh)} \sin(\theta) \end{aligned} \quad (3.19)$$

where θ is the angle between the current and the direction of the mass fluxes, a is the wave amplitude, ω the angular frequency. POM, POLCOMS, and ROMS calculate the Stokes drift in a similar manner as Delft3D-FLOW.

3.4.2 Surface stress

Not all circulation models modify the formulation of the wind shear-stress to account for the effect of waves. POLCOMS adjusts the surface stress to be consistent in terms of conservation of momentum in a two-way coupled system, according to the formulation of [Janssen et al. \(2004\)](#):

$$\tau_w = \tau_a - \rho g \int_0^{2\pi} \int_0^{w_h} \frac{k}{w} (S_{in} + S_{nl} + S_{ds}) dw d\theta \quad (3.20)$$

where τ_w is the modified surface shear-stress, τ_a is the total wind stress and the second term on the right hand side represents the stress acting on waves ([Bolaños et al., 2011](#)). The terms S_{in} , S_{nl} and S_{ds} are the source terms from the wave model for respectively wind input, wave-wave interaction and dissipation.

The wind drag parameterization in FVCOM and POM is modified to account for the modified aerodynamic roughness of the sea due to waves, where the roughness of the sea depends strongly on wave age U_{10}/c . The sea surface roughness is modified according to [Donelan et al. \(1993\)](#):

$$z_0 = 3.7 \times 10^{-5} \frac{u_{10}^2}{g} \left(\frac{u_{10}}{c} \right)^{0.9} \quad (3.21)$$

where z_0 is the sea surface roughness, u_{10} is the wind speed at an elevation of 10 m and c is the phase velocity of the peak period. The drag coefficient C_D is determined with:

$$C_D = \left(\frac{\kappa}{\ln(10/z_0)} \right)^2 \quad (3.22)$$

where κ is the Von Kármán constant. The surface stress is given by:

$$\tau_s = \rho_a C_D U_{10}^2 \quad (3.23)$$

where ρ_a is the air density. The wind velocity U_{10} is the apparent wind, so the wind velocity relative to the current.

3.4.3 Wave force

The wave force in the horizontal momentum equations, is in all circulation models represented by the gradient of the radiation stress. Delft3D-FLOW thereby provides the opportunity to calculate the forcing, based on the dissipation rate in the wave model.

Radiation Stress In Delft3D-FLOW, the wave force F , bases on the gradients of the radiation stress tensor, is given by:

$$F_x = -\frac{1}{\rho h} \left(\frac{\partial S_{xx}}{\partial x} - \frac{\partial S_{xy}}{\partial y} \right) \quad \text{in the } x\text{-direction} \quad (3.24)$$

$$F_y = -\frac{1}{\rho h} \left(\frac{\partial S_{yy}}{\partial y} - \frac{\partial S_{yx}}{\partial x} \right) \quad \text{in the } y\text{-direction} \quad (3.25)$$

When a depth-averaged model is used, the radiation stress gradients are applied over the entire depth, while when a 3D model is used, the force due to radiation stress gradients is applied only at the surface layer d_1 of the vertical grid:

$$F_x = -\frac{1}{\rho d_1} \left(\frac{\partial S_{xx}}{\partial x} - \frac{\partial S_{xy}}{\partial y} \right) \quad \text{in the } x\text{-direction} \quad (3.26)$$

$$F_y = -\frac{1}{\rho d_1} \left(\frac{\partial S_{yy}}{\partial y} - \frac{\partial S_{yx}}{\partial x} \right) \quad \text{in the } y\text{-direction} \quad (3.27)$$

The radiation stresses are given by:

$$S_{xx} = \rho_0 g \int_0^\infty \int_0^{2\pi} \left(n - \frac{1}{2} + n \cos^2 \theta \right) N(\sigma, \theta) d\theta d\sigma \quad (3.28)$$

$$S_{xy} = \rho_0 g \int_0^\infty \int_0^{2\pi} (n \sin \theta \cos \theta) N(\sigma, \theta) d\theta d\sigma \quad (3.29)$$

$$S_{yx} = \rho_0 g \int_0^\infty \int_0^{2\pi} (n \sin \theta \cos \theta) N(\sigma, \theta) d\theta d\sigma \quad (3.30)$$

$$S_{yy} = \rho_0 g \int_0^\infty \int_0^{2\pi} \left(n - \frac{1}{2} + n \sin^2 \theta \right) N(\sigma, \theta) d\theta d\sigma \quad (3.31)$$

$$(3.32)$$

In contrary to both FVCOM and ROMS, the radiation stresses are applied are not depth-dependent. The radiation stresses (*Mellor, 2003, 2005; Mellor et al., 2008*) in FVCOM and ROMS are given by:

$$\begin{aligned}
S_{xx} &= kE \left[\frac{k_x k_x}{k^2} F_{CS} F_{CC} + F_{CS} F_{CC} - F_{SS} F_{CS} \right] + \frac{k_x k_x}{k} \frac{c^2}{L} A_R R_z \\
S_{xy} &= kE \left[\frac{k_x k_y}{k^2} F_{CS} F_{CC} \right] + \frac{k_x k_y}{k} \frac{c^2}{L} A_R R_z \\
S_{yy} &= kE \left[\frac{k_y k_y}{k^2} F_{CS} F_{CC} + F_{CS} F_{CC} - F_{SS} F_{CS} \right] + \frac{k_y k_y}{k} \frac{c^2}{L} A_R R_z
\end{aligned} \tag{3.33}$$

and the vertical radiations stresses are given by:

$$\begin{aligned}
S_{px} &= (F_{CC} - F_{SS}) \left[\frac{F_{ss}}{2} \frac{\partial E}{\partial x} + F_{CS}(1+s)E \frac{\partial(kD)}{\partial x} \right. \\
&\quad \left. - EF_{SS} \coth(kD) \frac{\partial(kD)}{\partial x} \right] \\
S_{py} &= (F_{CC} - F_{SS}) \left[\frac{F_{ss}}{2} \frac{\partial E}{\partial y} + F_{CS}(1+s)E \frac{\partial(kD)}{\partial y} \right. \\
&\quad \left. - EF_{SS} \coth(kD) \frac{\partial(kD)}{\partial y} \right]
\end{aligned} \tag{3.34}$$

Both models include surface roller in the equation, based on *Svendsen (1984)* and *Svendsen et al. (2002)*. The vertical distribution of the surface roller is given by:

$$R_z = 1 - \tanh \left(\frac{2z}{\gamma} \right)^4 \tag{3.35}$$

The roller area A_r can be calculated using the expression by *Svendsen (1984)*:

$$A_r = \frac{\alpha}{\sqrt{2}} H_s L Q_b \tag{3.36}$$

where α is a parameter with a value of 0.06 and Q_b is the fraction of breaking waves.

The wave forces F_x and F_y are, according to (*Mellor, 2005*), given by:

$$F_x = \frac{1}{\rho d_1} \frac{\partial S_{xx}}{\partial x} + \frac{1}{\rho d_1} \frac{\partial S_{xy}}{\partial y} - \frac{1}{\rho d_1} \frac{\partial S_{px}}{\partial z} \tag{3.37}$$

$$F_y = \frac{1}{\rho d_1} \frac{\partial S_{yx}}{\partial x} + \frac{1}{\rho d_1} \frac{\partial S_{yy}}{\partial y} - \frac{1}{\rho d_1} \frac{\partial S_{py}}{\partial z} \tag{3.38}$$

Though the formulations of the above presented wave forces are assumed to be presented in a correct way, corresponding to the implementation in the circulation models FVCOM and POM, the correct representation cannot be guaranteed. As the formulation of the depth dependent radiation stress is currently subject of research, the formulations change once in a while, and may result in adjustments in the circulation models, concerning the formulation of the radiation stresses.

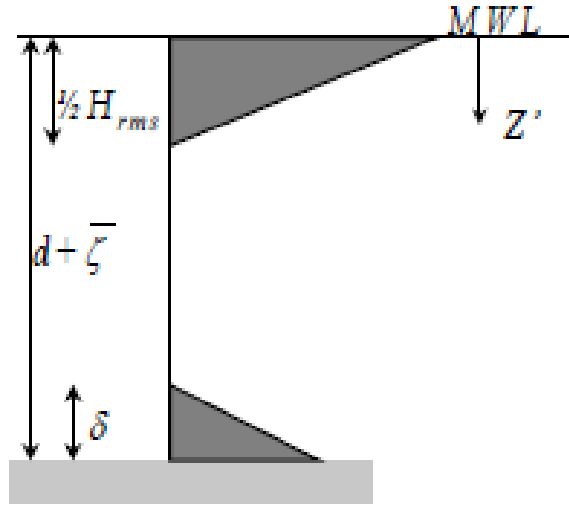


Figure 3.1: Vertical distribution of shear-stresses and turbulent kinetic energy (Deltares, 2011)

Wave energy dissipation rate

The modeling of radiation stress in numerical models can lead to spurious currents, as shown by [Dingemans et al. \(1987\)](#). When neglecting the divergence free part of the radiation stress, the remaining part is closely related to the wave energy dissipation. In Delft3D-FLOW, applying the wave force dependent on the dissipation rate is a possibility.

$$F_x = D \frac{k_x}{\omega} \quad (3.39)$$

$$F_y = D \frac{k_y}{\omega} \quad (3.40)$$

The total wave energy dissipation rate, D , per unit time is the sum of the energy dissipation due to bottom friction, whitecapping and wave breaking per unit time and is calculated in SWAN.

3.4.4 Streaming

The wave boundary layer thickness varies along the wave profile, which causes variation in the vertical orbital velocity. The degree of variation in the orbital velocity strongly depends on the roughness of the bed. Consequently, the horizontal and vertical orbital velocities are not exactly 90° out of phase, resulting in a net streaming in the direction of wave propagation and a finite time-averaged shear stress. The formulation is based on energy dissipation and decreases linearly with the boundary layer thickness δ ([Fredsoe and Deigaard, 1992](#)):

$$\tau_{streaming}(z) = \frac{\partial}{\partial z} \left[\frac{D_f \cos \theta}{\omega} \left(1 - \frac{d + \zeta - z}{\delta} \right) \right] \text{ for } d + \zeta - \delta \leq z \leq d + \zeta \quad (3.41)$$

The left hand side of Equation 3.41 is the residual term after averaging a vertical derivative of the advection terms over the wave period and is modeled in Delft3D-FLOW in a similar way as the wave force at the top layer, but at the bottom layer of the vertical grid (Figure 3.1). The dissipation due to friction D_f is given by:

$$D_f = \frac{1}{2\sqrt{\pi}} \rho_0 f_{w, fac} u_{orb}^3 \quad (3.42)$$

The friction factor f_w according to *Soulsby et al. (1993)* is given by:

$$f_{w, fac} = \min \left\{ 0.3, 1.39 \left(\frac{A}{z_0} \right)^{-0.52} \right\} \quad (3.43)$$

and A is given by:

$$A = \frac{u_{orb}}{\omega} \quad (3.44)$$

The wave boundary layer has a thickness δ given by:

$$\delta = H \min \left[0.5, 20 \max \left\{ \frac{ez_0}{H}, 0.09 \frac{k_s}{H} \left(\frac{A}{k_s} \right)^{0.82} \right\} \right] \quad (3.45)$$

Delft3D-FLOW is the only circulation model that accounts for the effect of streaming.

3.4.5 Bed boundary conditions

Delft3D-FLOW In Delft3D-FLOW, the mean bed shear-stress for combined waves and current $|\vec{\tau}_m|$ is given by a nonlinear relation between the mean bed shear-stress due to current alone $|\vec{\tau}_c|$ and the bed shear-stress due to waves alone $|\vec{\tau}_w|$ according to *Soulsby et al. (1993)*:

$$|\vec{\tau}_m| = Y(|\vec{\tau}_c| + |\vec{\tau}_w|) \quad (3.46)$$

with

$$Y = X1 + bX^p(1 - X)^q \quad (3.47)$$

The maximum bed shear-stress is important for modeling sediment transport and is given by:

$$|\vec{\tau}_{max}| = Z(|\vec{\tau}_c| + |\vec{\tau}_w|) \quad (3.48)$$

with:

$$Z = 1 + aX^m(1 - X)^n \quad (3.49)$$

and:

$$X = \frac{|\vec{\tau}_c|}{|\vec{\tau}_c| + |\vec{\tau}_w|} \quad (3.50)$$

where the parameters a , b , p , q , m and n depend on the friction model chosen and on the drag coefficient due to current C_{2D} , the wave current factor f_w and the angle between the direction of wave propagation and the current direction.

The drag coefficient C_{2D} is calculated with the use of the formulation of Chézy, Manning or White Colebrook. The bed shear-stress due to current is given by:

$$\vec{\tau}_c = \frac{g\rho_0 u |u|}{C_{2D}^2} \quad (3.51)$$

The wave-averaged bed shear-stress due to waves is given by:

$$|\vec{\tau}_w| = \frac{1}{2} \rho_0 f_w u_{orb}^2 \quad (3.52)$$

The orbital velocity is computed with the root-means square wave height H_{rms} and the wave period T according to the linear wave theory. The orbital velocity is given by:

$$u_{orb} = \frac{1}{4} \sqrt{\pi} \frac{H_{rms} \omega}{\sinh(kH)} \quad (3.53)$$

The friction factor is dependent on the orbital velocity, the wave angular frequency ω and the Nikuradse roughness length scale k_s and is given by:

$$f_w = \begin{cases} 0.00251 \exp \left[5.21 \left(\frac{A}{k_s} \right)^{-0.19} \right], & \frac{A}{k_s} > \frac{\pi}{2} \\ 0.3, & \frac{A}{k_s} \leq \frac{\pi}{2} \end{cases} \quad (3.54)$$

with:

$$A = \frac{u_{orb}}{\omega} \quad (3.55)$$

The bed shear-stress τ_b in the depth-averaged horizontal momentum equations is corrected for Stokes drift, as the bed is in rest and the equations are formulated in GLM velocities, and is given by:

$$\vec{\tau}_b = \frac{|\vec{\tau}_m|}{|u|} (\bar{u} - \bar{u}_s) \quad (3.56)$$

The bed shear-stress in case of a 3D model is applied as a boundary condition. The bed shear-stress due to current alone is modified by replacing the depth-averaged velocity by the velocity near the bed, assuming a logarithmic profile.

$$\vec{\tau}_b = \frac{|\vec{\tau}_m|}{|\vec{U}_{2D}|} (\vec{u} - \vec{u}_s) \quad (3.57)$$

where U_{2D} is the depth-averaged velocity, given by:

$$\vec{U}_{2D} = \frac{1}{h} \int_{-d}^{\zeta} \vec{u} dz \quad (3.58)$$

The mean bed shear-stress for combined waves and current is given by:

$$\vec{\tau}_m = \rho \vec{u}_* |\vec{u}_*| \quad (3.59)$$

where u_* is the shear stress velocity for waves and currents. The velocity in the first layer above the bed is given by:

$$\vec{u}_b = \frac{\vec{u}_*}{\kappa} \ln \left(1 + \frac{\Delta z_b}{2z_0} \right) \quad (3.60)$$

where Δz_b is the vertical distance to the computational grid point closest to the bed. The roughness length is modified due to waves according to:

$$\bar{z}_0 = \frac{\Delta z_b}{\exp \left(\kappa \frac{|\vec{u}_b|}{|\vec{u}|} \right) - 1} \quad (3.61)$$

ADCIRC The bottom friction in ADCIRC is calculated with the use of Manning's n formulation. The n is a spatially variable value that depends on the composition of the bottom. The roughness length z_0 is computed at the wave model time step.

$$z_0 = H \exp \left[- \left(1 + \frac{\kappa H^{1/6}}{n \sqrt{g}} \right) \right] \quad (3.62)$$

where n is the Manning n value, h is the water depth computed by ADCIRC and κ is the Von Kármán constant. To prevent unrealistic small roughness lengths in SWAN, Manning n values that are smaller than 0.03 are raised to $n \geq 0.03$. The roughness length computed by ADCIRC is used in the bottom friction formulation by (Madsen *et al.*, 1988) in SWAN. The values of n remain unchanged in ADCIRC.

FVCOM and ROMS Both FVCOM and ROMS use the same equations to account for enhanced bottom friction due to wave-current interaction. The bottom boundary layer is important for the solution of the shallow water equations. The boundary conditions for the momentum equations are determined with the use of the bottom boundary layer. It determines the stress exerted on the flow by the bottom:

$$\nu_v \frac{\partial u}{\partial \hat{\sigma}} = \tau_{b,x}, \quad \nu_v \frac{\partial v}{\partial \hat{\sigma}} = \tau_{b,y} \quad (3.63)$$

The user can choose either a simple quadratic drag-coefficient method or a more complex logarithmic formulation. The quadratic drag-coefficient method calculates the bottom shear-stress with the use of two spatially-uniform coefficients γ_1 and γ_2 :

$$\tau_{b,x} = \left(\gamma_1 + \gamma_2 \sqrt{u^2 + v^2} \right) u \quad (3.64)$$

$$\tau_{b,y} = \left(\gamma_1 + \gamma_2 \sqrt{u^2 + v^2} \right) v \quad (3.65)$$

where the user can choose between a linear or quadratic drag coefficient by setting either γ_1 or γ_2 to zero.

The logarithmic formulation assumes a logarithmic profile of the flow in the bottom-boundary layer:

$$|u| = \frac{u_*}{\kappa} \ln \left(\frac{z}{z_0} \right) \quad (3.66)$$

where κ is the Von Kármán constant, z_0 is the bottom roughness length, u_* the bottom shear velocity, $|u| = \sqrt{u^2 + v^2}$ and z is the elevation above the bottom. The bed shear-stress is then given by:

$$\tau_{b,x} = \frac{\kappa^2 u \sqrt{u^2 + v^2}}{\ln^2(z/z_0)} \quad (3.67)$$

$$\tau_{b,y} = \frac{\kappa^2 v \sqrt{u^2 + v^2}}{\ln^2(z/z_0)} \quad (3.68)$$

POM In [Xie et al. \(2001\)](#), [Xie et al. \(2003\)](#) and [Xie et al. \(2008\)](#), the bottom friction in POM is described. To account for wave-current interaction at the bottom, the bottom stress is calculated according to [Signell et al. \(1990\)](#) and [Davies and Lawrence \(1995\)](#). The modified bottom stress for wave-current interaction τ_b is composed of the maximum wave bed stress τ_w and the instant current bed stress τ_c :

$$\tau_b = \tau_c + \tau_w \quad (3.69)$$

The initial current bed stress is given by:

$$\tau_w = 0.5 f_w \rho u_{orb}^2 \quad (3.70)$$

where u_{orb} is the near-bed orbital velocity, that is given by:

$$u_{orb} = \frac{a_w \omega}{\sinh kh} \quad (3.71)$$

where a_w is the wave amplitude, ω the angular wave frequency and k is the wave number.

The wave friction factor f_w is determined with the use of *Jonsson (1966)* and *Jonsson and Carlsen (1976)*:

$$\frac{1}{4\sqrt{f_w}} + \log_{10} \left(\frac{1}{4\sqrt{f_w}} \right) = -0.08 + \log_{10} \left(\frac{A_b}{k_b} \right) \quad (3.72)$$

The current friction factor f_c is determined by *Davies and Lawrence (1995)*, and is given by:

$$f_c = 2 \left[\frac{\kappa}{\ln(30z_r/k_{bc})} \right] \quad (3.73)$$

where the reference height z_r is the height at which the slip condition is applied and k_{bc} is initially the Nikuradse roughness. The wave friction velocity U_{*w} and U_{*c} are given by:

$$U_{*w} = \left(\frac{\tau_w}{\rho} \right)^{1/2}, \quad (3.74)$$

$$U_{*c} = \left(\frac{\tau_c}{\rho} \right)^{1/2} \quad (3.75)$$

The combined friction velocity is given by:

$$U_{*cw} = (U_{*w}^2 + U_{*c}^2)^{1/2} \quad (3.76)$$

The combined bottom roughness k_{bc} is determined with:

$$k_{bc} = k_b \left[24 \frac{U_{*cw}}{U_w} \frac{A_b}{k_b} \right]^\beta \quad \text{with } \beta = \left(1 - \frac{U_{*c}}{U_{*cw}} \right) \quad (3.77)$$

where A_b is the near-bottom excursion amplitude. The determined value for k_{bc} will be used again in Equation 3.73. With the use of iteration a final value of f_c will be calculated.

3.4.6 Turbulence

Delft3D-FLOW uses a turbulence model to model the effect of turbulent mixing. Waves enhance the vertical mixing and are incorporated in the turbulence model by adding wave energy production and dissipation terms. Wave breaking contributes energy which is linearly distributed over a half wave height beneath the mean water surface. Enhanced turbulence due to bottom friction is linearly distributed over the thickness of the wave boundary layer δ (see Figure 3.1).

These processes are modeled by introducing source terms to the $k - \epsilon$ and $k - L$ turbulence models.

Breaking waves

The contribution due to breaking waves for the k -equation is given by:

$$P_{kw}(z') = \frac{4D_w}{\rho_w H_{rms}} \left(1 - \frac{2z}{H_{rms}} \right) \text{ for } 0 \leq z' \leq \frac{1}{2} H_{rms} \quad (3.78)$$

and for the ϵ -equation:

$$P_{\epsilon w}(z') = c_{1\epsilon} \frac{\epsilon}{k} P_{kw}(z') \quad (3.79)$$

The boundary conditions are modified as well. An extra term concerning the contribution of waves is introduced for both the k -equation, as for the ϵ -equation. The modified boundary conditions at the surface read:

$$k|_{\sigma=0} = k_{(wind)} + k_{(waves)} = k_{(wind)} + \left(\frac{2D_w \kappa}{\rho_w c_D} \right)^{\left(\frac{2}{3}\right)} \quad (3.80)$$

$$\epsilon|_{\sigma=0} = \epsilon_{wind} + \epsilon_{waves} = \epsilon_{wind} + \frac{4D_w}{\rho_w H_{rms}} \quad (3.81)$$

Bottom friction

The effect due to bottom friction is given by:

$$P_{kw}(z) = \frac{2D_f}{\delta} \left(1 - \frac{d + \zeta - z}{\delta} \right) \text{ for } d + \zeta - \delta \leq z \leq d + \zeta \quad (3.82)$$

where D_f represents the dissipation rate due to bottom friction.

The modification at the bottom is taken into account by adaption of the bottom roughness height, calculated in Equation 3.61.

POLCOMS uses the Mellor-Yamada level 2.5 turbulence close scheme ([Mellor and Yamada, 1982](#)) to estimate the vertical eddy viscosity and diffusivity with an algebraic mixing length. To account for turbulence generated due to surface wave breaking, the scheme is modified according to [Craig and Banner \(1994\)](#), where the surface condition reads:

$$lqS_q \frac{\partial b}{\partial z} = \alpha u_*^3 \text{ at } z = \zeta \quad (3.83)$$

where l is the turbulent length scale, q the turbulent velocity scale, b is the turbulent kinetic energy density (i.e. $q^2 = 2b$), α is a the wave energy factor with a value 100 and u_* is the wind friction velocity, determined in the model.

A modification of the turbulence surface condition is also included in ROMS, according to the theory of [Umlauf and Burchard \(2003\)](#), which ensures the model to account for surface fluxes of turbulence kinetic energy due to wave breaking.

Coupling procedure

In a two-way coupled system, the models force each other with information from the other model at a given interval, the coupling interval. As the computational time step in the circulation model is in general smaller than the coupling interval, the information received from the wave model is assumed to be constant during the computations in between the set interval.

An exemption is ADCIRC. ADCIRC extrapolates the radiation stress from SWAN at the beginning of the current interval and at the beginning of the previous interval for every time step during the current interval.

3.5 Conclusion

This chapter presented the governing equations used in the circulation models when coupled with a wave model. The models FVCOM, POM, ROMS and POLCOMS use a mode splitting technique that separates the governing momentum equations into two equations, an internal and external momentum equation. The first equation deals with depth dependent processes, such as baroclinic pressure, while the latter is depth independent and deals with external processes, such as barotropic pressure. ADCIRC differs from these models by using a Generalized Wave Continuity Equation apart from the momentum equations. The Generalized Wave Continuity Equation is a combination of the classic momentum equation and continuity equation. Delft3D-FLOW solves either the 2D depth-averaged or 3D non-linear shallow water equations, based on the incompressible 3D Navier-Stokes equations.

The transfer of wind energy to the water column is usually modeled with the use of a surface shear stress. To account for the modified aerodynamic roughness of the sea due to waves, the surface shear stress in FVCOM and POM is adjusted according to [Donelan et al. \(1993\)](#). None of the other models account for this modification of the roughness of the sea surface.

POLCOMS is the only model that splits up the wind energy into a part that is used to generate waves and a part that is used in the circulation model. The circulation model uses an adjusted surface stress expression, which is the difference between the surface stress that the system would have felt in the absence of waves and the wave stress.

All models use 2D radiation stress in both 2DH and 3D models, except FVCOM and ROMS, that uses 3D radiation stress. Only Delft3D-FLOW gives the possibility to use the dissipation rate to model the excess flux of momentum.

In Delft3D-FLOW, the bottom stress when waves are included is given by a nonlinear relation between the bed shear stress due to current alone and waves alone, according to the theory by [Soulsby et al. \(1993\)](#). The bed shear stress is corrected for Stokes drift. The Model-Coupling Toolkit described in [Warner et al. \(2008a\)](#) and [Warner et al. \(2008b\)](#) is used by FVCOM and ROMS. ADCIRC does not use an enhanced formulation for the bottom stress to account for the effect of waves, but adjust the n value of the Manning's n formulation to ensure realistic roughness lengths in SWAN. POLCOMS uses the bottom stress formulation according to ([Madsen, 1994](#)).

POM and POLCOMS use the turbulence close scheme by [Mellor and Yamada \(1982\)](#), which is modified by [Craig and Banner \(1994\)](#) to account for wave-current interaction.

It can be concluded that Delft3D-FLOW generally incorporates similar physical processes in its equations. Remarkably, Delft3D-FLOW does not account for the modification of sea roughness in the parameterization of its surface shear stress formulation, while FVCOM and POMS do. This is not just using a different parameterization, but ignoring a physical process completely. The opposite is valid for the incorporation of the dissipation rate, while none of the other models uses this type of formulation to replace the radiation stress.

Chapter 4

SWAN

4.1 Introduction

In Chapter 2 numerous studies are presented where two-way coupled models are used. Thereby a number of parameterizations of generation and dissipation processes in wave models are presented, that could have a significant effect on the behavior of the two-way coupled model.

SWAN (*Booij et al., 1999*) is, together with WAVEWATCH III and WAM, the most used wind and is a third generation wave model and is used to model wind, wave and swell effects. A difference between on the one hand WAVEWATCH III and WAM and on the other hand SWAN is that WAVEWATCH III and WAM are specifically designed for ocean application, while SWAN can be used on any scale relevant, such as coastal areas, estuaries and lakes.

The parameterizations discussed in Chapter 2 particularly play an important role in the coastal zone. This provides a plausible reason to prefer SWAN over WAM and WAVEWATCH III in this study. This chapter will present a number of relevant parameterizations from Chapter 2, with the goal to give proper insight in the parameterization of the physics in the model SWAN.

4.2 Physics in SWAN

4.2.1 Action balance equation

SWAN uses the action density spectrum $N(\sigma, \theta)$ rather than the energy density spectrum $E(\sigma, \theta)$ to describe waves. The rationale behind this is that action density is conserved when ambient currents are present, while energy density is not. The relation between action density and energy density is given by $N(\sigma, \theta) = E(\sigma, \theta)/\sigma$, where σ is the relative radian frequency. The action balance equation (*Booij et al., 1999*) is given by:

$$\begin{aligned} & \frac{\partial N(\sigma, \theta; x, y, t)}{\partial t} + \frac{\partial c_{g,x} N(\sigma, \theta; x, y, t)}{\partial x} + \frac{\partial c_{g,y} N(\sigma, \theta; x, y, t)}{\partial y} \\ & + \frac{\partial c_{\theta} N(\sigma, \theta; x, y, t)}{\partial \theta} + \frac{\partial c_{\sigma} N(\sigma, \theta; x, y, t)}{\partial \sigma} = \frac{S_{tot}(\sigma, \theta; x, y, t)}{\sigma} \end{aligned} \quad (4.1)$$

The first term on the left hand side represents the change of the wave action in time. The second and third term on the left hand side represent the propagation of action density in geographical space, with group propagation velocities $c_{g,x}$ and $c_{g,y}$ in respectively x - and y -space. The fourth term represents current-induced and depth-induced refraction, where c_θ is the propagation velocity in θ -space. The fifth term represents shifting of the relative frequency due to variation in depth and currents, where c_σ is the propagation velocity in σ space. The term S_{tot} on the right hand side represents the source term in terms of energy density, given by:

$$S_{tot}(\sigma, \theta) = S_{in}(\sigma, \theta) + S_{nl4}(\sigma, \theta) + S_{nl3}(\sigma, \theta) + S_{wc}(\sigma, \theta) + S_{bfr}(\sigma, \theta) + S_{br}(\sigma, \theta) \quad (4.2)$$

The first term on the right hand side represents generation by wind. The second and third term represent wave-wave interaction, with the second term representing quadruplet wave-wave interaction and the third term representing triad wave-wave interaction. The fourth, fifth and sixth term on the right hand side represent dissipation by means of whitecapping, bottom friction and depth-induced wave breaking.

Referring to Chapter 2, the source terms S_{in} , S_{bfr} and S_{br} are discussed in the literature study. The parameterizations of these source terms will be presented in the next sections. Though whitecapping is treated in the literature study in Chapter 2, it will not be discussed in this chapter, as the discussed differences in parameterizations are assumed to have a limited effect in the coastal zone.

4.2.2 Wind

Different wind drag parameterizations in SWAN not only might lead to different wave height, but eventually also to different wave forcing in the circulation model as a result of different wave heights and possible different locations of depth-induced wave breaking.

$$S_{in}(\sigma, \theta) = A + BE(\sigma, \theta) \quad (4.3)$$

The source term S_{in} represents wave growth by wind. S_{in} exists of a linear part A and a exponential part $BE(\sigma, \theta)$. The wind speed U_{10} used in SWAN is at an elevation of 10 m . The relation between U_{10} and the friction velocity U_* is presented in 4.4.

$$U_*^2 = C_D U_{10}^2 \quad (4.4)$$

Two formulations of the wind drag coefficient C_D are available in SWAN. The oldest is according to [Wu \(1982\)](#):

$$C_D = \begin{cases} 1.2875 \times 10^{-3} & \text{for } U_{10} < 7.5 \text{ m/s} \\ (0.8 + 0.065 U_{10}) \times 10^{-3} & \text{for } U_{10} \geq 7.5 \text{ m/s} \end{cases} \quad (4.5)$$

More recently [Zijlema et al. \(2012\)](#) formulated:

$$C_d = (0.55 + 2.97 \tilde{U} - 1.49 \tilde{U}^2) * 10^{-3} \quad (4.6)$$

in which $\tilde{U} = U_{10}/U_{ref}$ with $U_{ref} = 31.5 \text{ m/s}$.

While the wind drag coefficient C_D according to [Zijlema et al. \(2012\)](#) decreases during wind speed larger than 31.5 m/s , the wind drag coefficient increases during high wind speeds according to [Wu \(1982\)](#). Where the wind drag parameterization according to [Zijlema et al. \(2012\)](#) during high wind speeds is based on measurements, the wind drag parameterization according to [Wu \(1982\)](#) is based on extrapolation of values of C_D calculated at relatively low wind speeds.

The linear growth term A , which is basically used for initial wind growth, is modeled with the use of the formulation by [Cavaleri and Malanotte-Rizzoli \(1981\)](#).

$$A = \frac{1.5 \times 10^{-3}}{2\pi g^2} (U_* \max[0, \cos(\theta - \theta_w)])^4 H \quad (4.7)$$

θ_w is the wind direction, H is the filter and σ_{PM}^* is the peak.

SWAN provides two optional expression for the exponential wind growth. The first is due to [Komen et al. \(1984\)](#):

$$B = \max[0, 0.25 \frac{\rho_a}{\rho_w} (28 \frac{U_*}{c_{ph}} \cos(\theta - \theta_{wind}) - 1)] \sigma \quad (4.8)$$

The second expression is derived by [Janssen \(1989, 1991\)](#):

$$B = \beta \frac{\rho_a}{\rho_w} \left(\frac{U_*}{c_{ph}} \right)^2 \max[0, \cos(\theta - \theta_w)]^2 \sigma \quad (4.9)$$

with β is the Miles constant. The Miles constant is dependent on the non-dimensional critical height λ , according to the theory of [Janssen \(1991\)](#):

$$\beta = \begin{cases} \frac{1.2}{\kappa^2} \lambda \ln^4 \lambda, & \text{for } \lambda \leq 1 \\ 0, & \text{for } \lambda > 1 \end{cases} \quad (4.10)$$

where:

$$\lambda = \frac{gz_e}{c_{ph}^2} e^r \quad (4.11)$$

and

$$r = \frac{\kappa C}{U_* \cos(\theta - \theta_w)} \quad (4.12)$$

where κ is the Von Kármán constant and z_e is the effective surface roughness. The wind profile is given by:

$$U(z) = \frac{U_*}{\kappa} \ln \left(\frac{z + z_e - z_0}{z_e} \right) \quad (4.13)$$

The effective roughness length is:

$$z_e = \frac{z_0}{\sqrt{1 - \frac{|\vec{\tau}_w|}{|\vec{\tau}|}}} \quad (4.14)$$

and the total roughness length is respectively given by:

$$z_0 = \hat{\alpha} \frac{U_*^2}{g} \quad (4.15)$$

where the total surface stress $\vec{\tau}$ is:

$$\vec{\tau} = \rho_a |\vec{U}_*| \vec{U}_* \quad (4.16)$$

The wave stress $\vec{\tau}_w$ is given by:

$$\vec{\tau}_w = \rho_w \int_0^{2\pi} \int_0^\infty \sigma B E(\sigma, \theta) \frac{\vec{k}}{k} d\sigma d\theta \quad (4.17)$$

4.2.3 Bottom friction

Bottom friction in SWAN is modeled with the use of (4.18):

$$S_{bfr}(\sigma, \theta) = -\frac{C_{bfr}}{g} \left[\frac{\sigma}{\sinh(kd)} \right]^2 E(\sigma, \theta) \quad (4.18)$$

C_{bfr} is the bottom friction coefficient. The bottom friction C_{bfr} depends on the root-mean-square orbital velocity at the bottom $u_{rms,bottom}$:

$$u_{rms,bottom} = \left(\int_0^{2\pi} \int_0^\infty \frac{\sigma^2}{\sinh^2 kd} E(\sigma, \theta) d\sigma d\theta \right)^{1/2} \quad (4.19)$$

SWAN provides three options to calculate the bottom friction coefficient, which is the bottom friction coefficient according to JONSWAP, Collins or Madsen.

[Hasselmann et al. \(1973\)](#) suggested the value of $C_{bfr} = C_{JONSWAP} = 0.038$ for swell waves. Later [Bouws and Komen \(1983\)](#) suggested $C_{bfr} = C_{JONSWAP} = 0.067$ for wind-sea conditions on sandy bottoms, which is the default value in SWAN. [Zijlema et al. \(2012\)](#) had reasons to believe that the value $C_{bfr} = C_{JONSWAP} = 0.067$ by [Bouws and Komen \(1983\)](#) was too high and after reevaluation of that the value $C_{bfr} = C_{JONSWAP} = 0.038$ should also be used for wind-sea conditions.

$$C_{bfr} = C_f g u_{rms,bottom} \quad (4.20)$$

Collins (1972) suggests a different formulation of the bottom friction coefficient. He states the bottom friction coefficient in (4.18) is the product of a another friction coefficient C_f , g and the root-mean-square velocity $u_{rms,bottom}$ at the bottom, as in (4.20). A value of $C_f = 0.015$ is suggested by *Collins (1972)* and used as default value in SWAN.

$$C_{bfr} = C_{madsen} = \frac{f_w}{\sqrt{2}} u_{rms,bottom} \quad (4.21)$$

Madsen et al. (1988) is the third option for bottom friction in SWAN. Madsen suggests that C_{bfr} is a function of a coefficient f_w times the $u_{rms,bottom}$, divided by $\sqrt{2}$. The value of f_w depends on the ratio a_b/k_n , as in

$$f_w = 0.30 \quad \text{for } a_b/k_n < 1.57 \quad (4.22)$$

$$\frac{1}{4\sqrt{f_w}} + \log_{10} \left(\frac{1}{4\sqrt{f_w}} \right) = m_f + \log_{10} \left(\frac{a_b}{k_n} \right) \quad \text{for } a_b/k_n \geq 1.57 \quad (4.23)$$

4.2.4 Depth-induced wave breaking

The bore-based model by (*Battjes and Janssen, 1978*) is the default parameterization used in SWAN. The source term S_{br} is given by:

$$S_{br}(\sigma, \theta) = \frac{D_{tot}}{E_{tot}} E(\sigma, \theta) = -\frac{\alpha_{BJ} Q_b \tilde{\sigma}}{\beta^2 \pi} E(\sigma, \theta) \quad (4.24)$$

where H_{max} is the maximum wave height with a given depth: $H_{max} = \gamma d$. The breaker parameter γ has a default value of 0.73 and d is the depth. D_{tot} is the mean rate of energy dissipation per unit horizontal area due to depth-induced wave breaking and is expressed as:

$$D_{tot} = -\frac{1}{4} \alpha_{BJ} Q_b \left(\frac{\tilde{\sigma}}{2\pi} \right) H_{max}^2 = -\alpha_{BJ} Q_b \tilde{\sigma} \frac{H_{max}^2}{8\pi} \quad (4.25)$$

where the proportionality factor α_{BJ} has a default value of 1 in SWAN. The mean relative angular frequency $\tilde{\sigma}$ is given by:

$$\tilde{\sigma} = E_{tot}^{-1} \int_0^{2\pi} \int_0^{\infty} \sigma E(\sigma, \theta) d\sigma d\theta \quad (4.26)$$

and the fraction of depth-induced breakers Q_b is determined with:

$$Q_b = \begin{cases} 0 & \text{for } \beta \leq 0.2 \\ Q_0 - \beta^2 \frac{Q_0 - \exp(Q_0 - 1)/\beta^2}{\beta^2 - \exp(Q_0 - 1)/\beta^2} & \text{for } 0.2 < \beta < 1 \\ 1 & \text{for } \beta \geq 1 \end{cases} \quad (4.27)$$

The nkd-scaling parameterization (*Salmon et al., 2013*) is mentioned in the literature study as a promising new parameterization breaker parameter γ . The nkd-scaling parameterization is also

referred to as the βkd -scaling parameterization, but in this study the parameterization will be called the nkd -scaling parameterization. The nkd -scaling parameterization is given by:

$$\gamma_{nkd} = \gamma_{\beta-kd} = \gamma_1(\beta) / \tanh \left[\gamma_1(\beta) / \gamma_2(\tilde{k}d) \right] \quad (4.28)$$

The breaker parameter γ_{nkd} is dependent on a breaker parameter that represents the dependency on the bottom slope: $\gamma_1(\beta)$, and on a breaker parameter that represents the normalized wave number: $\gamma_2(\tilde{k}d)$. The formulation of the breaker parameter dependent on the bottom slope is:

$$\gamma_1(\beta) = \gamma_0 + a_1 \tan \beta \geq 0 \quad (4.29)$$

and the formulation of the breaker parameter dependent on the normalized wave number is:

$$\gamma_2(\tilde{k}d) = a_2 + a_3 \tilde{k}d \geq 0 \quad (4.30)$$

where γ_0 , a_1 , a_2 and a_3 are tunable coefficients. The characteristic wave number \tilde{k} is given by:

$$\tilde{k} = k_{-1/2} = \left[\int \int k^{1/2} E(\sigma, \theta) d\sigma d\theta / E \right]^{-2} \quad (4.31)$$

This lower order wave number is chosen, because it is not as sensitive for the presence of multiple peaks in the density spectrum or the the exact shape of the spectral tail, which appears not be accounted for entirely correct in all cases in 3_{rd} generation wave models.

The parameterization scales the dependency on both the bottom slope and the normalized wave number. The normalized wave number becomes less relevant in increasingly shallow water, which is represented in the formula by the hyperbolic tangent, which provides a smooth transition between both the breaker parameters γ_1 and γ_2 .

To not over-estimate the effect of very steep bottom slopes, a maximum bottom slope of $\beta = 1/10$ is imposed.

Chapter 5

Conclusion Literature Survey

The literature survey exists of a literature study, a description of the wave model SWAN and a description of the circulation models Delft3D-FLOW, ADCIRC, FVCOM, POLCOMS, POM and ROMS.

The two-way coupled system is an extremely difficult system to fully understand. Both the circulation model and the wave model need input from the opposite model. The water level and current calculated in the circulation model are determined by solving the shallow water equations, which exist of a lot of driving forces that all have their contribution to the final answer. Several studies demonstrated that adding the gradient of the radiation stress to the shallow water equations has a significant contribution to the calculated water level. The radiation stress is dependent on the total wave energy. Wind adds energy to waves, while bottom friction, depth-induced wave breaking and whitecapping dissipate wave energy. Bottom friction is dependent on the velocity at the bottom, which is calculated from the with linear wave theory.

Concisely, the goal formulated of the literature survey was to improve the understanding of the two-way coupled model and to determine at which subjects there still is a lot of progress to be made. In the literature study it was already mentioned that the relative importance of certain physical processes is strongly dependent on the location of the model and the size of the model. This is especially true for the driving forces of the system. The beneath presented list therefore does not include this conclusion, but elaborates on parameterizations and correct representation of the physics of which is not known what the effect is in a two-way coupled system. The most important subjects that need better understanding are summarized here:

1. During the last decade several attempts to derive a 3D formulation of the radiation stress (*Longuet-Higgins and Stewart, 1960*) in circulation models. Though a 3D formulation of the radiation stress would probably agree better with reality, it is demonstrated that errors occur due to the 3D formulation and a correct 3D formulation still has not been found. Even though these errors have been demonstrated, there are circulation models that still use a 3D formulation, which makes it difficult to decide whether the 3D formulation has advantages over the 2D formulation of the radiation stress and the error is taken for granted.
2. Recent research demonstrated that the wind drag used to determine the transfer of energy from the wind to waves decreases at high wind speeds, in contrary to what was assumed before: an increase of the wind drag at high wind speeds. A coefficient that is used in a quadratic law to determine the bottom friction was determined with a relatively high wind

drag at higher wind speeds. Reevaluation of the observations led to a decreased coefficient. The precise impact of this adjustment for the coupled system is unknown, especially at higher wind speeds. The existence of a relation between the wind drag in the circulation model and the wind drag in the wave model is proposed, but is generally ignored.

3. The exchange of information between the circulation model and the wave model happens at an adjustable interval: the coupling interval. The interval usually is a compromise between computational time and the temporal variance of the interacting processes. A guidance to which extent the limits of this interval reach, with respect to the temporal variance of the interacting processes, does not exist.
4. The bottom stress formulation in most circulation models is enhanced when the model is coupled with a wave model. The enhanced bottom stress formulation is a function of both the independent bottom stress due to waves and the bottom stress due to currents. A significant difference in bottom stress could occur when the choice has to be made to include or not include the effect of wave bottom stress into the circulation model.
5. Depth-induced wave breaking has a direct impact on the radiation stress, which implies that the choice of the depth-induced wave breaking parameterization could have a significant effect on the results of a model. Still, the *Battjes and Janssen (1978)*-formulation is widely applied. Recent research has led to the derivation of other promising parameterizations.
6. Delft3D-FLOW is the only model that gives the opportunity to use the dissipation rate (*Dingemans et al., 1987*) as a replacement for the radiation stress. The dissipation rate is associated with wave energy dissipation, which is assumed to be the part of the radiation stress that causes fluctuations in total radiation stress. The dissipation rate would lead to better results, as the gradient of the radiation stress could lead to spurious currents. *Alkyon (2009)* shows that model results improve in comparison with measurements, when using the radiation stress, instead of the dissipation rate. An explanation has not been found yet.

The above presented list of conclusions on what subjects still need further understanding will be a guidance in Chapter 6 of this study.

Chapter 6

Introduction numerical modeling

6.1 Introduction

Chapter 5 presents a list of conclusions that lack common understanding and need to be investigated to increase knowledge on the two-way coupled system that models the effect of wave-current interaction. This chapter will provide how these conclusion are used in the resulting part of this study and explains why choices are made. The goals formulated in Chapter 1 are rephrased here:

- To improve the understanding of a two-way coupled system
- To increase the knowledge on the reliability of the result of the two-way coupled system
- To identify the largest sources of uncertainty
- To advise on the direction on further improvement of the two-way coupled system

6.2 Numerical modeling

6.2.1 Introduction

The first goal of this study is to improve the understanding of the two-way coupled system used to model wave-current interaction. The second goal is to increase the knowledge on the reliability of the result of the two-way coupled system. A first step has been made in the literature survey by identifying the subjects that still need further understanding. These subjects are presented in Chapter 5. To improve the understanding and to increase knowledge on the reliability of the result of the two-way coupled model the above presented hypotheses will be investigated by using numerical models. It is believed that the best way to improve the understanding and knowledge can be obtained by using both field cases as schematized cases. The advantage of using a field case compared with a schematic case is that the use of a field case provides more insight in the relative importance of an effect for engineering practice, while the advantage of a schematic case is that the influence of a certain effect can better be isolated.

6.2.2 Delft3D-FLOW - SWAN model

The research questions that are formulated beneath will be investigated with the circulation model Delft3D-FLOW, coupled with the wave model SWAN. The choice of this models is based on the fact that they have proven in the past they are able to produce accurate results. Another important factor is that the topics that will be investigated can be investigated with both models. Though especially many other circulation models exist, as discussed in Chapter 3, that also could have been used, no obvious preference existed. To verify whether a two-way coupled model existing of Delft3D-FLOW and SWAN can model wave-current interaction appropriately, an idealized case is used where the result of the model is compared with the result of an analytical solution.

6.2.3 Demand on locations

The first and most important demand is that wave-current interaction should be a process that is both present and important at the chosen location. The second demand is measurements should be available to compare with the model results. This ensures that observations on whether an aspect is an improvement can be supported by better representation of reality.

6.2.4 Eastern Wadden Sea

Alkyon (2009) performed a hindcast of a storm at the Eastern Wadden Sea. The predicted water levels appeared to compare significantly better with measurements after including wave forcing, which proves that wave current interaction is important at this location. Thereby wave and water level measurements are available to compare with the computed results, which makes it possible to make a quantitative comparison. The eastern Wadden Sea is known for its complex bathymetry, which exists of many channels and flats. This complex bathymetry makes it hard to identify the processes that are responsible for possible computed differences when varying the coupling interval. To increase the understanding of the behavior of the two-way coupled models, first a schematized situation is used. The solution of the two-way coupled model will be compared with an analytical solution.

6.3 Choice of subjects

Due to lack of time, not all of the conclusions formulated in the previous chapter are investigated in this study. The consequence is that choices have to be made on which conclusions are investigated and in which direction the resulting part of this study will continue.

The comprehensive conclusions in Chapter 5 are numbered and the same order is followed here to provide a brief description of the conclusions.

1. The use of the 3D formulation of the radiation stress versus the 2D formulation of the radiation stress while the incorrectness of the 3D formulation is demonstrated.
2. Recent study showed that the wind drag decreases at higher wind speeds, in contrary to previously assumed to be true wind drag formulations where the wind drag increases during high wind speeds.

3. A guidance on the length of the coupling interval with respect to the temporal variance of the interacting processes does not exist.
4. The effect of the use of an enhanced bottom stress formulation to account for waves in the circulation model is not known.
5. Depth-induced wave breaking has a significant impact on the radiation stress. Recent studies provided new parameterizations of the depth-induced wave breaking. The effect on the radiation stress is unknown.
6. To model the excess flux of momentum by waves the radiation stress and the dissipation rate can be used in Delft3D-FLOW. It is claimed the dissipation rate leads to better results, because the radiation stress could lead to spurious results. To which extent this holds is unknown.

The 3D formulation of the radiation stress is investigated extensively last decade by numerous scientists world wide. Assuming the demonstrated errors in the formulation are correct and the provided solution to use the 2D formulation of the radiation stress, which has proven to be able to generate good results, does not urge to investigate this topic in this study.

Currently it is not exactly known where the coupling interval should be based on. A first demand would be that it should be able to represent the temporal variability of the interacting quantities (i.e. radiation stress, water level, current). A first estimate would be that the temporal variability of the interacting processes is dependent on the forcing of the system (i.e. wind field, boundary conditions), but to which extent and whether or not there are other processes that influence the quality of the result is unknown. The choice of the coupling interval will be further investigated in this study.

Recent studies show that the wind drag decreases at high wind speeds in contrary to the previously assumed increase of wind drag during high wind speeds. The effect of this implication on wave-current interaction is not known at higher wind speeds, while knowledge on the effect is important. Studies that use the two-way coupled model at locations where extensive calibration and validation during high wind speeds is not possible, do want to know the magnitude of the possible error of the model.

Depth-induced wave breaking is a process that has a reasonable share in dissipation in the coastal region, which has its share in gradients of the radiation stress. A new parameterization called the nkd-scale model parameterization shows promising results. The effect of a different depth-induced wave breaking parameter could influence the system, as it causes forces to be different.

6.4 Research questions

To investigate the above sketched uncertainties, research questions have been formulated. The topics mentioned are investigated in a particular order, which is not arbitrarily.

6.4.1 Coupling interval

The coupling interval should be chosen in a way that both the circulation model and the wave model receive information at such a rate that the computations are still accurate. The circulation

model is dependent on the wave force, while the wave model is dependent on the water level and current from the circulation model. Thereby changes in wind can play an important role, as water level, currents and wave growth are dependent on the wind. At this moment, it is not known what the effect is of the applied coupling interval on the accuracy of the model. This leads to the following research questions:

1. What is the effect of the applied coupling interval on the accuracy of the computed water level and wave conditions under storm conditions?
2. What are the dominant processes regarding the coupling interval?
3. What are the limits of the coupling interval to which the accuracy of the model is preserved?

6.4.2 Wind drag

Recently, studies show that the wind drag parameterization in wave models is significantly different from what was believed in the past. At high wind speeds, the transfer of wind energy is less than earlier believed. This not only has an effect on the computed wave conditions, but also on the total set-up. The following research questions are formulated:

1. What is the effect on total set-up of the fit wind drag parameterization compared with the conventional wind drag parameterization by *Wu (1982)* during high wind speeds?
2. At which wind speed differences between fit and *Wu (1982)* become significant?

6.4.3 Depth-induced wave breaking

As concluded in Chapter 5, a new parameterizations of depth-induced wave breaking is recently developed. This new parameterization, from now on referred to as the nkd (or beta-kd) -scaling model, shows significant reductions of computed errors for cases with horizontal bathymetries. When locally generated wave conditions are dominant, the significant wave height is typically underestimated, while when non-locally generated wave conditions are dominant, the significant wave height is typically over-estimated. The validation of the nkd-scaling model shows improvements in computed wave conditions in both cases. The nkd-scaling model is dependent on normalized wave number and local bottom slope, which is dependent on mean wave direction. Thereby the directional wave spreading in 2D cases appeared to have a significant influence on the significant wave height, which resulted in partitioning of the breaker index by directional wave spreading. The nkd-scaling model shows in some cases an improved prediction compared with computation with scaling according to *Battjes and Janssen (1978)* and *Ruessink et al. (2003)*, while in other cases the error increases when using the nkd-scaling model, which results in neither an improvement nor a deterioration on average.

In coastal zones, the dissipation due to depth-induced wave breaking is apparent to be the dominant dissipation process. The nkd-scaling model is likely to cause dissipation, and related radiation stress gradients, to occur at different location than when the Battjes & Janssen model is used. It is not known what the effect is on the two-way coupled model. Answering the following research question have to contribute to a better understanding of the role of depth-induced wave breaking on the two-way coupled model:

1. What is the effect of the nkd-scaling model on the magnitude and location of the wave force and subsequently on the water level and currents?

Chapter 7

Idealized case

7.1 Introduction

The coupling interval is investigated with the use of an idealized case and a field case. The idealized case investigates the influence of the coupling interval on the performance of the two-way coupled model with respect to an analytical solution. A quantitative comparison between the model results and the analytical solution will provide the necessary insight in the behavior of the two-way coupled model, which is required to analyze the influence of the coupling interval on the performance of the model during the field case. Discrepancies will be analyzed and an attempt will be made to provide a possible explanation.

The analytical solution as provided in Subsection 7.2.1 covers a 1D cross-shore solution with normally incident waves entering a uniform coast. The normally incident waves entering the uniform coast do not vary in time, which yields a stationary situation. Since the two-way coupled system is not a 1D-model, the model is set-up in a way that the solution only varies in cross-shore direction and that variations in alongshore direction are limited to the absolute minimum at the location of interest.

7.2 Method

7.2.1 Analytical solution

To compare the analytical solution with the model results, both calculations should be based on the same physical processes. Equation 7.1 describes the equilibrium between the radiation stress gradient and pressure term due to the water level gradient. Variation in radiation stress in the alongshore direction is neglected. Therefore the wave force F_x only exists of a the radiation stress gradient $-\partial S_{xx}/\partial x$ in the x -direction. The radiation stress gradient is dependent on the dissipation of energy. Outside the surf zone energy dissipation due to depth-induced wave breaking is less than the increase of energy due to shoaling, which results in a positive radiation stress gradient, yielding a negative water level gradient. Inside the surf zone the radiation stress gradient is negative (energy dissipation due to depth-induced wave breaking is larger than the increase in energy due to shoaling), which results in a positive water level gradient. To keep the solution simple and

understandable, other processes responsible for wave energy dissipation, such as bottom friction and whitecapping are neglected. For the same reason wave-wave interactions and input of wave energy due to wind are left out of the equation. This does not introduce any problems, because the interest is in the response of the two-way coupled system, and not in modeling all physical processes correctly.

$$F_x = -\frac{\partial S_{xx}}{\partial x} = \rho g h \frac{\partial \bar{\eta}}{\partial x} = \rho g (h_0 + \bar{\eta}) \frac{\partial \bar{\eta}}{\partial x} \quad (7.1)$$

The solution is stationary, what makes the balance between wave energy (E) and dissipation due to depth-induced wave breaking (D_w) can be solved with the use of Equation 7.2.

$$\frac{\partial E c_g \cos \theta}{\partial x} = -D_w \quad (7.2)$$

where c_g is the wave group speed. For normally incident waves ($\theta = 0$) entering a uniform coast, the equation reduces to:

$$\frac{\partial E c_g}{\partial x} = -D_w \quad (7.3)$$

To compare both solutions, dissipation due to depth-induced wave breaking has to be determined equally in both solutions. The solution provided in SWAN by *Battjes and Janssen (1978)* is chosen to implement in the analytical solution:

$$D_w = \alpha_{BJ} * Q_b * \frac{H_{max}^2}{8\pi} \quad (7.4)$$

where $\alpha_{BJ} = 1$, the fraction of breaking waves Q_b (which is dependent on the ratio H_{rms}/H_{max}) and the maximum wave height at a given depth $H_{max} = \gamma * h$. The wave breaking index γ is 0.73. In order to calculate the wave force, first the radiation stress had to be calculated, which is dependent on the water depth.

The analytical solution is calculated with the use of Matlab. The scripts used to calculate are presented in Appendix A. The solution is found with the use of an iterative procedure. The iterative procedure stops when the maximum difference between the result of the last and the penultimate calculation is smaller than $1 \times 10^{-15} m$. This condition is met after 11 iterations. At the same time, the wave force F_x is calculated.

7.3 Model set-up

7.3.1 Grid and bathymetry

The analytical solution requires that the bathymetry exists of a uniform slope. The solution is only valid when there is no variation in alongshore direction, which requires that this is similar in the simulation. To ensure that the variation in alongshore direction is negligible, the distance in alongshore direction is chosen to be four times as large compared with the distance in cross-shore

direction and magnitudes larger compared with depth and magnitude of the setup. The uniform slope is based on the average slope at the Eastern Wadden Sea. The depth decreases from roughly 20 m offshore to almost 0 m over a distance of 20 km , which yields an average slope of 1 : 1000. This slope is chosen to be the slope of the bathymetry. The depth at the boundary has to be chosen in such a way that there is no wave energy dissipation due to depth-induced wave breaking. With the above presented parameterization of depth-induced wave breaking, the first waves start to break at a depth between 35 and 40 m . To create some space between the location of waves starting to break and the boundary, the depth at the offshore boundary is chosen to be 50 m . Given the uniform slope, this makes that the grid covers an area of 50 \times 200 km . The computational grid exists 250 \times 1000 grid cells. The grid cells are equidistant in both m - and n -direction, with a distance of 200 m in both the m -direction and n -direction. The bathymetry is shown in Figure 7.1.

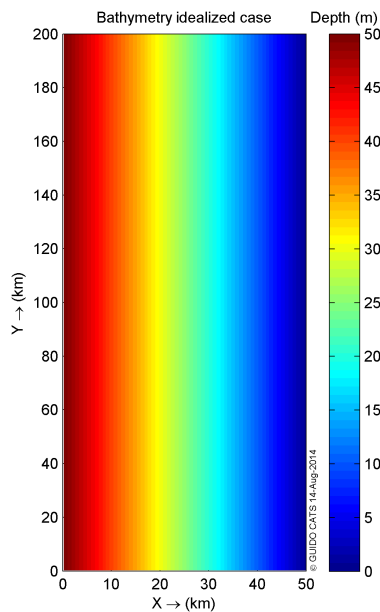


Figure 7.1: Bathymetry idealized case

7.3.2 Model set-up Delft3D-FLOW

The initial water level is 0 m at the entire domain. The seaward boundary in the cross-shore direction is uniform in alongshore direction. A water level of 0 m is imposed at this boundary. Because the first waves start to break at a considerable distance from this boundary, it is assumed that the radiation stress gradient is small and the absence of setup or set-down is justified. After a considerable amount of attempts, the following boundary conditions appeared to give the best result. A Neumann boundary condition is used at the alongshore boundaries. With a Neumann boundary condition the water level gradient is imposed, which is in this case 0 at both alongshore boundaries.

A Chézy coefficient of 100 $m^{1/2}s^{-1}$ is used, which ensures that the influence of the bottom friction is relatively small. The small influence of bottom friction is necessary because of the absence of bottom friction in the analytical solution. The water density is set at $\rho_w = 1023 \text{ kgm}^{-3}$, which is similar to the water density at the Wadden Sea. Observations points are located in the cross-shore

direction at the center of the domain, which is the cross-section where the analytical solution is compared with the model results.

7.3.3 Model set-up SWAN

The water level, currents and bathymetry are provided by Delft3D-FLOW. There is no wind used during the simulation and the bathymetry does not evolve during the simulation. At the northern boundary waves enter the domain. The direction of the wave is perpendicular to the coast and the directional spreading is defined as the power m , which is a way to define the directional spreading in SWAN. The directional spreading should be accommodated by the spectral resolution, which is 10^0 in this computation. The directional spreading can therefore not be less than 10^0 , which is the value used at the wave boundary ($m=30$ is equal to a directional spreading of 10.2^0). The only physical process that is included in the computation is depth-induced wave breaking. The wave breaking index $\gamma = 0.73$ and $\alpha_{BJ} = 1$. Wave-wave interactions, bottom friction, whitecapping, refraction and frequency shift are turned off. The accuracy criteria have been sharpened from the default values to a maximum relative change between $H_{m0} - T_{m01} : 0.002$, a relative change with respect to mean value of $H_{m0} : 0.002$ and $T_{m01} : 0.002$ at 99.8% of the wet grid points. The maximum number of iterations is increased from the default number of 15 to 80. These numerical accuracy criteria have been sharpened with the reason to avoid spurious effects due to numerical inaccuracy.

The wave height and mean wave period T_{m01} that enter the domain have its origin at the wave boundary conditions that are used in [Alkyon \(2009\)](#). The wave boundary conditions were obtained from wave buoys measurements at Schiermonnikoog Noord and Westereems West. During the storm the highest significant wave heights measured were in the order of 8 m , with an associated mean wave period in the order of 11 s .

7.4 Results

The water level computed with the two-way coupled system Delft3D-FLOW - SWAN and the water level according to the analytical solution are shown in the left figure of Figure 7.2 and the wave force in the cross-shore direction, F_x , is shown in the right figure. The wave force in the cross-shore direction shows that F_x is a little bit larger in case of Delft3D-FLOW. The initial water level of 0 m combined with the wave forcing at the start of the run caused a shock in water movement. The water level computed by the two-way coupled model shows large oscillations at the start of the run until an equilibrium situation will be reached. Though the amplitude of the oscillation decreases, it does not become constant during the simulated period of two days and the water level keeps varying both at shoreline and at the location of maximum set-down. The water level has a sinusoidal shape with a period of approximately 4 hours (Figure 7.3).

To make a comparison between the water level computed and the analytical solution, the mean water level during the second day is taken. From the figures in Figure 7.3 it can be obtained that the water level oscillates around a fairly constant water level. This resulted in the presented line Figure 7.2. The root-mean-square error between the averaged water level and the analytical solution is 0.01 m , while the largest differences are located near shore. The location of maximum set-down computed by the model is located 1.1 km closer to shore, while the difference in water level is very small (0.003 m).

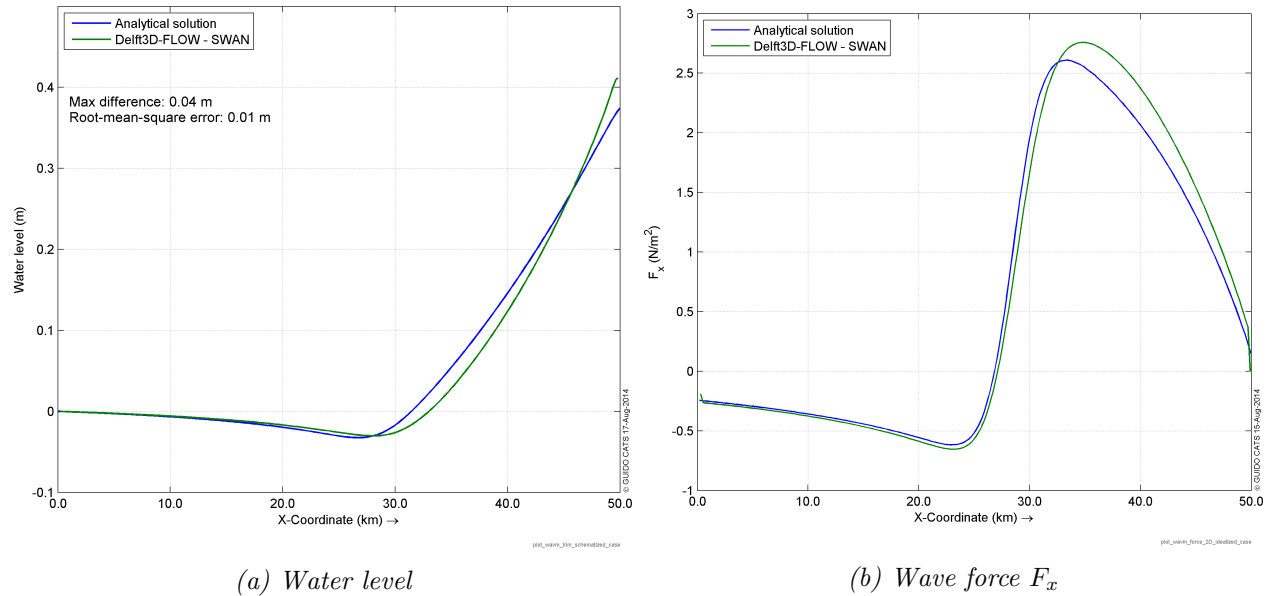


Figure 7.2: Cross-shore comparison between analytical solution and two-way coupled Delft3D-FLOW - SWAN model

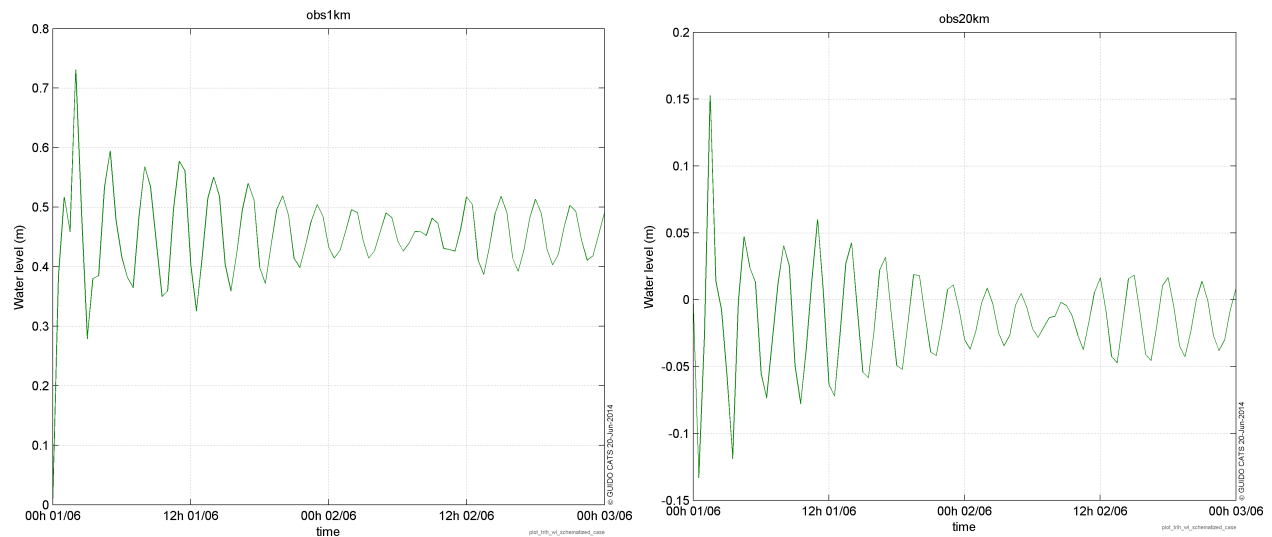


Figure 7.3: Water level and water level differences at 9 November 2007 12:00 hours

7.5 Analysis

The set-up of this model had the goal to diminish alongshore gradients as much as possible, as these are not accounted for in the analytical solution. The set-up of the model as described in Section 7.3.3 showed rather good results compared with grids of which the ratio between the cross-shore distance and alongshore distance was larger. At the center of the domain all variables only vary in the cross-shore direction.

Variations in coupling interval appeared not to have any influence. The computed wave forces hardly varied in time. An explanation lies in the fact that the influence of the variation of the

water level is limited with respect to depth-induced wave breaking. The largest fluctuations in water level occur near the shore line. The wave force is directed shore-wards from a depth of approximately 25 *m*, with its maximum at a depth of approximately 12 *m*.

The mean wave direction is directed to shore in the interest area (the center of the domain). The mean wave direction and directional spreading in the domain decreases when entering shallower water. This is not the case at areas adjacent to the alongshore boundaries. At the seaward boundary, the wave energy enters the domain with a mean wave direction pointed to shore. Due to directional spreading not all waves propagate in the mean wave direction, but propagate in an angle relative to the mean wave direction. At locations not adjacent to the alongshore boundaries, these waves come with the same amount from both the eastern- and the western direction, which ensures that the mean wave direction remains constant. At locations near the alongshore boundaries there are no waves coming from the alongshore boundary, so the mean wave direction turns towards the alongshore boundaries. This effect could be limited by limiting the directional spreading to a minimum.

The not perpendicular to the coast mean wave direction adjacent to the alongshore boundaries causes that the wave force has an alongshore component. This alongshore component causes (small) currents in the alongshore direction, and during some periods of the simulation little gyres appear at both ends. The effect on the solution presented above is limited, because the boundaries are chosen far away enough from the center of the domain to have effect.

7.6 Conclusion

The purpose of this simulation was to assess whether the two-way coupled model consisting of Delft3D-FLOW and SWAN is able to reproduce an analytical solution. As the analytical solution does not incorporate any other processes than depth-induced wave breaking, the settings in the model were adjusted to minimize the effect of other processes. It is obtained that the combination Delft3D-FLOW and SWAN is able to reproduce the analytical solution with sufficient accuracy to use both models with enough confidence further in this study.

Further, the idealized case can be used to investigate other effects in this study. In that case, the processes that are not taken into account in these reproduction of the analytical solution, will be accounted for.

Chapter 8

Coupling interval

8.1 Introduction

Now that the model has proven it can reproduce wave-current interaction with sufficient accuracy, the influence of the coupling interval on wave-current interaction is investigated with the use of the 9 november 2007 storm at the Eastern Wadden sea. The research questions as formulated in Chapter 6 are rephrased:

1. What is the effect of the applied coupling interval on the accuracy of the computed water level and wave conditions under storm conditions?
2. What are the dominant processes regarding the coupling interval?
3. What are the limits of the coupling interval to which the accuracy of the model is preserved?

The Subsection 8.2 will explain in more detail the method how to derive answers to the formulated research questions. The model set-up will be extensively discussed before the results will be presented and analyzed.

8.2 Method

Wave-current interaction is a continues process. When modeling wave-current interaction, a coupling interval is introduced to transfer information from one model to the other. The coupling interval should be chosen in a way the information that is transferred, represents the temporal variability of the coupled quantities radiation stress, water level and current in a adequate way.

The temporal variability of the radiation stress is dependent on the energy density spectrum, which is dependent on the input by wind and dissipation of wave energy. The temporal variability of water level and currents is dependent on various processes including the tidal cycle, forcing due to radiation stress and forcing due to wind and pressure.

The wind and the wave boundaries of the model are based on data with an interval of 10 minutes (this will be discussed in the following subsection). The recorded wind velocity and direction are the momentarily measured values. During a storm, the variation in wind velocity and direction increases. The wave boundary conditions are given by a variance density spectrum, extended with

the average direction and directional spreading. The aim of a wave spectrum is to describe the sea surface as a stochastic process and not to describe in detail one observation of the sea surface. A wave spectrum usually represents a sea-state that covers a period of time of 15-30 minutes, which will ensure it is short enough to be stationary and long enough to have reasonably reliable averages [Holthuijsen \(2007, Chapter 3\)](#). The wave boundary conditions thus has a shorter interval than the value that it represents, which causes an overlap of data.

Both the wind conditions and the wave boundary conditions are based on data entries with a 10 minute interval. The wind speed and direction are interpolated linearly to the time step (6 s) in DELFT3D-FLOW, which is a commonly used technique. Decreasing the coupling interval will automatically lead to the use of the interpolated wind values in SWAN. At the same time, wave boundary conditions are demanded by SWAN, which also have to be obtained by interpolation. Among many possibilities, linear interpolation is chosen, which is assumed not to force the model with unrealistic values and strokes with the way the wind is interpolated.

Velocities can change rather rapidly in direction and magnitude due to wind and tidal effects. Waves are subjected to ambient current, and large velocity changes might lead to large force gradients. Decreasing the coupling interval provides a smoother transition in velocity change. On the other end, it might turn out that the coupling interval is already sufficient to represent the temporal variability of the coupled quantities and larger intervals will suffice too. This introduces an urge to know at which interval the model does not function any more and results become noticeably worse.

In [Alkyon \(2009\)](#) a hindcast was performed for the above mentioned storm. The coupling interval used during that study was based on the availability of the wave boundary conditions, i.e. 10 minutes. This investigation will use the 10 minute coupling interval as a reference to compare mutual changes. With the above remarks in mind, the coupling interval will be decreased to 5 minutes to investigate the importance of the change of ambient current and wave force. The effect of an increased coupling interval is investigated by increasing the coupling interval to 30 minutes, 60 minutes, 120 minutes, 180 minutes and 240 minutes. The intervals are chosen such that they are a multiple of 10 or that 10 is a multiple of the chosen interval. This will provide the opportunity to compare model results with both water level measurements as wave spectra measurements.

8.3 Model set-up Eastern Wadden Sea

8.3.1 Grid

The hydrodynamic grid is presented in Figure 8.1. The blue lines are the grid lines and the black lines is the land boundary. The number of visualized grid lines is reduced with a factor 3. Both Delft3D-FLOW and SWAN use the same grid.

8.3.2 Bathymetry

A combination of depth soundings in 2001, 2005 and 2006 and a bathymetry of the German area from 2005 are used to obtain the bathymetry. The most recent bathymetric information for each point is used. Where no information was available, bathymetric information from the Kuststrook

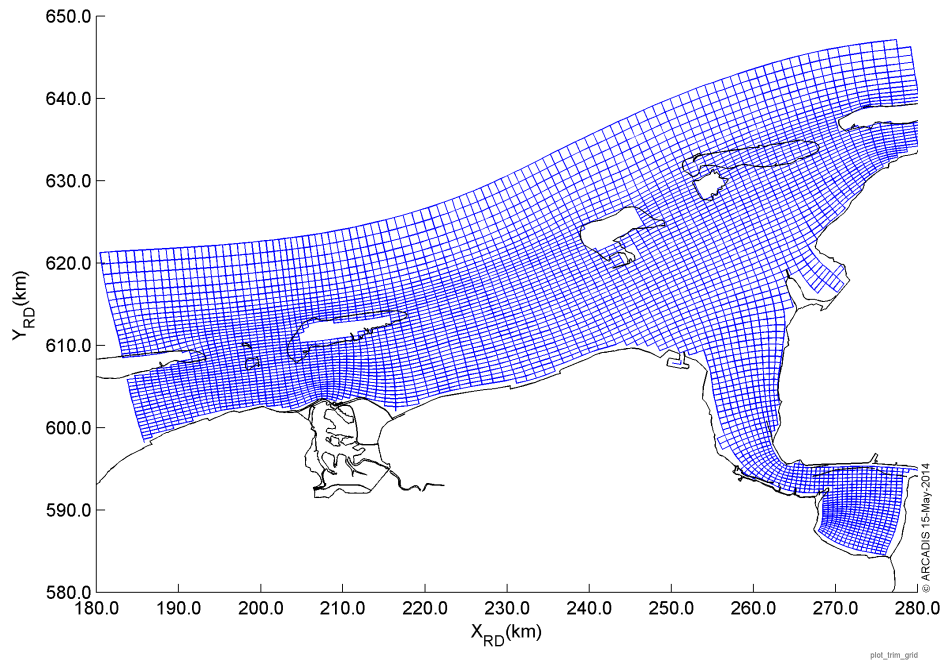


Figure 8.1: Computational grid Eastern Wadden Sea (thinned 3 times)

model was used. This resulted in the most up-to-date bathymetry possible at that time. There is no use to update the bathymetry for this study. The bathymetry is presented in Figure 8.2.

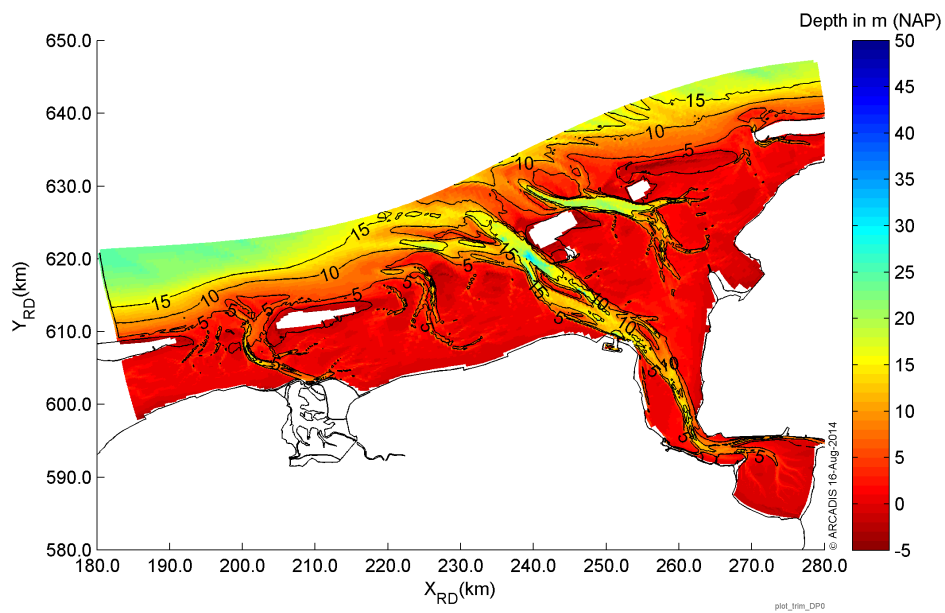


Figure 8.2: Bathymetry of the Eems-Dollard model with contour lines at depths of 5, 10 and 15 m

8.3.3 Delft3D-FLOW boundary conditions

The Eems-Dollard model has boundaries adjacent to the North Sea outside of the Wadden Sea and an open boundary at the west side of the domain, inside the Wadden Sea. In *Alkyon* (2009), the derivation of the boundary conditions is described. Riemann boundary conditions are applied at the boundaries adjacent to the North Sea. The Riemann boundary conditions were derived with the use of the larger models Kustgrof and Kustfijn. Optimal settings were applied for Kustgrof and Kustfijn.

8.3.4 Wave boundary conditions

The wave boundary conditions during the storm of November 2007 are based on measurements at the wave buoys Westereems West (WEW1) and Schiermonnikoog Noord (SON). The boundary outside the Wadden Sea is divided in three pieces: west, north and east. At the western boundary, wave boundary conditions bases on measurements from SON and at the eastern boundary the wave boundary conditions are based on measurements from WEW1. At the northern boundary, a combination of both measurement stations is applied. At both ends of the northern boundary wave boundaries based on the measurements are applied. Due to shallow conditions, wave boundary conditions were reduced at that location to 50% of the measured significant wave height at WEW1. To avoid large gradients in wave boundary conditions, at both sides of the reduced wave boundary conditions, the wave boundary conditions are linearly interpolated between towards the measured values.

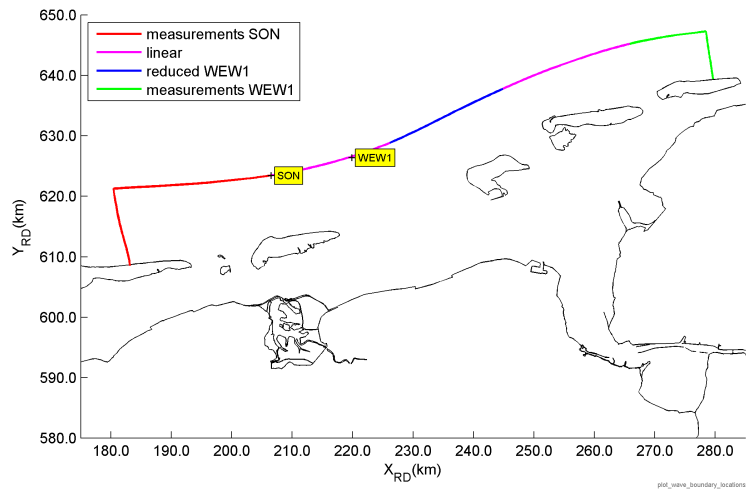


Figure 8.3: Orientation of wave boundary conditions

In Figure 8.4, the significant wave height H_{m0} and the spectral wave period T_{m01} are given. The red dots indicated with OND are the values at the shallow water boundary. The significant wave height is lowered with 50% during the storm based on the values at WEW1, while the spectral wave period of OND is equal to that at WEW1.

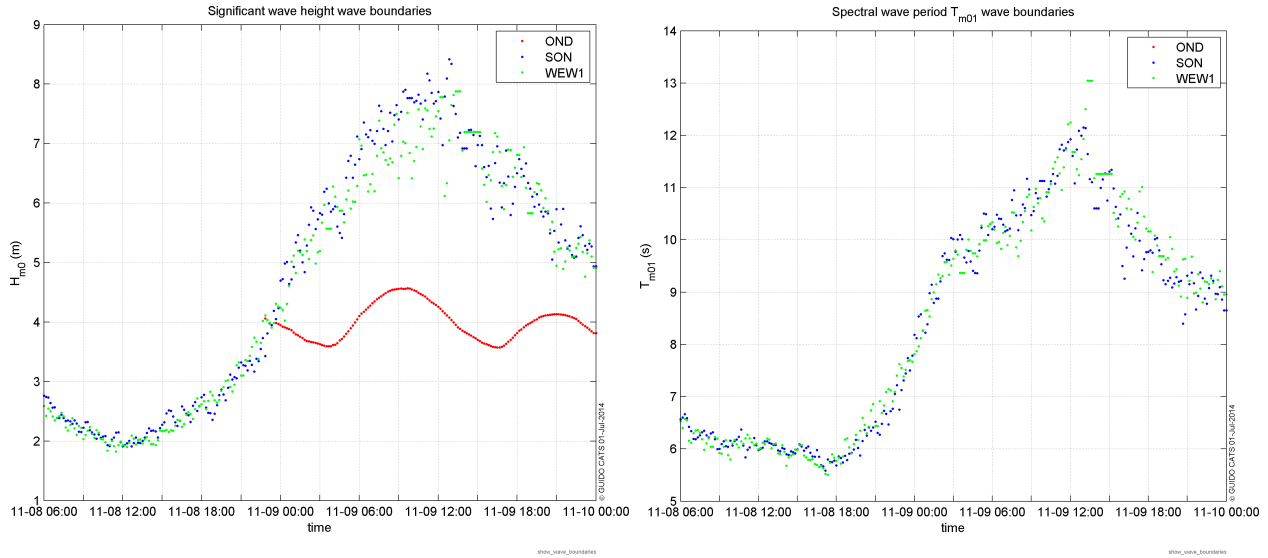


Figure 8.4: Significant wave height and spectral wave period T_{m01} at boundaries

8.3.5 Wind

In *Alkyon* (2009), HIRLAM wind fields are used for the models Kustgrof and Kuststrook model. Both the wind fields obtained with HIRLAM and measurements have been used as an input to the Eems-Dollard model. The computed outcome of the model is compared with measurements. The best results were achieved with the use of a spatial uniform wind field, based on the measurements at Huibertgat (Figure 8.5).

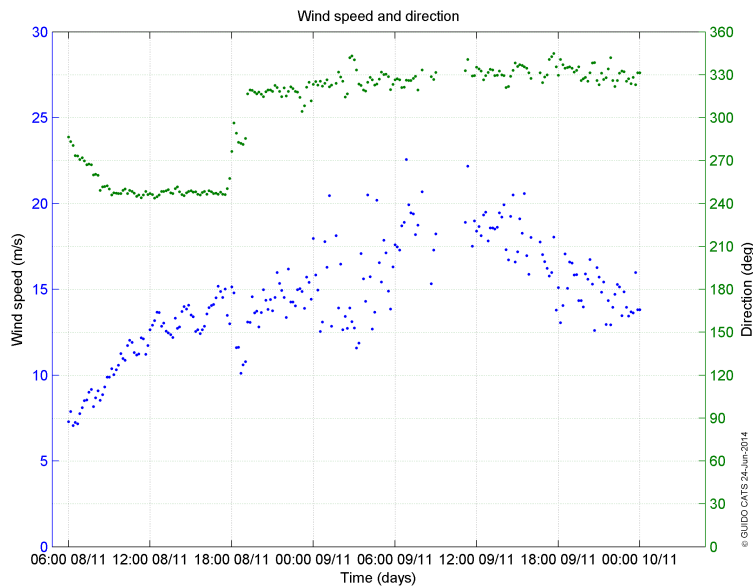


Figure 8.5: Wind speed and direction at Huibertgat

8.3.6 Model settings

Delft3D-FLOW

The wind drag parameterization in Delft3D-FLOW is a linear function that is fitted to the [Charnock \(1955\)](#) wind drag parameterization between 5 m/s and 25 m/s, which is based on the range of wind speeds during the simulation of the storm. Below 5 m/s and above 25 m/s the differences between [Charnock \(1955\)](#) wind drag parameterization and the parameterization in Delft3D-FLOW increase. Delft3D-FLOW provides the opportunity to specify the wind drag with the use of a piece-wise linear function with three break point: A, B and C. A linear dependency of wind drag C_d on wind speed U_{10} is specified at A: $C_d^A = 0.0008$ and $U_{10}^A = 0$ m/s, B: $C_d^B = 0.0092$ $U_{10}^B = 100$ m/s and C: $C_d^C = 0.0092$ $U_{10}^C = 100$ m/s.

$$C_d(U_{10}) = \begin{cases} C_d^A & \text{for } U_{10} \leq U_{10}^A \\ C_d^A + (C_d^B - C_d^A) \frac{U_{10} - U_{10}^A}{U_{10}^B - U_{10}^A} & \text{for } U_{10}^A \leq U_{10} \leq U_{10}^B \\ C_d^B + (C_d^C - C_d^B) \frac{U_{10} - U_{10}^B}{U_{10}^C - U_{10}^B} & \text{for } U_{10}^B \leq U_{10} \leq U_{10}^C \\ C_d^C & \text{for } U_{10}^C \leq U_{10} \end{cases} \quad (8.1)$$

The roughness formula of Manning is used for bottom roughness. The bottom roughness is spatially varying. At the North Sea the roughness is $0.022 \text{ m}^{-1/3}\text{s}$, at the Wadden Sea $0.021 \text{ m}^{-1/3}\text{s}$ decreasing in the Eems-Dollard estuary to $0.016 \text{ m}^{-1/3}\text{s}$ in the Eems river mouth. In the river Eems the bottom roughness decreases to $0.012 \text{ m}^{-1/3}\text{s}$ at Herbrum.

The viscosity has a uniform value of $10 \text{ m}^2/\text{s}$. Diffusivity has a spatially varying value with $30 \text{ m}^2/\text{s}$ at the North Sea and the Wadden Sea, increasing to $50 \text{ m}^2/\text{s}$ at the Eems-Dollard estuary. $400 \text{ m}^2/\text{s}$ at the river Eems mouth and $200 \text{ m}^2/\text{s}$ at the river Eems. The Dollard has a value of $100 \text{ m}^2/\text{s}$. The calibration of these settings was performed in [Alkyon \(2008\)](#).

The open source version Delft3D 2399 of the Delft3D suite is used in this study to examine the effects of the chosen subjects. Delft3D-FLOW is part of this suite.

SWAN settings

The model settings of SWAN are not changed compared with [Alkyon \(2009\)](#). Wave forcing is applied with the use of radiation stress. Depth-induced wave breaking is applied according to Battjes & Janssen with the default values for $\alpha = 1$ and $\gamma = 0.73$. Non-linear triad interactions are included according to [Eldeberky and Battjes \(1995\)](#), with $\alpha = 0.1$ and $\beta = 2.5$. Bottom friction is accounted for with the use of JONSWAP, with a value of $\chi = 0.067 \text{ m}^2 \text{ s}^{-3}$. Whitecapping is applied according to [Komen et al. \(1984\)](#). The processes wind growth, refraction and frequency shift are included in the simulation.

Numerical settings exist of the choice of the numerical solving schemes and the criterion of ending the wave computation at an requested accuracy. The default options provided by Delft3D-WAVE are applied, with exception of the accuracy criterion that sets the percentage of wet grid points where the set criteria have to be met. This criterion is raised from 98% to 99%. The SWAN

computations are performed in stationary mode. These settings are similar to the settings used in (Alkyon, 2009).

In this study SWAN version number 40.91 is used, which is different compared with SWAN version number 40.51 AB used in (Alkyon, 2009). SWAN version number 40.91 provides a number of options that were not available in SWAN version number 40.51 AB, such as the depth-induced wave breaking nkd-scaling parameterization, the *fit* wind drag parameterization according to Zijlema *et al.* (2012).

8.4 Results

The results of the computations will be compared with measurements and the performance of the model using different coupling intervals will be determined by comparing the computed values with measurements. Water level measurements were performed at different locations than the wave measurements. Unfortunately the current is not measured. The wave measurements have been converted to energy density spectra. From these spectra the significant wave height H_{m0} , the spectral wave period $T_{m-1,0}$, T_{m01} and T_{m02} , the mean wave direction DIR and the directional spreading $DSPR$ are derived. The results are assessed with the use of visual interpretation of the mentioned parameters at the entire model domain, as well as a statistical analysis of the runs with different coupling intervals.

8.4.1 Visual interpretation water level

The water level during the storm is influenced by the excess flux of momentum due to the presence of waves. This excess flux of momentum is represented by wave force in this simulation. Due to the use of different coupling intervals, the wave force exerted on the water differs for each of the coupling intervals used. The wave force causes set-up and set-down. The contribution of the wave force on the water level can be quantified by determining the set-up due to wave force. To determine the set-up due to waves, an extra simulation is performed where the forcing due to waves was not included. Subtraction from the computed water level including waves results in the set-up due to waves.

The storm starts at approximately 9 November 2007 00:00 hours. At this time, the set-up and set-down due to waves is limited, with a set-up between 0.1-0.2 *m* within the Wadden Sea interior and a set-down of a few centimeters at the ebb-tidal deltas. During the storm, the water level rises and at approximately 9 November 2007 09:00 hours high water is reached (Figure 8.6a). The set-up due to waves rose to approximately 0.3-0.4 *m* at the coast of Groningen and Friesland, while at the Eems-Dollard channel and at the coast of Germany the set-up is in the order of 0.1 *m*. The set-down has moved further towards the North Sea. After high water, the set-up increases even further inside of the Wadden Sea interior, with maxima of nearly 0.5 *m* off the coast of Groningen and Friesland (Figure 8.6b). It appears that the contribution of the wave set-up on the water level is dependent on the phase of the tide, where a correlation between set-up and water level is found. Figure 8.6c shows the computed and measured water level at Lauwersoog and the difference between the computed water level and the measured water level. Figure 8.6c shows the wave set-up. It can be obtained that the peaks of the set-up coincide with low water. An extra peak at 9 November 2007 at approximately 8:00 hours cannot be explained by coinciding with low water. A large gradient in the wave boundary condition is the most probable cause for this effect. The

mutual differences seem to be rather small, with exception of the computed wave set-up for the simulations with a 120 and 240 minute coupling interval. The largest wind speed is observed around 9 November 2007 12:00 hours, while the largest wave boundary conditions and the largest set-up at the whole domain is visually obtained at times around 9 November 2007 13:30 hours, which is approximately during the peak of the storm. After low water, the strength of the storm decreases and the wave set-up decreases along with it.

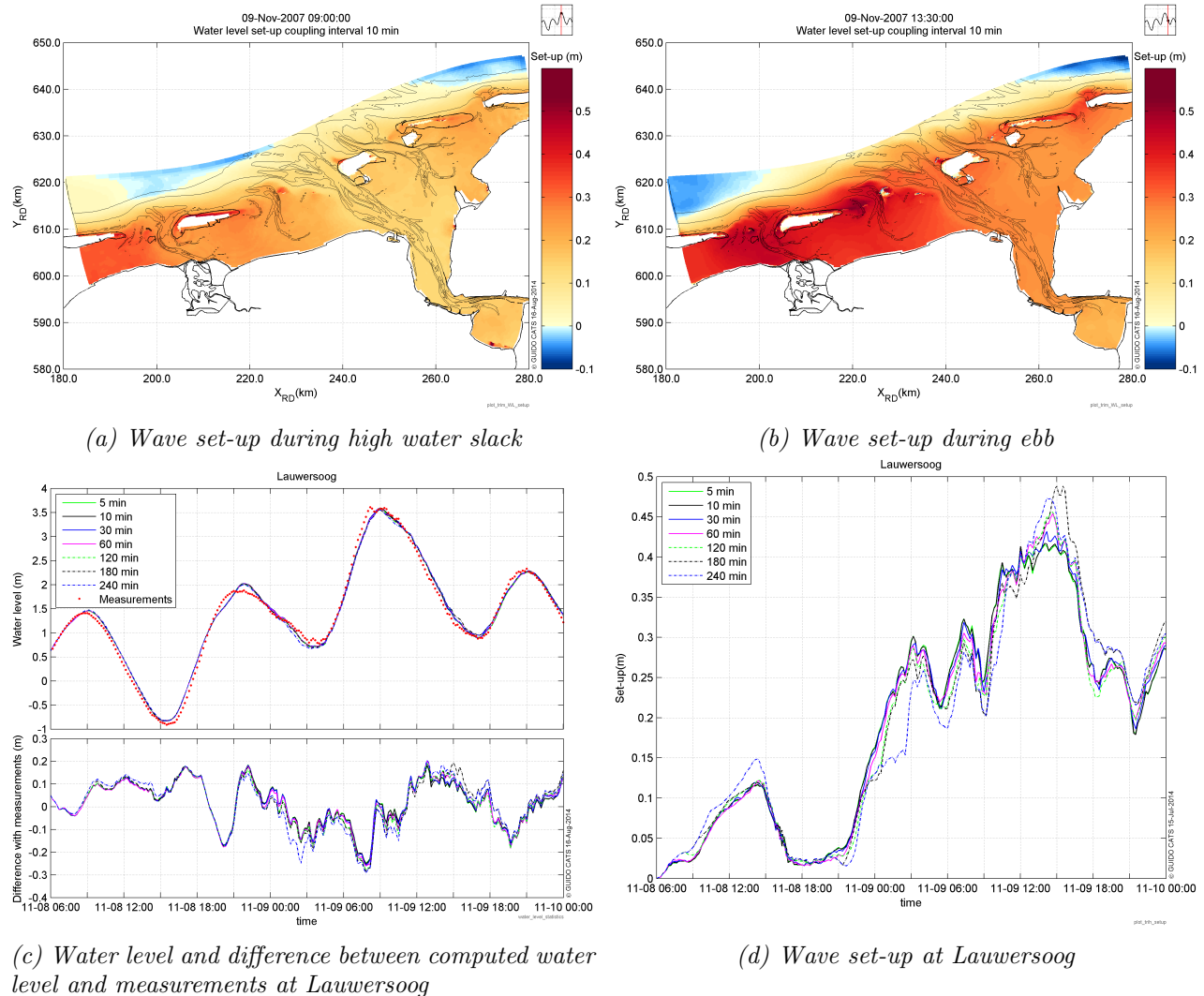


Figure 8.6: Wave set-up during high water slack (9 November 2007 09:00 hours) and wave set-up during ebb (9 November 2007 13:30 hours).

Differences in computed water level when applying different coupling intervals occur when wave forces deviate. Generally, it is observed that the water levels computed with larger coupling intervals tend to be lower at high water and higher at low water than water levels computed with a shorter coupling interval. An explanation is that when relatively short coupling intervals are applied, assume 10 minutes, the force has a constant value during the length of this interval. Every wave computation new boundary conditions are used, that are based on measurements at the time of the computation. The amount of energy that enters the domain has a high correlation with the wave forces. Hence, the wave energy mostly dissipates at the edge of the ebb-tidal delta outside of

the Wadden Sea. This ensures large gradients in radiation stress, which equals wave force. When applying a relatively large coupling interval, wave force is generally underestimated before the peak of the storm in terms of wave boundary conditions, while it generally is overestimated after the peak of the storm.

In principle, every simulation with a different coupling interval applied has its own 'path'. The initial conditions are equal, but forcing the water body with a force for a different period of time will force the water body to adjust. The water level and currents will be different for each simulation. The next wave computation is dependent on the water level and currents, which influences again the computation of the wave conditions. This is a circular process, which makes it extremely hard to predict on forehand which way it will go. In this case the largest wave boundary conditions are obtained after high water, which causes that the highest water level is underestimated when applying a large coupling interval, as wave forces are under-estimated before the peak of the storm.

The highest water level during the simulation at every single grid cell is obtained for all simulations with different coupling intervals. The highest water level computed when a 5 minute coupling interval is applied is approximately equal compared with the highest water level computed when a 10 minute coupling interval is applied. Applying larger coupling intervals causes lower highest water level. The differences increase gradually, with maximum differences in the order of 5 centimeter for the 240 minute coupling interval.

8.4.2 Statistical analysis water level

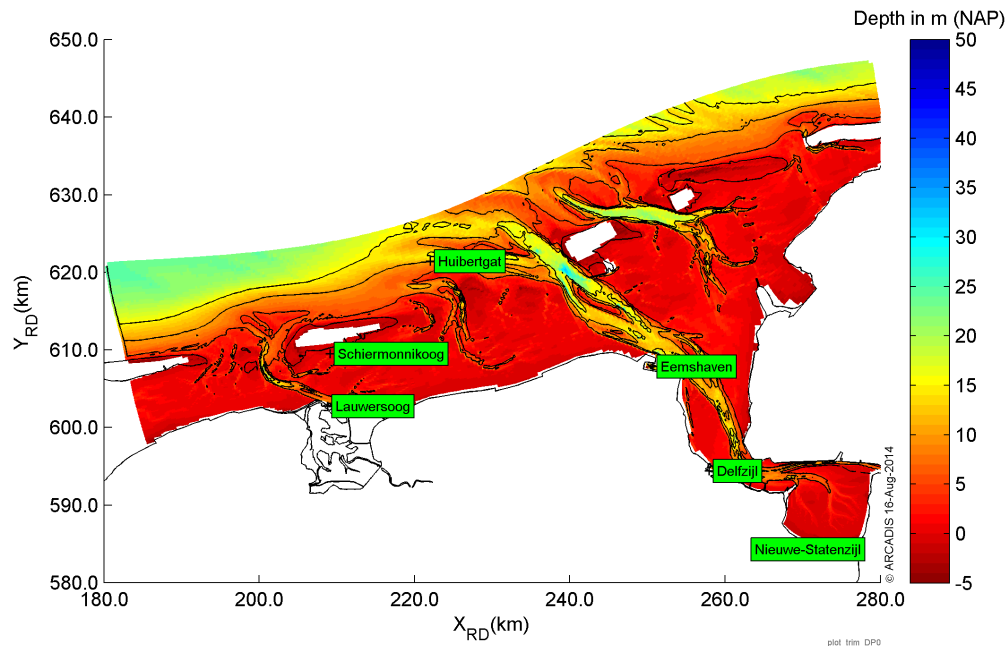


Figure 8.7: Locations of water level measurement buoys

A statistical analysis is performed to make a quantitative comparison between the different coupling intervals used. The results of each of the simulations are compared with measurements. The water level measurements are performed at six different locations: Schiermonnikoog, Lauwersoog,

Huibertgat, Eemshaven, Delfzijl and Nieuwe Statenzijl (Figure 8.7).

minutes	5 min	10 min	30 min	60 min	120 min	180 min	240 min
Schiermonnikoog	0.161	0.162	0.163	0.166	0.169	0.168	0.177
Lauwersoog	0.095	0.095	0.097	0.100	0.102	0.105	0.113
Huibertgat	0.069	0.069	0.070	0.070	0.066	0.070	0.071
Eemshaven	0.136	0.136	0.137	0.139	0.141	0.140	0.142
Delfzijl	0.149	0.150	0.149	0.151	0.152	0.150	0.152
Nieuwe-Statenzijl	0.663	0.663	0.664	0.665	0.666	0.667	0.666

Table 8.1: RMS error of computed water levels compared with water level measurement (unit in m). The value represents the RMS error (m) during 8 November 2007 06:00 - 10 November 2007 00:00

Table 8.1 shows the root-mean-square (RMS) error of the computed water levels at the measurement stations. The root-mean-square error is defined as:

$$RMSE = \sqrt{\frac{\sum_{i=1}^N (x_{pred,i} - x_{meas,i})^2}{N}} \quad (8.2)$$

The root-mean-square error during the simulation period is presented for the coupling intervals at the different locations in Table 8.1. One can obtain that at non of the measurement stations the performance of the model improves nor decays significantly according to the RMSE. The prediction of the water level at the location Nieuwe-Statenzijl is significantly worse than at the other locations. An explanation of the poor prediction at Nieuwe-Statenzijl is provided by the narrow channel towards Nieuwe-Statenzijl, which is schematized poorly, and causes the water level buoy to dry. Around low water the computed water level does not fall below NAP +1 m. As the focus of the study lies in observing and explaining obtained differences due to variations in the coupling interval, no effort has been put in resolving this issue. Huibertgat is the only station located outside the Wadden Sea interior. In general, the prediction of the water level looks rather insensitive for the variation in coupling interval according to the computed root-mean-square error.

As obtained with the visual interpretation of the water level, the wave set-up starts to increase when the storm starts. To assess whether the wave set-up has an influence on the predictive capability of the model, the root-mean-square error is also computed for the day of the storm on itself. The result are presented in Table 8.2. Inspection of this table shows that also during the days the predictive skill of the model does not deteriorate significantly. The visual interpretation of the water level showed that water levels computed with relatively large coupling intervals are generally lower during high water, and higher during high water. This is apparent not to have a large influence on the computed root-mean-square error.

Compared with the root-mean-square error computed for the entire simulation, the predictive capacity of the model does not or barely decrease. In contrary to the other stations, the root-mean-square error significantly decreases at the Nieuwe-Statenzijl, which is a result of the earlier mentioned poor schematization of the narrow channel in that area. Its effect becomes less when the water level rises and the root-mean-square error decreases.

The maximum water level during a storm is an important parameter for safety assessment of flood defenses. The maximum computed and measured water levels at the stations are shown in Table 8.3:

minutes	5	10	30	60	120	180	240
Schiermonnikoog	0.169	0.169	0.172	0.177	0.182	0.180	0.193
Lauwersoog	0.093	0.094	0.098	0.103	0.107	0.110	0.122
Huibertgat	0.085	0.085	0.086	0.085	0.081	0.086	0.087
Eemshaven	0.170	0.170	0.170	0.174	0.176	0.176	0.178
Delfzijl	0.190	0.190	0.190	0.193	0.194	0.191	0.193
Nieuwe-Statenzijl	0.329	0.329	0.331	0.335	0.339	0.337	0.346

Table 8.2: RMS error of computed water levels compared with water level measurement (unit in m). The value represents the RMS error (m) for the day of the storm (9 November 2007 00:00 - 10 November 2007 00:00)

minutes	5	10	30	60	120	180	240	meas
Schiermonnikoog	3.504	3.502	3.503	3.495	3.491	3.467	3.468	3.53
Lauwersoog	3.590	3.592	3.577	3.576	3.573	3.550	3.551	3.61
Huibertgat	3.105	3.106	3.087	3.079	3.075	3.088	3.086	3.11
Eemshaven	3.557	3.557	3.545	3.537	3.533	3.536	3.531	3.85
Delfzijl	4.052	4.053	4.042	4.032	4.026	4.030	4.021	4.21
Nieuwe-Statenzijl	4.564	4.564	4.548	4.542	4.546	4.555	4.542	4.90

Table 8.3: The highest water level (m) computed during the simulation for all used coupling intervals. The value on the right is the maximum water level measured.

From Table 8.3 it can be obtained that the maximum water levels at the stations are generally, slightly lower when applying a larger coupling interval, though the differences are in the order of centimeters. This was already observed with the visual interpretation. The largest differences between the highest water level computed when a 5 minute and a 240 minute coupling interval was applied was at the Wadden Sea interior to the coast of Groningen and Friesland. This is where the stations Lauwersoog and Schiermonnikoog are located, and it is observed that the largest mutual differences are obtained at this location.

8.4.3 Visual interpretation wave conditions

Visual interpretation of the modeled wave conditions happens by inspecting the computed wave spectra mutually and with measurements, and by comparing the spectral wave parameters H_{m0} , $T_{m-1,0}$, T_{m01} , T_{m02} mean wave direction and directional spreading over the whole model domain. Comparing the computed quantities for all simulations at the same time is only possible every 12 hours, as the computations of the simulation with an applied coupling interval of 180 minutes and 240 minutes only coincide every 12 hours. This does not put a restriction on other time instants where the computed values from these simulation are not present.

Visual interpretation of wave spectra

Uithuizer Wad During low water, the wave buoy stranded, even during the storm, and a significant amount of measurements is not useful because of this reason. During ebb, the computed spectra show significant differences with the measured spectra. The measured spectra show that most energy is at low-frequency under 0.2 Hz , while computed spectra show that most wave energy

is at much higher frequencies. Though mutual differences between the simulations are obtained, these are much smaller than the differences with the measurements. In general it can be concluded that the amount of total energy is somewhat larger for the simulation with relatively large coupling intervals, while the mutual shape does not differ.

Wierummer Wad In general, all the computed wave spectra resemble the measured wave spectra very well. There hardly is any difference noticeable due to differences in applied coupling interval. The peak spectral density is under-estimated a little by the model. The frequency range of the measured wave spectra only reach from 0.02-0.5 Hz . A significant amount of time the computed spectral density contains spectral density at frequencies larger than 0.5 Hz . Though this does not cause a problem when visually interpreting wave spectra, this might lead to a problem when a statistical analysis is made. The next section will elaborate on how that problem is handled.

Westereems Oost During the storm the peak of the measured energy density spectrum is rather constant and lies at a value of approximately 0.08 Hz . The computed energy density resembles the measured wave spectra reasonably well, though the peak spectral density is under-estimated during a significant part of the time. Time instant where all computations coincide, show that the computed energy density spectra are identical, except for 18:00 hours 9 November 2007, which is after the heaviest part of the storm, and still the mutual differences are very small. The location of Westereems Oost is rather close to the boundary of the model and this might explain the little difference between the computed wave spectra for the simulations.

Pieterburen Wad The peak spectral density is rather good computed by the model for all simulations. The spectrum is generally much wider compared with the spectra at Westereems Oost. During flood, it appears that lower frequencies are under-estimated by the model. The measured spectra show that there is a considerable amount of wave energy density for frequencies lower than 0.2 Hz , while there hardly is any energy density computed for these frequencies. During ebb, the measurements show that low-frequency wave energy is absent. This indicates that opposing currents cause that low-frequency wave energy does not penetrate in to the Wadden Sea. The measured spectra during ebb are more narrow than the computed spectra. Mutual differences between the simulation are present after the start of the storm, but the mutual differences are significantly smaller compared with the difference with the measurements.

Visual interpretation wave conditions

The computed significant wave height shows very little response to difference in applied coupling interval. During the storm, the largest differences in computed significant wave height between the simulations with 10 and 240 minutes are in the order of 10 cm at most. These differences are mainly found at the northern edge of the ebb-tidal delta and in the channels in between the islands, while inside the Wadden Sea interior the largest differences are even smaller. It is observed that the simulation with a coupling interval of 240 minutes shows higher values for the significant wave height during low water. A relation with the earlier observed higher water level during low water when a relatively large coupling interval is applied can be made. During high water, the opposite is true and the computed significant wave height appears to be a little bit lower for the simulation with the 240 minute coupling interval. At the northern edge of the ebb-tidal delta, the

significant wave height lies in the range of 3-6 m, which makes the differences too small to speak of a significant effect. Simulations with intermediate coupling intervals show similar tendency, but the mutual differences are smaller. The simulation with the 5 minute coupling interval does not show differences with the simulation with the 10 minute coupling interval. It can be concluded that visually, the differences in significant wave height are very small.

The spectral wave periods $T_{m-1,0}$, T_{m01} and T_{m02} all show little variation when different coupling intervals are applied. Mean wave direction and directional spreading also appear to be insensitive for the applied coupling interval. It can be concluded that the effect of the differences in water level do not significantly affect the wave computations, at least this could not be visually obtained. The statistical analysis should verify whether this observation holds.

8.4.4 Statistical analysis wave conditions

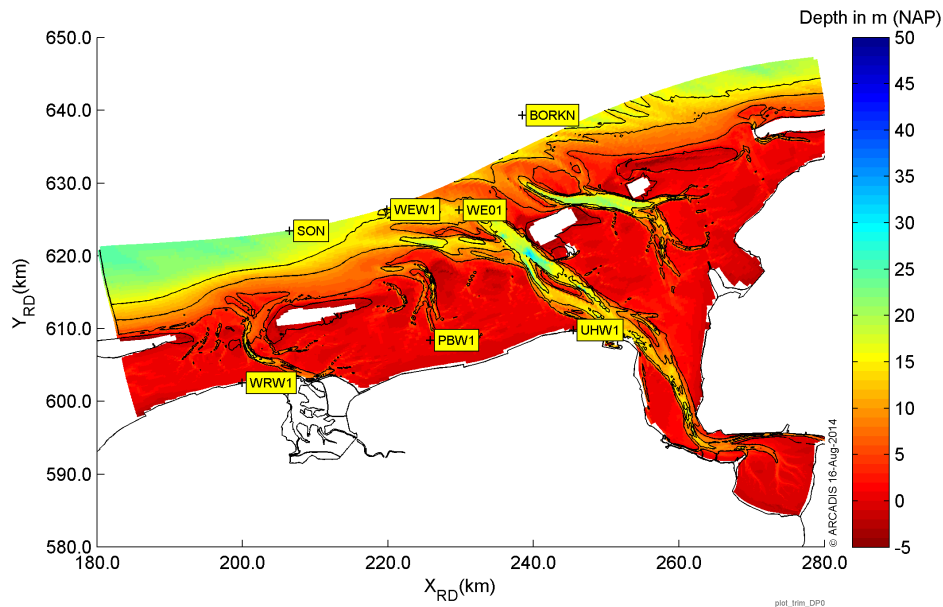


Figure 8.8: Locations of the wave buoys Westereems West (WEW1), Schiermonnikoog Noord (SON), Westereems Oost (WEO1), Pieterburenwad (PBW1), Uithuizerwad (UHW1), Wierumerwad (WRW1)

The computed significant wave height H_{m0} and the spectral periods $T_{m-1,0}$, T_{m01} , T_{m02} are compared with the measured values at the buoy locations Westereems Oost (WEO1), Pieterburenwad (PBW1), Uithuizerwad (UHW1) and Wierumerwad (WRW1) (Figure 8.8). The measured quantities are derived from the 1-dimensional energy density spectrum. The frequency range of the measured wave spectra lies between 0.03 Hz and 0.5 Hz. To make a fair comparison, the same range from the computed spectra is used to calculate the spectral quantities. Table 8.4 gives the root-mean-square error (RMSE, Equation 8.2), scatter index (SI) and relative bias (RBIAS) for the quantities derived from the 1-dimensional energy density spectrum. The scatter index is given by:

$$SI = \frac{RMSE}{x_{mean,measured}} * 100\% \quad (8.3)$$

and the relative bias is given by:

$$RBIAS = \frac{x_{mean,pred} - x_{mean,meas}}{x_{mean,meas}} * 100\% \quad (8.4)$$

The mean wave direction (DIR) is given in degrees. The predictive capability of the model is not given by the RMSE, but by the mean absolute error (MAE). The mean absolute error is given by:

$$MAE = \frac{1}{N} \sum_{i=1}^N |DIR_{pred,i} - DIR_{meas,i}| \quad (8.5)$$

where the exact way of computing the difference is given by:

$$|DIR_{pred,i} - DIR_{meas,i}| = 180 - |180 - |\theta_{pred,i} - \theta_{meas,i}|| \quad (8.6)$$

To avoid the use of unreliable data due to shallow water, data entries measured when the water depth was lower than 1.5 *m* were omitted from the statistical analysis. The value of 1.5 *m* is based on [Alkyon \(2009\)](#), where the same value is used. The number of data entries used to determine the above presented statistical quantities depends on the lesser of the number of measurements and the number of computed values. Inherent on increasing the coupling interval is that less wave calculations are made. The result is that there is less data to compare with measurements. In some of the above provided equations, the mean value of the measured quantity is used. This mean value is calculated with data entries that are measured at times equally to the computed values. When there are more computed values than measurements, only computed values that coincide with times of the measurements are used.

Station	min	H_{m0}			$T_{m-1,0}$			T_{m01}			T_{m02}			DIR		DSPR
		RMSE	SI	RBIAS	RMSE	SI	RBIAS	RMSE	SI	RBIAS	RMSE	SI	RBIAS	MAE	MAE	
WRW1	5	0.07	9.15	-0.09	0.29	7.93	-0.48	0.18	5.88	2.06	0.17	5.76	3.38	32.88	-	
	10	0.07	9.16	-0.08	0.29	7.97	-0.47	0.18	5.90	2.05	0.17	5.77	3.37	32.89	-	
	30	0.07	8.84	0.05	0.29	7.96	-0.75	0.18	5.93	2.04	0.17	5.79	3.40	33.28	-	
	60	0.07	8.66	0.09	0.32	8.65	-1.60	0.18	6.05	1.79	0.17	5.80	3.26	33.20	-	
	120	0.08	10.18	-1.66	0.32	8.84	-1.77	0.18	6.08	1.34	0.16	5.65	2.75	33.31	-	
	180	0.10	13.79	-2.26	0.40	11.44	-1.84	0.22	7.46	1.63	0.19	6.69	3.05	33.89	-	
240	0.15	20.45	-6.38	0.48	13.48	-4.18	0.26	8.57	-0.38	0.20	7.21	1.23	32.85	-		
UHW1	5	0.20	20.01	-19.58	0.76	14.87	-12.80	0.23	5.99	-4.50	0.11	3.33	-1.39	65.34	-	
	10	0.20	20.01	-19.58	0.76	14.84	-12.76	0.23	5.97	-4.48	0.11	3.32	-1.37	65.33	-	
	30	0.20	20.05	-19.63	0.77	15.18	-13.28	0.23	6.17	-4.65	0.12	3.43	-1.47	65.34	-	
	60	0.20	20.65	-20.20	0.80	15.70	-13.99	0.24	6.30	-4.98	0.12	3.42	-1.72	65.32	-	
	120	0.22	22.29	-21.88	0.88	17.05	-15.57	0.26	6.81	-5.63	0.13	3.65	-2.19	65.25	-	
	180	0.26	25.43	-24.70	0.88	17.13	-15.84	0.28	7.40	-6.48	0.14	4.12	-3.01	65.31	-	
240	0.31	28.60	-27.84	1.01	19.44	-18.27	0.33	8.59	-7.50	0.18	5.11	-3.84	63.26	-		
WEO1	5	0.41	10.87	-1.77	1.23	11.90	-10.42	1.37	16.19	-15.18	1.36	18.13	-17.36	6.15	3.20	
	10	0.41	10.87	-1.79	1.23	11.88	-10.41	1.36	16.17	-15.16	1.36	18.11	-17.34	6.15	3.20	
	30	0.42	10.98	-1.61	1.22	11.78	-10.44	1.36	16.17	-15.23	1.36	18.12	-17.39	5.96	3.20	
	60	0.41	10.75	-1.38	1.24	11.98	-10.69	1.39	16.52	-15.58	1.39	18.47	-17.74	5.90	3.31	
	120	0.40	10.49	-0.76	1.28	12.33	-10.86	1.42	16.87	-15.79	1.41	18.74	-17.89	6.23	2.98	
	180	0.43	11.16	-2.63	1.08	10.39	-9.14	1.32	15.70	-14.72	1.36	18.03	-17.19	6.33	3.24	
240	0.45	11.85	-2.02	1.16	11.14	-9.85	1.31	15.44	-14.41	1.32	17.54	-16.67	7.38	3.50		
PBW1	5	0.13	15.25	7.65	1.11	23.80	-16.98	0.51	13.96	-9.18	0.38	11.16	-7.43	22.24	13.43	
	10	0.13	15.21	7.61	1.11	23.82	-17.00	0.51	13.97	-9.20	0.38	11.17	-7.44	22.21	13.40	
	30	0.14	15.36	7.91	1.11	23.77	-16.99	0.51	13.93	-9.15	0.38	11.13	-7.38	22.14	13.45	
	60	0.14	15.96	8.99	1.12	24.01	-16.74	0.51	13.98	-8.76	0.38	11.12	-7.02	22.48	13.59	
	120	0.16	18.96	10.20	1.12	24.14	-16.15	0.51	14.17	-8.24	0.38	11.31	-6.57	22.18	13.53	
	180	0.16	18.97	8.24	1.08	23.66	-15.00	0.51	14.27	-8.24	0.38	11.51	-6.72	23.66	13.81	
240	0.22	24.93	7.60	1.15	25.10	-14.61	0.54	15.11	-8.03	0.41	12.25	-6.57	22.07	13.64		

Table 8.4: Statistical parameters RMSE, SI, RBIAS of H_{m0} (m), $T_{m-1,0}$ (s), T_{m01} (s) and T_{m02} (s), and statistical parameter MAE of DIR (deg) and DSPR (deg) for the coupling intervals 5 min, 10 min, 30 min, 60 min, 120 min, 180 min and 240 min at the wave buoy locations Westereems-Oost (WEO1), Pieterburenwad (PBW1), Uithuizerwad (UHW1) and Wierumerwad (WRW1). The units of RMSE and MAE are similar to the unit of the quantity. The values of SI and RBIAS are presented as percentages.

The wave buoy Westereems Oost lies outside the Wadden Sea interior, rather close to the model boundaries. The prediction of the significant wave height H_{m0} is predicted accurate at this location, with a root-mean-square error in the range of 0.41-0.45 m for all applied coupling intervals. The scatter index remains in the range of the 10-12%. The prediction of the spectral wave periods $T_{m-1,0}$, T_{m01} , T_{m02} are under-predicted by the model, but tend to be slightly better when a larger coupling interval is applied. The mean wave direction and directional spreading are predicted accurately, with again a slight increase in accuracy when the used coupling interval increases. Figure 8.9 shows the computed H_{m0} and T_{m01} at Westereems Oost. The left figure shows that the prediction of H_{m0} hardly deviates when different coupling intervals are applied. On 8 November 2007 between 09:00 and 15:00 hours and a day later on 9 November 2007 between 09:00 and 15:00 hours it is obtained by visual interpretation of the figure that the computed significant wave height is less accurate. During these periods water is flowing out of the Wadden Sea and the observation may be related with ebb-currents. The right figure shows the computed T_{m01} . Though Table 8.4 shows that the spectral wave periods are predicted best when a 180 minute or 240 minute coupling interval is applied at this location, the figure shows that due to these large coupling intervals small variations are missed. The turning point in the lines show when a SWAN computation was performed.

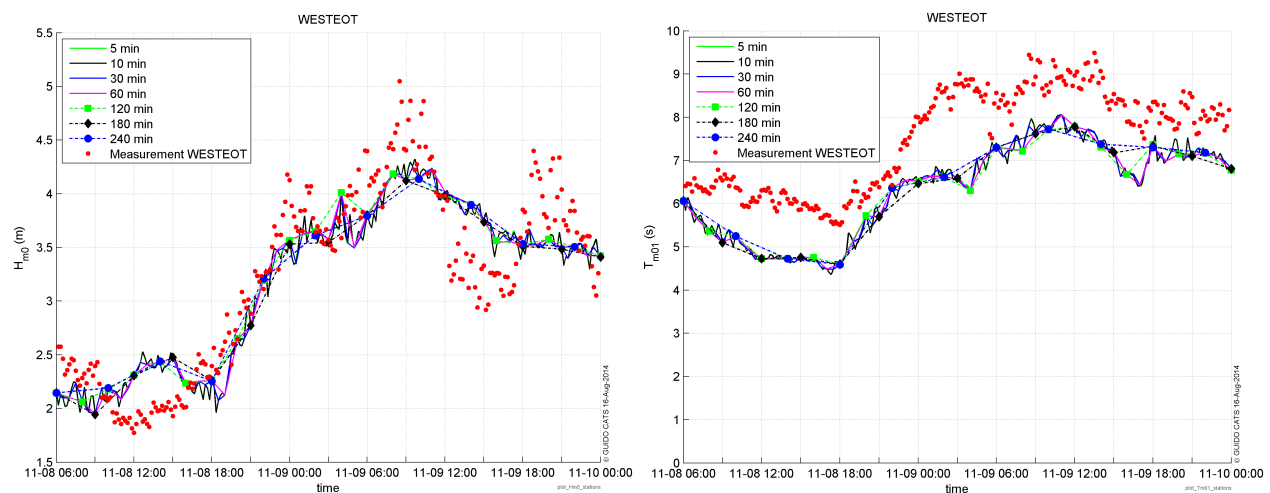


Figure 8.9: Significant wave height H_{m0} and spectral wave period T_{m01} at Westereems Oost. For the coupling intervals of 120 min, 180 min and 240 min, the markers represent the time instants when a wave computation is performed.

The wave buoys Pieterburen Wad, Uithuizer Wad and Wierummer Wad are located inside the Wadden Sea interior. The directional wave spreading was not measured at the wave buoys Wierummer Wad and Uithuizer Wad. The consequence is that the prediction of the directional wave spreading could not be verified. From the table it obtained that the mutual differences of the computed directional wave spreading are very small at Pieterburen Wad, which means that variation in coupling interval does not has an effect on the prediction of the directional wave spreading at the location of these wave buoys. This observation is also verified for the computed directional wave spreading at Wierummer Wad and Uithuizer Wad and at these locations the mutual differences also appear to be small, especially at Wierummer Wad, though this interpretation is based on visual observations.

At Wierummerwad, the prediction of the significant wave height and spectral wave periods is very accurate compared with the prediction of these quantities at the other buoy locations. The accuracy

does hardly vary with a variation of the coupling interval up to values of 120 minutes for the applied coupling interval. Using larger values, the accuracy decreases, which is particularly true for the prediction of the significant wave height when a 240 minute coupling interval is applied.

At Uithuizer Wad the general tendency is that the accuracy of the computed significant wave height and spectral wave periods decreases when a larger coupling interval is applied. Especially when a coupling interval larger or equal to 120 minutes is applied, the accuracy of the model results decreases significantly.

The prediction of the significant wave height at Pieterburen Wad becomes less accurate when the length of the coupling interval is increased. The scatter index of H_{m0} grows from 15.25% when a 5 minute coupling interval is applied, to 24.93% when a coupling interval of 240 minutes is applied. The prediction of the spectral wave periods appears to be hardly sensitive for the applied coupling interval. Only when a 240 minute coupling interval is applied, the accuracy appears to diminish, though differences are not that large.

The accuracy of the model with respect to the prediction of the mean wave direction is best at Westereems Oost. The accuracy increases when the length of the applied coupling interval is increased. At Uithuizerwad, the mean wave direction is predicted poorly compared with the other wave buoys, with a mean absolute error between $60-65^{\circ}$, but the mutual differences are small. An explanation for this poor accuracy might lie in the fact that the used bathymetry is too coarse at the location of Uithuizer Wad and refraction of waves plays an important role at this location. At Pieterburenwad the differences in computed mean wave direction are small due to the variation of the coupling interval. The prediction of the directional wave spreading is accurate, though not as accurate as at Westereems Oost.

It can be concluded that the quality of the prediction by the model does deteriorate inside the Wadden Sea interior when a large coupling interval is used. Outside the Wadden Sea only measurements from one wave buoy are available. The comparison with the computed values indicates a slight improvement in the prediction of the significant wave height H_{m0} and all spectral wave periods when the length of the coupling interval is increased. An important remark is that the number of data entries when large coupling interval are applied is limited, which makes the computed statistical values less reliable. However, the origin of the obtained differences in accuracy does not lie in the fact that the computed values mutually differ that much, but in the fact that the data-set on which the statistical analysis is performed is much smaller. The effect of a computation with a relatively large difference with the measurements increases in weight when the data-set is smaller.

8.4.5 Analysis

During the storm, the set-up due to waves started to differentiate for the simulations. As mentioned above, the computed wave conditions hardly vary at coinciding time entries, which makes it trivial that the set-up due to waves is not caused by different wave conditions directly. The only other option left is that the applied coupling interval has effect on the wave set-up by the time the wave force is constant in the circulation model. The wave boundary conditions based on the measurement at Schiermonnikoog Noord (SON) increase in variance density until approximately 9 November 13:30 hours. The waves entering the Wadden Sea dissipate most of their energy due to depth-induced wave breaking at the tidal inlets of the Wadden Sea. As the waves will break at the edge of the ebb-tidal flats, larger waves at the northern model boundary only means larger radiation

stress gradients at the ebb-tidal flats. These radiation stress gradients are directly associated with the wave force, which will increase under the assumption that the waves that enter towards the ebb-tidal flats relatively grow faster than the water level rises. This appears to be true, as the locations where the largest wave force occurs moves a little bit offshore towards larger depths. In the situation that wave force is increasing and the coupling interval is large, the wave force is underestimated for an significant amount of time, which causes that the set-up is underestimated. The opposite is true when the wave force decreases: the wave force and the set-up are both overestimated. Wave force at the entrance of the Eems-Dollard channel appears to be absent, what can be explained by the reduced wave boundary conditions applied at that region and the large, shallow ebb-tidal delta that already caused waves to dissipate energy outside the domain.

The location of the largest wave force is not significantly influenced due to the set-up. What is meant, is that the wave force does not move towards the coast significantly while this could be a result of the set-up together with the depth-limited conditions that cause wave breaking. The northern edge of the ebb-tidal delta is associated with rather steep slopes that reach values well over 0.45 (*Alkyon, 2009*). This ensures that even when the set-up causes waves to reach further on the ebb-tidal delta, this is quickly outweighed by the decreased depth and the location of the largest wave forces does not significantly differs. In Subsection 8.4.1 the observation was made that the wave set-up shows a correlation with the phase of the tide. Peaks in set-up appeared to coincide with low water, while minima in set-up were obtained during high water. The wave force does not appear to be influenced by the phase of the tide, which excludes that as an explanation. A plausible explanation is that during low water, the inertia of the water body is less and the wave force has a larger influence.

An explanation for the fact that the wave conditions hardly vary when the coupling interval is changed, is a direct result of the above posed solution for the differences in water level. The waves dissipate energy at the ebb-tidal deltas near the tidal inlets of the Wadden Sea. In the interior of the Wadden Sea, the wave conditions are believed to be locally generated, depth-limited wind waves. All simulation show that wave penetration is limited. It was observed that the model underpredicts low-frequency wave energy at near-shore measurement stations. These low-frequency waves are associated with wave penetration through the tidal inlets (*Alkyon, 2009*). Values for H_{m0}/d of approximately 0.4 are obtained at the shallow tidal flats at the Wadden Sea interior. At the deep tidal channels these depth-limited conditions do not apply. The water levels inside the Wadden Sea interior for simulations with respectively a 5 and 240 minute coupling interval differ at most 10 cm locally, which is not enough to create significant differences in wave conditions between the two simulations.

8.5 Conclusions

What is the effect of the applied coupling interval on the accuracy of the computed water level and wave conditions under storm conditions? The computed water levels for the simulation do not perform significantly worse for simulations with relatively large coupling intervals, though the computed results tend to be slightly better when the coupling interval is shorter. The wave set-up is responsible for the obtained differences in water level.

The effect of the chosen coupling interval is hardly noticeable on any of the wave conditions. The differences that occur in water level due to the coupling interval are too small to have a significant effect on the wave conditions.

What are the dominant processes regarding the coupling interval? The water level appears to be most influenced by wave set-up. The wave set-up is both dependent on wave boundary conditions and to a lesser extent to the phase of the tide. During the storm, the gradient of the wave force appears to be large enough to cause differences in wave set-up when applying different coupling intervals. The wave force grows until the time that the highest wave boundary conditions are used, which is a result of larger amounts of wave energy entering the domain. Increasing the coupling interval causes an under-estimation of the wave force on the water body during growing wave boundary conditions, while the opposite holds when the wave boundary conditions.

The effect of differences in water level and current due to the different applied coupling intervals appears not to be large enough to have a significant effect on the wave conditions. A statistical analysis showed both small increases and decreases in accuracy of wave parameters between relatively large and relatively small coupling intervals. This appeared to be more likely the result of the size of the data-set instead of the diverging conditions, as the mutual differences at the times wave computations were made hardly differ.

What are the limits of the coupling interval to which the accuracy of the model is preserved? Though the statistical result do not show clearly where the accuracy of the model starts to worsen, a preference to a relatively small coupling interval is from a physical stand of view the best option. Looking closely to the computed water levels and mutual differences between the simulations shows that the differences between values computed with 5 and 10 minutes coupling intervals are in the order of millimeters. Computations made with a 30 minute interval also shows very good resemblance with the computations made with 5 and 10 minutes coupling intervals. Even larger coupling intervals do show increasingly larger differences with the computations with the smaller intervals. An important remark is that the coupling interval does not cause that the model computes completely unrealistic values during any of the simulations.

Chapter 9

Wind drag

9.1 Introduction

The transfer of energy by wind to waves is modeled in both Delft3D-FLOW and SWAN by a friction wind velocity u_* , which is dependent on the wind velocity u_{10} at 10 m elevation. The relation between the u_* and u_{10} is given by a wind drag coefficient. Recent study ([Zijlema et al., 2012](#)) shows that the wind drag coefficient decreases at higher wind speeds and starts to show increasing differences from approximately 20 m/s from wind drag parameterization by [Wu \(1982\)](#) and [Charnock \(1955\)](#).

As this new wind drag parameterization, called *fit*, can both be used in the circulation model and in the wave model, this is likely to cause significant differences in both computed water level and wave conditions. Certainly when applied in a relatively large model on the scale of, lets say, the North Sea, compared with the conventional wind drag parameterization by [Wu \(1982\)](#) and [Charnock \(1955\)](#).

Coastal areas generally ask for more detailed grids with significant smaller grid cells as the interacting of the dominant processes becomes more complex, compared to models that cover large areas (e.g. the North Sea). The water level and current boundary conditions for models at coastal areas are generally derived by nesting the model in larger models that are driven by tidal constituents and wind. The wave boundary conditions can both be based on measurements at or near the coastal model boundary or by the nesting of a wave model. When using a two-way coupled model, both the circulation model and the wave model use a different wind drag relation to represent the transfer of wind energy to respectively the water body (current, water level) and to waves.

The transfer of wind energy is assumed to be limited, due to limited fetch in the detailed coastal models, especially for waves, as these are expected to break before they reach shore. Though the fetch is relatively short in coastal models, the wave height will be influenced by the choice of the wind drag parameterization in the wave model. The choice of the wind drag parameterization in the wave model will not only affect the prediction of waves, but also the inherent wave force, as this is a result of large radiation stress gradients, which are dependent on gradients in dissipation of wave energy. This might cause that the location and magnitude of the wave set-up are different between simulations with different wind drag formulations in the wave model. On the other hand, the wind drag parameterization in the circulation model influences the water level. This also will cause waves to dissipate at different locations. As these processes interact, the effect of the fit

wind drag parameterization on total set-up is unknown, compared to the conventional [Wu \(1982\)](#) wind drag formulation in SWAN and the [Charnock \(1955\)](#) wind drag parameterization in Delft3D-FLOW.

It thereby is important to get an estimate at which wind speed the differences due to the formulations start to become significant. When for example hypothetical storms are simulated with a two-way coupled model to generate water level data at sea defenses where no measurements are available, the influence of the choice of wind drag parameterization and the relating uncertainty can be assessed.

1. What is the effect of the fit wind drag parameterization compared with the conventional wind drag parameterization by [Wu \(1982\)](#) in SWAN?
2. What is the effect when the fit wind drag parameterization is applied in both Delft3D-FLOW and SWAN?
3. At which wind speed differences in total set-up, wave set-up and wave conditions become significant?

9.2 Method

To assess the effect of the *fit* wind drag parameterization by [Zijlema et al. \(2012\)](#) on the total set-up, and at which wind speed significant differences occur, is first investigated with the bathymetry used to investigate the performance of the two-way coupled model in Chapter 7. [Zijlema et al. \(2012\)](#) show that differences in wind drag, compared with [Wu \(1982\)](#), are in the order of 10% at a wind speed of 20 *m/s*, while this increases to 30% for wind speeds of 32.6 *m/s*. The differences in wind drag coefficient becomes larger than 30 % at wind speed larger than 32.6 *m/s*.

To assess the differences between simulations using the *fit* wind drag and both the [Wu \(1982\)](#) wind drag in SWAN and [Charnock \(1955\)](#) in Delft3D-FLOW, wind speeds of 20, 30, 40, 50 and 60 *m/s* are used in the idealized bathymetry, used in Chapter 7. The following combinations of parameterization are assessed:

1. [Charnock \(1955\)](#) [Wu \(1982\)](#)
2. [Charnock \(1955\)](#) [Zijlema et al. \(2012\)](#)
3. [Zijlema et al. \(2012\)](#) [Zijlema et al. \(2012\)](#)

As a matter of convenience, the combinations will be abbreviated to 1. Charnock-Wu, 2. Charnock-Fit and 3. Fit-Fit.

The wind drag parameterization in [Alkyon \(2009\)](#) in Delft3D-FLOW is based on [Charnock \(1955\)](#) with an α parameter of 0.032, which is equal to the wind drag parameterization used to determine the water-level- and current boundary conditions in the WAQUA-IN-SIMONA environment. The value of the wind drag coefficient C_D is visualized in Figure 9.1 for the three parameterizations. The Delft3D-FLOW software environment does not allow to directly choose the *fit* wind drag parameterization or the [Charnock \(1955\)](#), when the model is compiled with the default settings. The *fit* wind drag parameterization is therefore implemented, while the [Charnock \(1955\)](#) wind drag parameterization can be represented by a formulation based on a linear dependency, which shows good accuracy for wind speeds between 5 *m/s* and 30 *m/s*. This ensures that the wind drag is correctly represented during the storm of 9 November 2007. For larger wind speeds, the wind drag

parameterization is adjusted in such a way that the C_D value in Delft3D-FLOW is identical to the C_D value used by [Charnock \(1955\)](#) at a given wind speed. The wave boundary conditions exist of a JONSWAP spectrum with a mean period of 11 s and a significant wave height of 8 m, which is identical to the largest wave boundary conditions during the storm of 9 November 2007 at the eastern Wadden Sea. Both the wind speed and the wave boundary conditions are gradually increased to their final values from the start of the simulation to prevent a shock wave in the water motion. The wind speed is increased from 0 m/s to its final value in six hours and the wave boundary conditions are increased in eight hours. The total simulation time is 24 hours, which provides the water body sixteen hours to adjust to the forcing, which is considered long enough to obtain a stationary situation.

In contrary to the idealized case used in Chapter 7, where with exception of depth-induced wave breaking all processes were turned off, all processes are incorporated.

After the simulation using the idealized bathymetry, the same combinations of wind drag parameterizations in Delft3D-FLOW and SWAN are used to assess the effect at the eastern Wadden Sea during the storm of 9 November 2007.

9.3 Assessment of S_{in}

The wind drag is not more than a parameterization from wind speed at a 10 m elevation and the u_* , which does not necessary mean that the value of S_{in} shows similar behavior. In SWAN, the wind input is formulated as $S_{in}(\sigma, \theta) = A + BE(\sigma, \theta)$. A describes linear wave growth according to [Cavaleri and Malanotte-Rizzoli \(1981\)](#), which is relatively small compared to the exponential growth described by $BE(\sigma, \theta)$ during high wind speed conditions. The default parameterization of B is by [Komen et al. \(1984\)](#), which is also used in this case. In both A and B the friction velocity u_* is used. First an assessment of the magnitude of S_{in} will be made under varying conditions. The wind drag coefficient dependent on the wind speed is shown in Figure 9.1. It is visible that as wind speed grows, the difference in wind drag coefficient increases.

The exponential wave growth, represented by the term B is not only dependent on u_* , but also on the phase velocity c , the ratio ρ_{air}/ρ_{water} (the densities of respectively the air and the water), the frequency and the angle between wind and wave direction. For convenience, the formulation of B by [Komen et al. \(1984\)](#) is rephrased here:

$$B = \max \left[0, 0.2 \frac{\rho_a}{\rho_w} \left(28 \frac{u_*}{c} \cos(\theta_{wave} - \theta_{wind}) - 1 \right) \sigma \right] \quad (9.1)$$

The phase velocity c can be determined for every frequency present in the wave spectrum with the use of the dispersion relation, under the condition the depth is known. The only parameter that changes due to the difference in wind drag parameterization is u_* , which makes it obvious that B is influenced by it. The value of S_{in} can easily be assessed and the differences between S_{in} for the wind drag by [Wu \(1982\)](#) and the wind drag by ([Zijlema et al., 2012](#)) can be obtained, which is visualized in Figure 9.2.

A JONSWAP variance density spectrum is assumed with parameters that coincide with the largest boundary conditions during the storm of 9 November 2007. It is visual that the magnitude of S_{in} is larger when the wind drag by [Wu \(1982\)](#) is applied in Figure 9.3. Where S_{in} seems to be unlimited

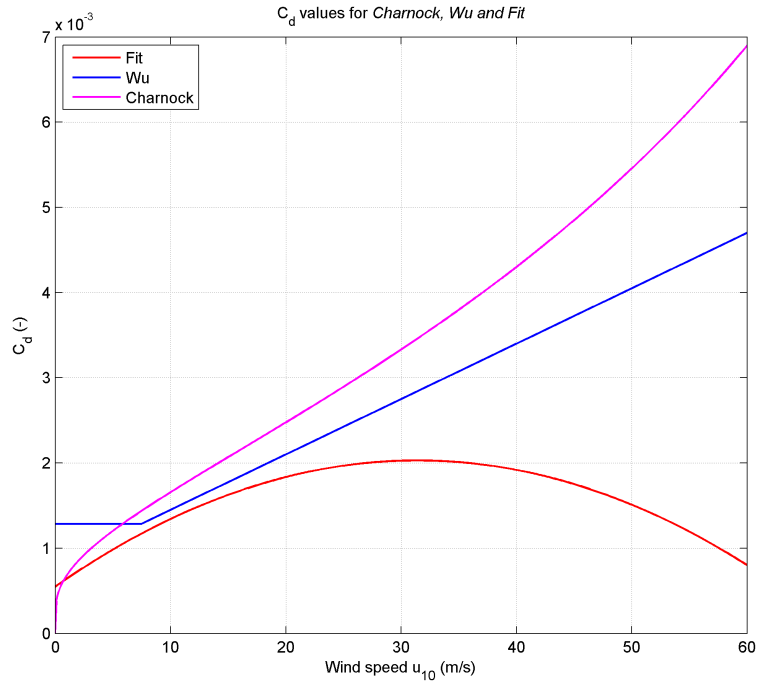


Figure 9.1: The wind drag coefficient Wu (Wu, 1982) and Fit (Zijlema et al., 2012) presented with respect to the wind speed

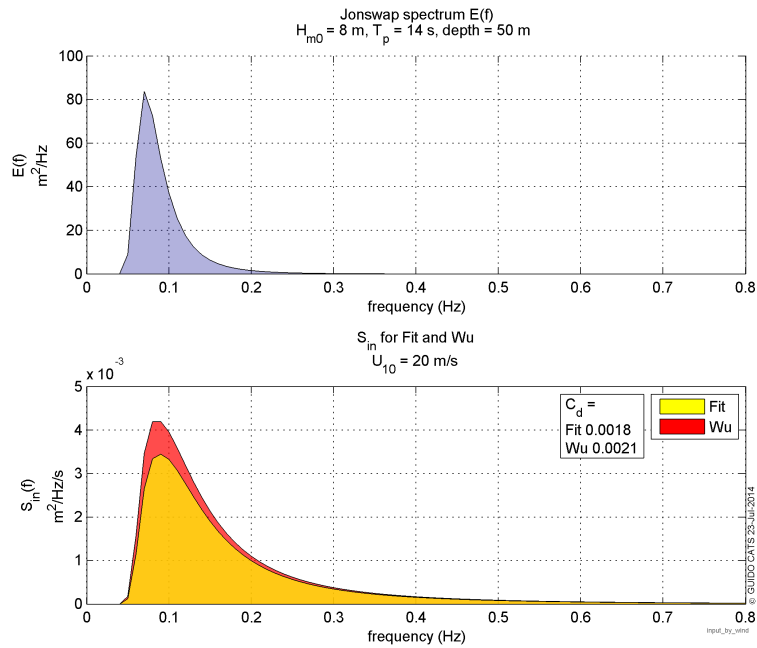


Figure 9.2: The JONSWAP variance density spectrum with a significant wave height of $H_{m0} = 8$ m and peak period $T_p = 14$ s at a depth of 50 m. The wind speed is 20 m/s. The lower figure shows S_{in} for both Wu and Fit .

in the case of Wu , the fit wind drag parameterization shows it maxima for S_{in} at a wind speed of 52 m/s. This has been observed for many variations of H_{m0} , T_p and depth. The explanation is that the spectral shape of JONSWAP causes this effect. The highest value of S_{in} would be different

when the spectral shape was chosen differently.

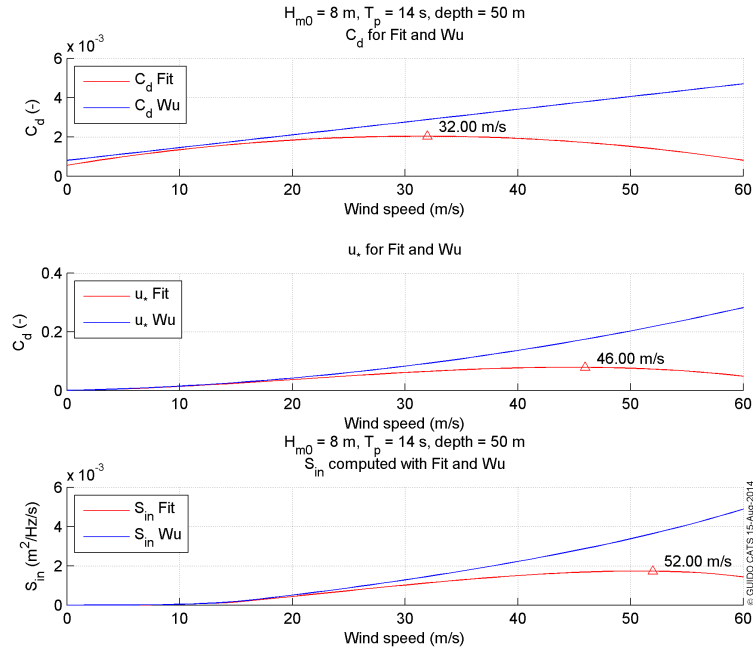


Figure 9.3: The term S_{in} dependent on wind speed, u_* is visualized in the middle figure and at the bottom figure the S_{in} is presented.

9.4 Idealized case

9.4.1 Results idealized case

From figure 9.3 it can be obtained that the difference between S_{in} is approximately 10% at a wind speed of 20 m/s and it rapidly increases to approximately 20% at 30 m/s and approximately 70% at a wind speed of 60 m/s. Simulation have been performed to assess the effect of these differences in S_{in} , not only on wave growth, but also on set-up. At the offshore boundary the wave conditions match with the largest wave conditions during the storm of 9 November 2007: H_{m0} of 8 m and a T_{m01} of 11 s. The wind speed is gradually increased, which results in values of 20, 30, 40, 50 and 60 m/s.

Figure 9.4 shows the computed water levels with the combinations of wind drag parameterizations indicated in Section 9.2. The coast is located at the right hand side of the figures and the direction of wind and the propagation of waves are perpendicular to the coast. It is visible that the water level is hardly affected by the choice of the wind drag parameterization in SWAN, as the red and the green are almost exactly the same, except when the wind speed is 60 m/s. In this case, the water level is a bit lower at locations farther offshore, while this does not apply closer to shore, where the maximum water levels are found.

The difference between the computed water level with the fit parameterization in Delft3D-FLOW is significant, while the difference in water level when the [Charnock \(1955\)](#) wind drag parameterization is used, is small, even at high wind speeds. This indicates that the wave set-up is not significantly influenced by the wind drag parameterization.

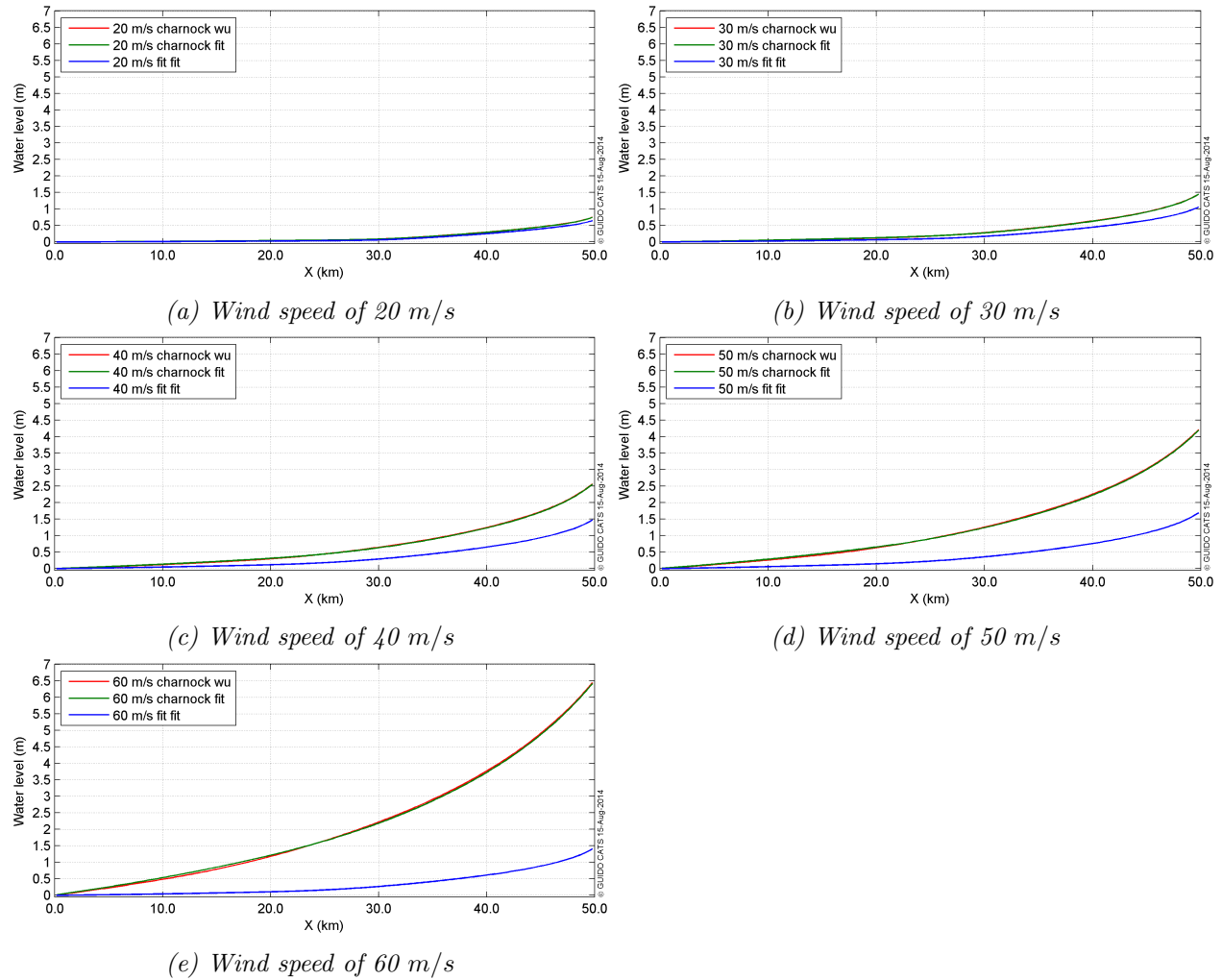


Figure 9.4: The computed water level for the combinations of Charnock, Wu and Fit for wind speeds of 20, 30, 40, 50 and 60 m/s.

Table 9.1 shows the maximum computed water levels. The difference between the *fit* wind drag parameterization and *Charnock* (1955) in Delft3D-FLOW is approximately 10 cm during a wind speed of 20 m/s. This difference rapidly increases during higher wind speeds, with a difference of approximately 5 m during a wind speed of 60 m/s.

Wind speed	20 m/s	30 m/s	40 m/s	50 m/s	60 m/s
Charnock - Wu	0.75	1.45	2.57	4.21	6.44
Charnock - Fit	0.74	1.44	2.56	4.19	6.41
Fit - Fit	0.64	1.06	1.47	1.69	1.41

Table 9.1: Maximum water level (m) for the combinations of wind drag parameterizations.

The differences obtained during high wind speeds are enormous. The set-up during high wind speeds when Charnock is applied in Delft3D seems to be not realistic, especially not for wind speeds of 50 and 60 m/s. The literature study already mentioned wind drag parameterization that are capped of to not overestimate wave growth and set-up during hindcasts. *Dietrich et al.*

(2011b) caps off the wind drag parameterization of [Garratt \(1977\)](#) at a value of $C_D = 0.0035$, which would be at a wind speed of approximately 35 m/s for Charnock and at approximately 45 m/s for Wu when this value would be applied for these parameterizations. The result would be that u_* grows linearly with increasing wind speed (when the wind speed is larger than 35 and 45 m/s for respectively Charnock and Wu), instead of progressively and the difference with fit-fit would still be enormous.

The wave set-up is computed by subtracting the water level computed by a Delft3D-FLOW stand alone simulation from the water level computed with the two-way coupled model. Table 9.2 shows the contribution of the wave set-up to the water level. Noteworthy is that the wave set-up during high wind speeds is higher when Fit-Fit is used, compared with Charnock-Fit. Clearly, the influence of the wind drag parameterization in Delft3D-FLOW is noticeable.

Wind speed	20 m/s	30 m/s	40 m/s	50 m/s	60 m/s
Charnock - Wu	0.29	0.28	0.27	0.26	0.23
Charnock - Fit	0.29	0.28	0.26	0.24	0.20
Fit - Fit	0.30	0.29	0.29	0.29	0.30

Table 9.2: Maximum wave set-up (m) for the combinations of wind drag

The wave forces computed hardly differ mutually during wind speeds of 20 and 30 m/s . During wind speeds of 40 m/s and higher, the wave force in case of Charnock-Wu shows larger forces. This is not visible in the maximum computed wave set-up. The differences in wave force between Charnock-Fit and Fit-Fit are smaller, though the wave force near shore in case of Charnock-Fit is larger. This is a result of the larger water depth, which allows the significant wave height to be larger, closer to shore. Before the largest amount of waves start to break, the significant wave height is nearly similar in case Charnock-Fit and Fit-Fit. Remarkably, the wave set-up is largest for Fit-Fit during high wind speeds. The probable cause lies in the fact that in case of Fit-Fit a similar force in magnitude is exerted on a water body that is smaller (lower water levels). This causes that the effect of the force becomes larger. This observation has already been made in Chapter 8.

9.5 Wadden Sea case

9.5.1 Visual interpretation water level

The water levels in case of Charnock-Wu and Charnock-Fit hardly vary during the storm of 9 November 2007. Differences are in particular observed in the Eems-Dollard channel and the Dollard estuary (Figure 9.5a. The largest difference between Charnock-Wu and Fit-Fit are at most in the order of 30 cm at Nieuwe-Statenzijl, while at Delfzijl the difference is in the order of 14 cm at most (Figure 9.5b. Similar to what is observed in the idealized case, the largest difference in water level is caused by the wind drag parameterization in Delf3D-FLOW, while the wave set-up hardly differs. At the buoy locations Delfzijl and Nieuwe-Statenzijl (both located inside or near the Eems-Dollard channel), the differences are larger. The computed set-up when Fit-Fit is applied is out of phase with the computed wave set-up when Charnock-Wu and Charnock-Fit is applied, which results in a difference oscillating around zero.

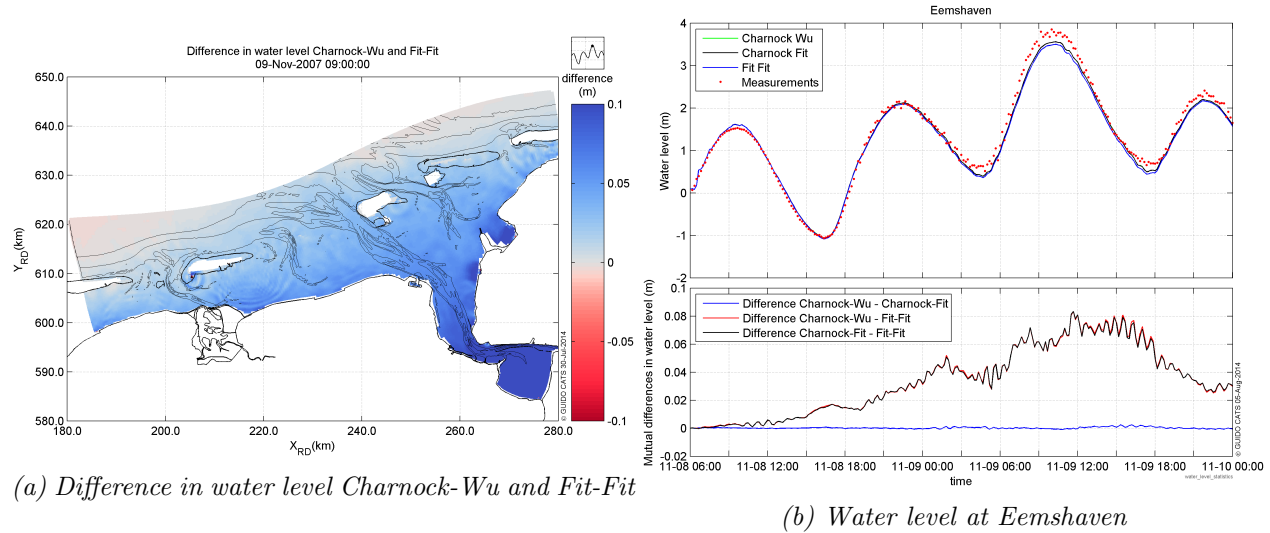


Figure 9.5: (a) Difference in water level between Charnock-Wu and Fit-Fit at 9 November 2007 09:00 hours. Blue indicates that the water level is higher in case of Charnock-Wu. (b) The upper figure shows the water level at Eemshaven during the simulation period. The lower figure shows the mutual differences. A positive value indicates the first mentioned combination of wind drag parameterizations has a higher water level, compared with the latter combination.

9.5.2 Statistical analysis water level

The root-mean-square error for the day of the storm is presented in Table 9.3. In general, the performance of the model is better when using the *Charnock* (1955) parameterization in Delft3D-FLOW, which is obviously a biased observation, as the model was calibrated with this setting. A second observation is that there is almost no difference between Charnock-Wu and Charnock-Fit.

Wind drag	Charnock-Wu	Charnock-Fit	Fit-Fit
Schiermonnikoog	0.169	0.169	0.173
Lauwersoog	0.094	0.094	0.105
Huibertgat	0.085	0.085	0.080
Eemshaven	0.170	0.170	0.215
Delfzijl	0.190	0.190	0.251
Nieuwe-Statenzijl	0.329	0.328	0.346

Table 9.3: Root-mean-square error water level for the day of the storm (9 November 2007 00:00 hours - 10 November 2007 00:00 hours)

The highest water levels are not surprisingly lower when Fit-Fit is applied, compared with Charnock-Wu and Charnock-Fit (Table 9.4). The causes a (larger) underestimation of the highest water level during the simulation period. At the stations inside the Wadden Sea interior, a clear difference can be obtained between Lauwersoog and Schiermonnikoog on the one hand side, and Eemshaven, Delfzijl and Nieuwe-Statenzijl on the other hand side. The latter stations already underestimated the highest water level significantly, and the underestimation when Fit-Fit is applied grew. The closer the station is located near the Wadden Sea interior, the less the difference is. The mutual difference between Charnock-Wu and Fit-Fit is 20 cm at Nieuwe-Statenzijl, while this difference is

9 *cm* at Delfzijl and 8 *cm* at Eemshaven.

Wind drag	Charnock-Wu	Charnock-Fit	Fit-Fit	meas
Schiermonnikoog	3.50	3.50	3.49	3.53
Lauwersoog	3.59	3.59	3.55	3.61
Huibertgat	3.11	3.11	3.09	3.11
Eemshaven	3.58	3.56	3.50	3.85
Delfzijl	4.05	4.05	3.96	4.21
Nieuwe-Statenzijl	4.56	4.57	4.36	4.90

Table 9.4: The highest water level measured during the simulation period (8 November 2007 06:00 hours - 10 November 2007 00:00 hours)

9.5.3 Visual interpretation wave conditions

The difference in significant wave height between Charnock-Fit and Fit-Fit is small. The difference with Charnock-Wu is mainly in the Eems-Dollard channel, with higher significant wave heights that are at most approximately 0.15 *m* higher when Charnock-Wu is applied, compared with Charnock-Fit and Fit-Fit. An explanation is that waves are not depth-limited in this channel and the fetch is relatively large (multiple times the distance from the northern boundary to the edge of the ebb-tidal deltas), which provides the opportunity to the wind to have an influence on the significant wave height.

9.5.4 Statistical analysis wave conditions

From Table 9.5, it can be seen that none of the computed parameters is affected significantly by using the different wind drag parameterizations. The differences obtained by visual inspection are too small to have an impact on the performance of the model in a statistical way. Considering the significant wave height, only at Uithuizerwad small differences in root-mean-square error can be seen, which is the wave measurement buoy closest to the Eems-Dollard channel. The wave periods do not show mutual differences larger than 0.03 *s*. The mean wave direction and the directional do not seem to be affected either. It can be concluded that the use of different wind drag parameterizations does hardly has an influence on the computed wave conditions during the storm of 7 November 2007. This was also expected to be the case, considering the results of the idealized case using a maximum wind speed of 20 *m/s*, which is approximately the highest wind speed during the storm.

9.6 Conclusion

What is the effect of the fit wind drag parameterization compared with the conventional wind drag parameterization by Wu (1982) in SWAN? It can be concluded that the contribution of the wind drag parameterization in SWAN hardly has an effect on the wave set-up. The total set-up in the idealized case during a wind speed of 60 *m/s* is 6.44 *m* when Charnock-Wu is applied. In case Charnock-Fit is applied, the total set-up is only 3 *cm* lower. The differences

		H_{m0}			$T_{m-1,0}$			T_{m01}			T_{m02}			DIR	DSPR
Station	wave-breaking	RMSE	SI	RBIAS	RMSE	SI	RBIAS	RMSE	SI	RBIAS	RMSE	SI	RBIAS	MAE	MAE
WRW1	Charnock-Wu	0.07	9.16	-0.08	0.29	7.97	-0.47	0.18	5.90	2.05	0.17	5.77	3.37	32.89	-
	Charnock-Fit	0.07	9.21	-1.23	0.29	7.86	-0.15	0.18	5.81	1.98	0.16	5.66	3.26	32.88	-
	Fit-Fit	0.07	9.47	-2.42	0.30	7.97	-0.74	0.18	5.82	1.61	0.16	5.59	2.96	32.47	-
UHW1	Charnock-Wu	0.20	20.01	-19.58	0.76	14.84	-12.76	0.23	5.97	-4.48	0.11	3.32	-1.37	65.33	-
	Charnock-Fit	0.20	20.26	-19.83	0.76	14.91	-12.78	0.22	5.90	-4.40	0.11	3.24	-1.24	65.39	-
	Fit-Fit	0.22	22.05	-21.68	0.78	15.29	-13.15	0.24	6.35	-4.97	0.12	3.51	-1.82	65.24	-
WEO1	Charnock-Wu	0.41	10.87	-1.79	1.23	11.88	-10.41	1.36	16.17	-15.16	1.36	18.11	-17.34	6.15	3.20
	Charnock-Fit	0.41	10.89	-2.42	1.20	11.59	-10.03	1.34	15.84	-14.76	1.34	17.82	-16.99	6.17	3.21
	Fit-Fit	0.42	10.93	-2.42	1.21	11.68	-10.12	1.35	15.98	-14.91	1.35	17.98	-17.15	6.15	3.19
PBW1	Charnock-Wu	0.13	15.21	7.61	1.11	23.82	-17.00	0.51	13.97	-9.20	0.38	11.17	-7.44	22.21	13.40
	Charnock-Fit	0.13	14.53	5.49	1.11	23.75	-17.01	0.51	14.17	-9.52	0.39	11.40	-7.77	22.22	13.42
	Fit-Fit	0.13	14.29	4.40	1.13	23.98	-17.47	0.52	14.39	-9.91	0.39	11.60	-8.12	22.30	13.51

Table 9.5: Statistical parameters RMSE, SI, RBIAS of H_{m0} (m), $T_{m-1,0}$ (s), T_{m01} (s) and T_{m02} (s), and statistical parameter MAE of DIR (deg) and DSPR (deg) for the simulation with depth-induced wave breaking parameterizations Battjes & Janssen and nkd-scaling model at the wave buoy locations Westereems-Oost (WEO1), Pieterburenwad (PBW1), Uithuizerwad (UHW1) and Wierumerwad (WRW1). The units of RMSE and MAE are similar to the unit of the quantity. The values of SI and RBIAS are presented as percentages.

in significant wave height already becomes significant with a difference of approximately 3 m between the maximum significant height computed with Charnock-Wu and Charnock-Fit, although the fetch is limited in the idealized case. This does not result in large differences in set-up, which is a result of the wave force, that does not show that large variations due to the different wind drag parameterization in SWAN. During a wind speed of 20 m/s, the significant wave height hardly differs.

It is evident that larger wind speeds have a large influence on the water level set-up by means of wind stress on the water body on the scale of a coastal model, compared with the indirect set-up by waves due to higher wind speeds. The result is that the parameterization of the wind drag does not influence the amount of set-up due to waves on this scale. In reality, the wave boundary conditions are in a greater or lesser extent a function of the wind speed. That variation is not taken into account in this idealized case, as it depends on the direction, fetch and time, which are all not known. This idealized case therefore should not be interpreted as a nested model where the boundary conditions are generated by the same conditions, but purely as an experimental set-up.

At the Wadden Sea case, the effect of the fit wind drag parameterization in SWAN had no effect on the set-up during the storm of 9 November 2007. The effect on computed wave conditions also is negligible. After the performance of the simulations in the idealized case, this was not a surprising result. The maximum wind speed during the storm of 9 November 2007 does hardly reach a value of 20 m/s and the time it does, is limited.

What is the effect when the fit wind drag parameterization is applied in both Delft3D-FLOW and SWAN? In case of the idealized case, the differences in set-up rapidly increase when the wind speed is increased. The set-up is significantly lower when Fit is applied in Delft3D-FLOW. A non-linear effect is that the wave set-up is higher when Fit-Fit is applied, compared with Charnock-Fit, during high wind speeds of 50 m/s and 60 m/s.

The significant wave height is similar when Fit-Fit is applied, compared with Charnock-Fit, until wind speeds are reached that cause significant differences in set-up. This significant difference in set-up causes that the significant wave height is higher in case of Charnock-Fit, as H_{max} in the

depth-induced wave breaking formulation of *Battjes and Janssen* (1978) is dependent on the water depth.

The Wadden Sea case shows a difference in water level of approximately 8 *cm* at most at a large part of the Wadden Sea interior. The difference in the Eems-Dollard channel and the Dollard estuary are larger, with differences up to 30 *cm* at Nieuwe-Statenzijl. Differences due to wave set-up are generally small. This is a result of the small difference in significant wave height and other wave periods.

At which wind speed differences in set-up and wave conditions become significant? At the Wadden Sea, the differences already become significant for the storm of 9 November 2007, while the maximum wind speed is limited. This mainly is a result of the wind drag parameterization in Delft3D-FLOW. It is clear that the set-up mainly is caused due to wind stress in the circulation model, while the effect of wave force is an indirect effect of the difference in radiation stress gradients, that experience only relatively small changes due to adjusted wind drag parameterizations. The effect during the storm of 9 November 2007 is off course a result of the calibration of the model with the used Charnock wind drag. As this wind drag parameterization also was used in the determination of the boundary conditions in the circulation model, the comparison is actually not a fair one. Using lower bottom friction values is probable to give a better results for the computed water levels, compared with the measurements.

What the exact effect is at the eastern Wadden Sea for storms with higher wind speeds is unknown, but the idealized case showed that larger differences can be expected due to the choice of the wind drag parameterization. While the Fit wind drag is based on measurements during high wind speeds, the Charnock and Wu wind drag parameterization are not. The result might even be that extreme water levels with long return periods, based on statistics, physically cannot ever be reached.

Chapter 10

Depth-induced wave breaking

10.1 Introduction

As mentioned in Chapter 6, the effect of the new depth-induced wave breaking parameterization, the nkd-scaling model, on wave force and subsequently, the water level and currents is not known. Verification of the nkd-scaling model showed that it improves the prediction of significant wave height at locations where the bathymetry is mainly horizontal. This appears to be the case both when waves are generated locally and non-locally. The formulated research question is rephrased:

- What is the effect of the nkd-scaling model on the magnitude and location of the wave force and subsequently on the water level and currents, compared with the Battjes & Janssen depth-induced wave breaking formulation?

10.2 Method

To investigate the effect of the nkd-scaling model (NKD) on wave force, and subsequently on water level and currents, the storm of 9 November 2007 at the eastern Wadden Sea is used again. The eastern Wadden Sea is known for its steep ebb-tidal deltas. Thereby it is known that the wave conditions inside the Wadden Sea interior are predominantly generated locally. This is expected to generate differences between simulations that use the Battjes & Janssen parameterization (BJ) and the nkd-scaling model parameterization. The differences can be compared mutually and with measurements. The aim is not only to verify whether one parameterization is possibly better than the other, but also to understand what causes the differences.

10.3 Model settings

The model settings will be equal to *Alkyon* (2009) for both SWAN and Delft3D-FLOW. These settings are already discussed extensively in Section 8.3. The only variation between the two simulations is the parameterization of the depth-induced wave breaking, which is described below.

10.3.1 Depth-induced wave breaking

The first simulation uses the default Battjes & Janssen parameterization, which is discussed in Section 4.2.4. The nkd-scaling parameterization is not yet discussed explicitly and will be here subsequently. The Battjes & Janssen parameterization uses a constant breaker parameter γ , which is 0.73. The nkd-scaling model provides an alternative for the breaker parameter γ , which is dependent on the normalized wave number $\tilde{k}d$ and the bottom slope β :

$$\gamma_{nkd} = \gamma_{\beta-kd} = \gamma_1(\beta) / \tanh \left[\gamma_1(\beta) / \gamma_2(\tilde{k}d) \right] \quad (10.1)$$

The breaker parameter γ_{nkd} is dependent on a breaker parameter that represents the dependency on the bottom slope: $\gamma_1(\beta)$, and on a breaker parameter that represents the normalized wave number: $\gamma_2(\tilde{k}d)$. The formulation of the breaker parameter dependent on the bottom slope is:

$$\gamma_1(\beta) = \gamma_0 + a_1 \tan \beta \geq 0 \quad (10.2)$$

and the formulation of the breaker parameter dependent on the normalized wave number is:

$$\gamma_2(\tilde{k}d) = a_2 + a_3 \tilde{k}d \geq 0 \quad (10.3)$$

where γ_0 , a_1 , a_2 and a_3 are tunable coefficients which are applied in their default values in this case. The characteristic wave number \tilde{k} is given by:

$$\tilde{k} = k_{-1/2} = \left[\int \int k^{1/2} E(\sigma, \theta) d\sigma d\theta / E \right]^{-2} \quad (10.4)$$

This lower order wave number is chosen, because it is not as sensitive for the presence of multiple peaks or the the exact shape of the spectral tail, which appear not be accounted for entirely correct in all cases in 3_{rd} generation wave models.

The parameterization scales the dependency on both the bottom slope and the normalized wave number. The normalized wave number becomes less relevant in increasingly shallow water, which is represented in the formula by the hyperbolic tangent, which provides a smooth between both the breaker parameters γ_1 and γ_2 .

To not over-estimate the effect of very steep bottom slopes, a maximum bottom slope of $\beta = 1/10$ is imposed.

10.4 Results

10.4.1 Visual interpretation water level

The water level when using NKD leads generally to lower water levels inside the Wadden Sea interior. Especially during the storm these differences are visible, as the absolute contribution of the wave set-up starts to increase. It is visible that the wave force using NKD causes that waves arriving at the ebb-tidal delta dissipate generally at a larger depth, thus further offshore, compared with the scaling according to BJ. The water level in the western part of the eastern Wadden Sea, at the coast of Groningen and Friesland, is most influenced by the use of the different breaker parameterizations. The water level difference lies between 0.05-0.10 *m*.

During ebb after high water during the storm, the water level computed when NKD is applied, starts to become higher at the Wadden Sea in the area between Schiermonnikoog and the Eems-Dollard channel (Figure 10.1). This is a result of the larger wave force that is located near the northern boundary of the model. At the ebb-tidal delta, waves entering the domain immediately start to break when BJ is applied, while this is not true for situations when NKD is applied. This causes that wave force is located at different locations and the largest wave forces when NKD is applied are close to the Wadden Sea compared with the wave force when BJ is applied. Thereby, when NKD is applied, significant wave forces are present inside the Wadden Sea interior, while when BJ is applied, wave force inside the Wadden Sea is absent.

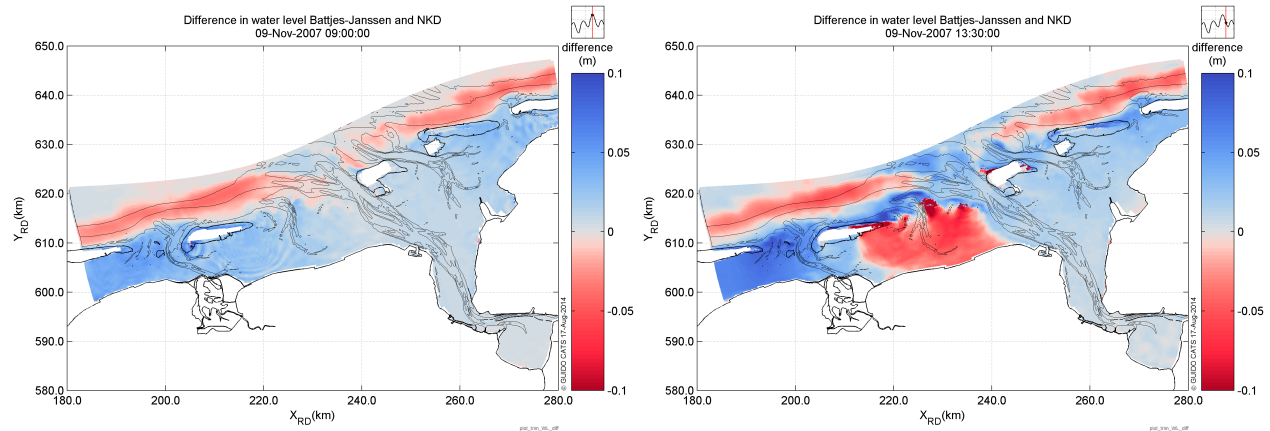


Figure 10.1: Difference in water level between simulations with Battjes & Janssen and nkd-scaling model at high water and ebb during the day of the storm.

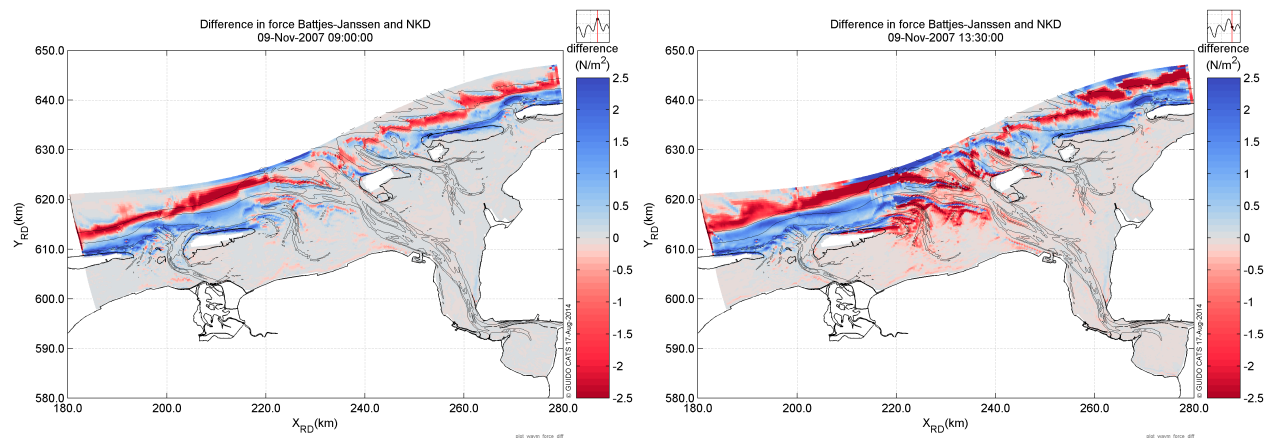


Figure 10.2: Difference in force between simulations with Battjes & Janssen and nkd-scaling model at high water and ebb during the day of the storm.

The differences in computed water level are largest at measurement buoy Schiermonnikoog, which lies inside the Wadden Sea interior between the island Schiermonnikoog and the coast. During the storm, the water level computed when NKD is applied first is lower with maxima up to 5 cm. After high water during the storm, the computed water level is higher when NKD is applied. During the day of the storm the mutual difference in wave set-up is approximately 10-15% lower when NKD is applied at Lauwersoog, until ebb, which gives approximately a 7% higher wave set-up at Lauwersoog (Figure 10.3).

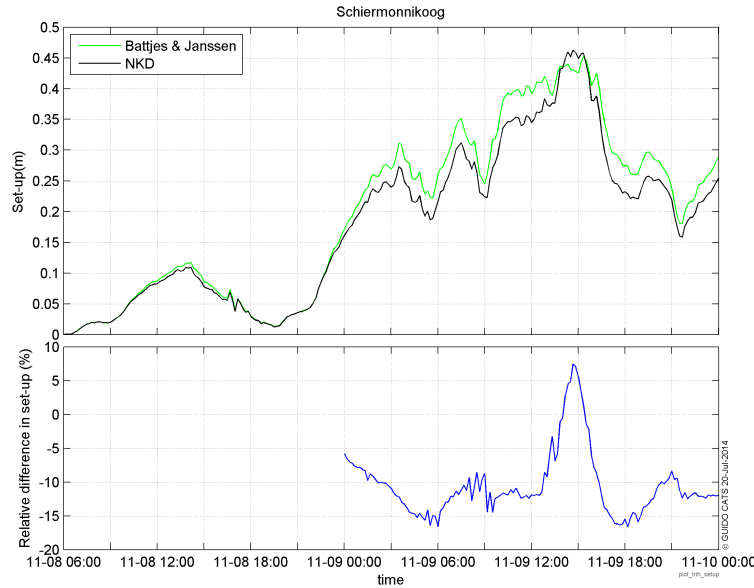


Figure 10.3: Wave set-up between simulations with Battjes & Janssen and nkd-scaling model at Schiermonnikoog. The lower figure shows a blue line that represents the relative difference between the set-up computed with the nkd-scaling model with respect to the set-up computed with Battjes & Janssen.

The observations from water level buoy Lauwersoog are very similar to those from water level buoy Schiermonnikoog, where the set-up with BJ is generally larger than the set-up with NKD. The relative differences are in the same order as at Schiermonnikoog. The relative differences at Huibertgat are even larger, with differences up to almost 30%. These relative differences are generally observed when the absolute set-up is small (order of a few centimeters), which makes the relative difference very sensitive for absolute differences.

10.4.2 Statistical analysis water level

The root-mean-square errors of the computed water levels at the measurement buoys are presented in Table 10.1. It is important to note that the root-mean-square error is not only the result of wave set-up. Part of the root-mean-square error is the result in erroneous water level prediction due to errors in the tidal constituents and due to (direct) wind set-up. Differences between the computed root-mean-square errors can only be blamed to the use of different depth-induced wave breaking parameterizations. It can be obtained that the water level prediction does not significantly changes when looking for the whole period of the simulation. However, this result is biased, as wave set-up is relatively small before the start of the storm.

To reduce the effect of the period before the storm, this computed value of the root-mean-square error presented in Table 10.2 is based on data only on the day of the storm (9 November 2007 06:00 hours - 10 November 2007 00:00 hours). It is visible that at the measurement buoys Schiermonnikoog and Lauwersoog the root-mean-square error increases when NKD is applied. At the other stations, the root-mean-square error stays equal, what implies that the influence of the choice of the depth-induced wave breaking parameter does not make a significant difference at that locations with respect to the water level. This observation agrees with the observation that the differences in water level are observed particularly at the Wadden Sea interior at the coast of Groningen and

	Battjes & Janssen	NKD
Schiermonnikoog	0.16	0.17
Lauwersoog	0.09	0.10
Huibertgat	0.07	0.07
Eemshaven	0.14	0.14
Delfzijl	0.15	0.15
Nieuwe Statenzijl	0.66	0.66

Table 10.1: Root-mean-square error water level for period 8 November 2007 06:00 hours - 10 November 2007 00:00 hours

Friesland, where the measurement stations Schiermonnikoog and Eemshaven are located.

	Battjes & Janssen	NKD
Schiermonnikoog	0.17	0.19
Lauwersoog	0.09	0.11
Huibertgat	0.09	0.09
Eemshaven	0.17	0.17
Delfzijl	0.19	0.19
Nieuwe Statenzijl	0.33	0.33

Table 10.2: Root-mean-square error water level (m) for the day of the storm (9 November 2007 06:00 hours - 10 November 2007 00:00 hours)

The maximum water level during the simulation period is presented in Table 10.3. It can be obtained that also here the largest differences between the simulation can be found at the stations Schiermonnikoog and Lauwersoog, where in both cases the water level predicted when BJ is applied is a respectively 0.02 m and 0.03 m higher. At Eemshaven, the water level is 0.01 m higher when BJ is applied, while at Nieuwe Statenzijl the maximum water level is 0.01 m higher when NKD is applied.

	Battjes & Janssen	NKD	meas
Schiermonnikoog	3.50	3.48	3.53
Lauwersoog	3.59	3.56	3.61
Huibertgat	3.11	3.11	3.11
Eemshaven	3.56	3.55	3.85
Delfzijl	4.05	4.05	4.21
Nieuwe Statenzijl	4.56	4.57	4.90

Table 10.3: The highest water level (m) measured during the simulation period (8 November 2007 06:00 hours - 10 November 2007 00:00 hours)

10.4.3 Visual interpretation wave conditions

Visual interpretation wave parameters at domain

Generally, waves entering the ebb-tidal delta dissipate energy farther offshore when NKD is applied. This causes that the significant wave height at the ebb-tidal deltas is lower when NKD is applied. In

Alkyon (2009), the observation was made that low frequency waves propagating through the tidal inlets are refracted to the sides of the channel after which they are dissipated on the tidal flats. This observation was made when BJ was applied. When NKD is applied, this low frequency waves do not directly dissipate during ebb. This is visible by a difference of more than 3 s of $T_{m-1,0}$ at the area near Pieterburen Wad. This phenomenon is not visible during flood. The low-frequency waves appear to enter the Wadden Sea interior especially by refracting from the Eems-Dollard channel. The directional wave spreading also is larger in this area when NKD is applied, which seems logical, as the refracted waves have a different direction as the locally generated waves.

Visual inspection energy density spectra

Westereems Oost The spectral shape is very similar for both simulations. During the peak of the storm, both simulations compute a double peaked spectrum, while the measurements do not resemble the second peak at the higher frequencies. Especially when NKD is applied, the energy density of the second peak is overestimated. Visually it looks like BJ therefore resembles the measured spectra somewhat better.

Wierummer Wad During the storm, the wave energy density is higher when BJ is applied, compared with the wave energy density when NKD is applied. This observation generally holds for all frequencies. The energy density spectrum computed when BJ is applied, looks like to resemble the measured wave spectra better.

Uithuizer Wad The largest difference between the computed wave spectra occur during the storm. The wave spectra when NKD is applied, are double peaked during the period between 9 November 2007 12:00 hours till 15:00 hours, which is during the peak of the storm. This is contrary to the wave spectra computed when BJ is applied. The lower frequency peak of the double peaked spectrum might be caused by offshore wave energy that penetrated the Wadden Sea interior.

Pieterburen Wad The differences between the computed wave spectra are very small at Pieterburen Wad. From approximately 9 November 2007 12:00 hours, differences in computed spectra between NKD and BJ start to occur. The shape of the spectra is more or less similar, but the general observation is that the peak energy density is larger. Thereby a larger amount of low-frequency energy ($f \leq 0.1Hz$) is obtained when NKD is applied. This is particularly true on 9 November 2007 between 13:00 - 14:00 hours, which is during ebb after the highest water level during the storm. Figure 10.4 shows an example of the computed and measured wave spectra.

10.4.4 Statistical analysis wave conditions

Table 10.4 shows the root-mean-square error, the scatter index and the relative bias of the parameters H_{m0} , $T_{m-1,0}$, T_{m01} , T_{m02} and gives the mean absolute error of the mean wave direction and the directional wave spreading.

The accuracy of the prediction of the significant wave height does not improve at any of the wave buoys due to applying NKD. The prediction of the spectral wave periods does neither improve when NKD is applied. At station Westereems Oost, which lies outside the Wadden Sea interior and

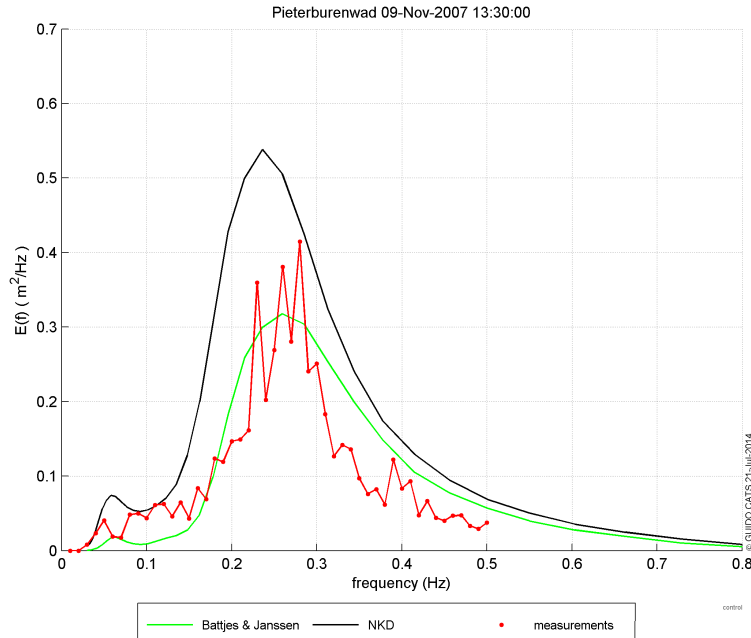


Figure 10.4: Energy density spectrum on 9 November 2007 13:30 hours at Pieterburen Wad. The computed spectra when BJ (green), NKD (black) are visible, just as the measured spectrum (red).

Station	wave-breaking	H_{m0}			$T_{m-1,0}$			T_{m01}			T_{m02}			DIR	DSPR
		RMSE	SI	RBIAS	RMSE	SI	RBIAS	RMSE	SI	RBIAS	RMSE	SI	RBIAS	MAE	MAE
WRW1	BJ	0.07	9.16	-0.08	0.29	7.97	-0.47	0.18	5.90	2.05	0.17	5.77	3.37	32.89	-
	NKD	0.14	17.40	-13.50	0.40	10.70	-5.29	0.21	6.70	-1.43	0.16	5.55	0.25	31.83	-
UHW1	BJ	0.20	20.01	-19.58	0.76	14.84	-12.76	0.23	5.97	-4.48	0.11	3.32	-1.37	65.33	-
	NKD	0.31	30.98	-21.54	0.84	16.50	-14.91	0.22	5.82	-4.49	0.11	3.09	-0.59	66.48	-
WEO1	BJ	0.41	10.87	-1.79	1.23	11.88	-10.41	1.36	16.17	-15.16	1.36	18.11	-17.34	6.15	3.20
	NKD	0.67	17.51	7.54	1.29	12.45	-10.87	1.32	15.67	-14.55	1.28	17.08	-16.21	5.73	3.93
PBW1	BJ	0.13	15.21	7.61	1.11	23.82	-17.00	0.51	13.97	-9.20	0.38	11.17	-7.44	22.21	13.40
	NKD	0.19	21.34	10.51	1.18	25.22	-17.93	0.53	14.51	-9.35	0.39	11.46	-7.39	22.04	13.32

Table 10.4: Statistical parameters RMSE, SI, RBIAS of H_{m0} (m), $T_{m-1,0}$ (s), T_{m01} (s) and T_{m02} (s), and statistical parameter MAE of DIR (deg) and DSPR (deg) for the simulation with depth-induced wave breaking parameterizations Battjes & Janssen and nkd-scaling model at the wave buoy locations Westereems-Oost (WEO1), Pieterburenwad (PBW1), Uithuizerwad (UHW1) and Wierumerwad (WRW1). The units of RMSE and MAE are similar to the unit of the quantity. The values of SI and RBIAS are presented as percentages.

is mostly affected by the wave boundary conditions, the significant wave height is under-predicted when BJ is applied, while it over-predicted when NKD is applied. [Salmon et al. \(2013\)](#) show that BJ generally overestimates the significant wave height under these conditions, which is corrected by NKD. In this case the opposite is true.

The other three wave buoys are located inside the Wadden Sea interior. Most waves are locally generated. [Salmon et al. \(2013\)](#) state that BJ generally underestimates significant wave height when locally generated waves dominate and that NKD solves this matter. This is not true at this particular case. Only at Pieterburen Wad, the relative bias of the significant wave height when applying NKD is larger than the relative bias for BJ. It already was mentioned earlier that NKD showed generally larger energy density during the storm, especially during ebb.

The mutual computed mean absolute errors for the mean wave direction and the directional wave

spreading do not differ significantly for any of the wave buoys, while it was observed that especially during ebb, the mutual differences near the Eems-Dollard channel increased. Though the wave buoy at Uithuizer Wad also lies in this region, it seems not affected. Probably its location is too close to shore to notice this effect, while the prediction of the mean wave direction and directional spreading already are poor at this location.

10.5 Analysis

Two matters attract special attention:

1. Dissipation occurs at larger depths when NKD is applied, compared with when BJ is applied. This causes that the magnitude of the wave force is different in both simulations and is located at different locations.
2. Penetration of non-locally generated waves in the Wadden Sea interior is found to be present to a larger extent when NKD is applied. At the same time, the wave set-up at Schiermonnikoog and Lauwersoog becomes larger when NKD is applied, while before this happened, the wave set-up when BJ is applied was larger.

Waves entering the ebb-tidal deltas dissipate at larger depths when NKD is applied, which automatically means that $\gamma_{nk d} < \gamma_{BJ} = 0.73$. The value of $\gamma_{nk d}$ is dependent on both the steepness of the bottom slopes of the ebb-tidal deltas and the value of $\tilde{k}d$, where a larger value of $\tilde{k}d$ and an increasingly steep bottom slope both mean a higher value of $\gamma_{nk d}$. It is apparent that the combination of both in this case results in a lower value of γ compared with BJ, at for example Friesche Zeegat. The result of NKD is that the wave force is spread over a larger area with somewhat lower values compared with BJ, which causes that the wave force is more concentrated and closer to the tidal inlets. Figure 10.5 shows an example where this is visible, especially at the entrance of the Friesche Zeegat.

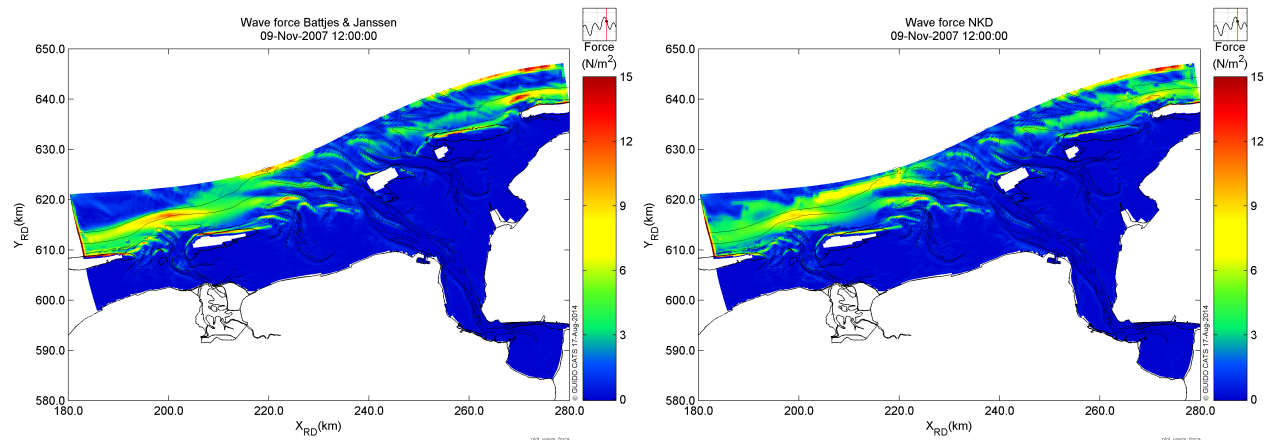


Figure 10.5: The wave force when using Battjes & Janssen (left figure) and the wave force when using nkd-scaling model (right figure) at 9 November 2007 12:00 hours.

The water level station which is probably most influenced by the wave force behind the Friesche Zeegat is Lauwersoog, while Schiermonnikoog is also likely to experience wave set-up due to wave force behind the Friesche Zeegat. At both locations it is obtained that wave set-up is approximately

15% lower when NKD is applied at 9 November 2007 12:00 hours. Before this time, there hardly was any difference in significant wave height at the Wadden Sea interior, which indicates that approximately the same amount of energy has dissipated outside the Wadden Sea. It can be concluded that the location and concentration of the wave force influences the wave set-up in the Wadden Sea interior.

During ebb, the wave set-up when NKD is applied increases at much faster rate than when BJ is applied. This is best visible at water level stations Schiermonnikoog and Lauwersoog. Ebb is considered to be between high water slack (9 November 2007, 09:40 hours) and low water slack (9 November 2007, 16:20 hours). From approximately 9 November 2007 12:00 hours, significant differences in computed wave height inside the Wadden Sea interior are visible, which is believed to be partly the result of non-locally generated waves, as it is the result of the locally generated waves that are able to grow larger when using NKD.

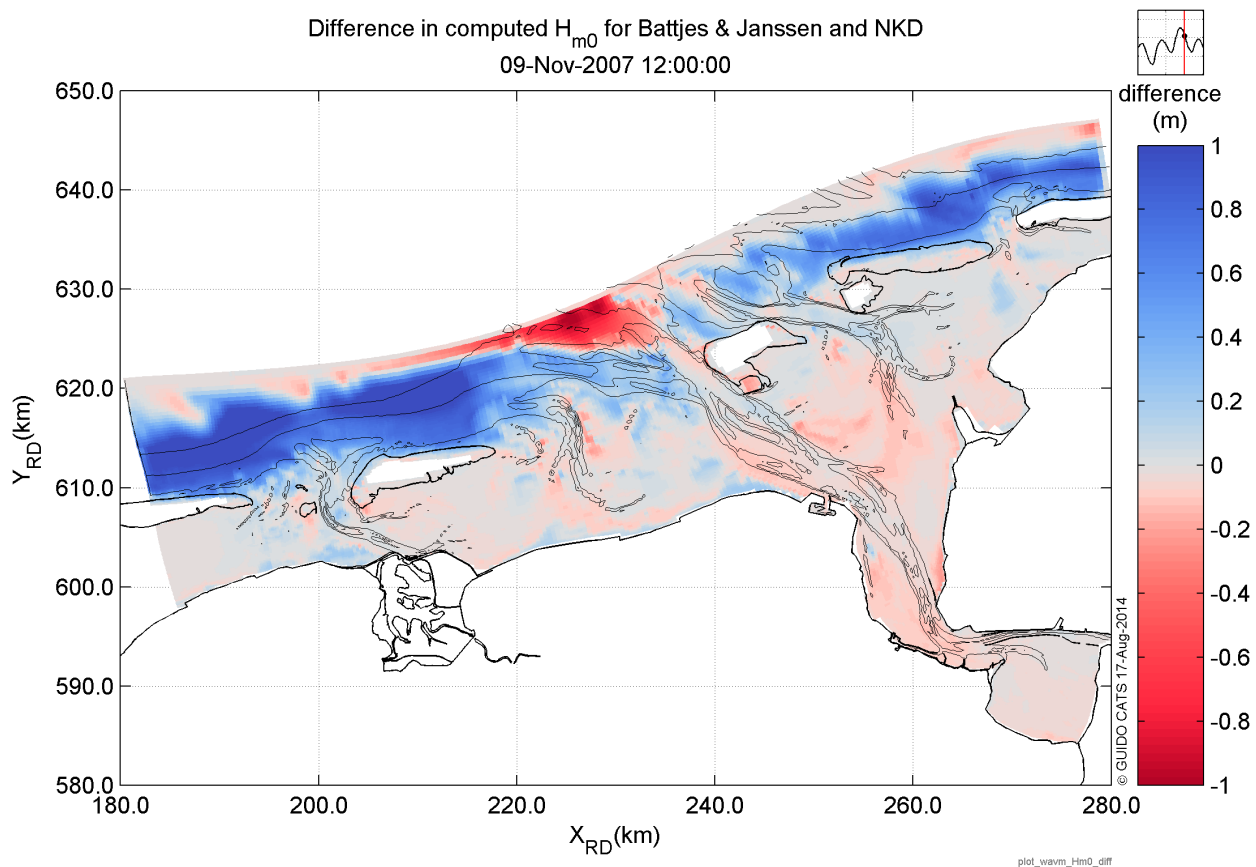


Figure 10.6: Difference in significant wave height between BJ and NKD. Blue indicates that at that specific location the value of H_{m0} is higher when BJ is applied, while the opposite is true for red.

This observation is shown in Figure 10.6. At Friesche Zeegat, the significant wave height is lower when NKD is applied, which is caused by dissipation at larger depth (explained above). From this time on, the significant wave height computed with NKD is higher at the Eems-Dollard channel and at the area of the Pieterburen Wad and Uithuizer Wad (the whole shoal, not the wave measurement buoy). It already was observed in [Alkyon \(2009\)](#) that North Sea waves penetrate further in the tidal channels during ebb and that due to opposing currents these North Sea waves are refracted towards the borders of the tidal channels, where they dissipate when arriving at the shallow shoals.

These observations were made when BJ was applied. In case NKD is applied, the North Sea waves do not dissipate that quickly and penetrate further into the Wadden Sea interior. This not only causes relatively low-frequency waves to enter the Wadden Sea interior, but it also gives waves the opportunity to dissipate their energy closer to the Wadden Sea. This results in wave force closer to the Wadden Sea and subsequently the wave set-up when NKD is applied increases during ebb.

10.6 Conclusion

What is the effect of the nkd-scaling model on the magnitude and location of the wave force and subsequently on the water level, compared with the Battjes & Janssen depth-induced wave breaking formulation? When North Sea waves enter the Wadden Sea, they arrive at a steep ebb-tidal delta. NKD is dependent on the bottom slope and on the normalized wave number. Wave energy is dissipated already at larger depth when NKD is applied. The result is that the wave force is spread at a larger area and the wave set-up is lower when using NKD, compared with the wave force when BJ is applied. The wave force when BJ is applied is more concentrated at the entrance of the tidal inlets, which causes a higher wave set-up in the Wadden Sea interior.

During ebb, North Sea waves penetrate closer towards the Wadden Sea when NKD is applied at the ebb-tidal delta which enters the Eems-Dollard channel. A similar explanation can be used: because the waves dissipate closer to the Wadden Sea at these shallow locations when NKD is applied, the related wave force is also closer towards the Wadden Sea and causes the wave set-up to be larger during ebb when NKD is applied.

Chapter 11

Conclusions

11.1 Introduction

Numerical modeling introduces errors by definition, which is no different for numerical modeling of wave-current interaction. In case of a two-way coupled system, the computed outcome of the model exists of errors, that are caused due to the wrong or incomplete representation of the physics in the models, numerically introduced errors and in incorrect forcing of the system. Beforehand, it was unknown what the magnitude of the errors was and what is responsible for the largest errors. Not knowing the uncertainty range of model outcomes is something that is highly undesirable, especially as these sort of models are used for the assessment of the safety of citizens. A better understanding of the two-way coupled model is essential to succeed in this assignment. Knowing what the largest influences are on the result of the model, gives an advantage in making an attempt to reduce this uncertainty. Hence, when an error is introduced in a certain aspect and it affects all other aspects, the total error will be significantly larger than when this introduced error does hardly affect other aspects. A literature study was performed to find out which subjects contain the largest uncertainties at the moment.

11.2 Literature survey

The literature study showed that physical processes or driving forces cannot be categorized as important or not, as it strongly depends on the location and the model schematization which aspects appear to be important. Besides of this, six conclusion were formulated that focused on the parameterization of physical processes or on aspects that affect the physical representation of processes in the model. Three of the formulated conclusions on subjects that need better understanding are further investigated in this study. The subjects chosen involve the choice of the coupling interval and on what is should be based, the influence of a new wind drag parameterization ([Zijlema et al., 2012](#)) in the wave model, compared with the former default parameterization in SWAN ([Wu, 1982](#)) and the effect of a new depth-induced wave breaking parameterization ([Salmon et al., 2013](#)) compared with the default depth-induced wave breaking parameterization in SWAN ([Battjes and Janssen, 1978](#)). Besides of these subjects, the most important conclusion based on the literature survey are:

- A physical process or driving force cannot be categorized as important or not, as it strongly depends on the location and the model schematization which aspects appear to be important.
- The inclusion of a depth-dependent formulation of the radiation stress in the circulation model would physically be more realistic, but a correct formulation has not been derived yet. Until that time, the use of the 2D formulation of the radiation stress appears to suffice with sufficient accuracy.
- Enhanced bottom friction due to waves in the circulation model is incorporated in the circulations models Delft3D-FLOW, FVCOM, POM and ROMS. All these models use different parameterizations, and Delft3D-FLOW offers numerous parameterizations of the wave-enhanced bottom friction term. The effect on the two-way coupled model is not known.
- Both radiation stress and dissipation rate can be used in Delft3D-FLOW to account for the excess flux of momentum. Though the dissipation rate should have the advantage that it is more stable, compared with modeling radiation stress, studies showed *Alkyon* (2009) that the opposite is true. An explanation has not been found.

11.3 Numerical modeling

Three of the formulated conclusions on subjects that need better understanding are further investigated in the second part of this study. The subjects chosen involve the choice of the coupling interval and on what it should be based, the influence of a new wind drag parameterization (*Zijlema et al.*, 2012) in the wave model, compared with the former default parameterization in SWAN (*Wu*, 1982) and the effect of a new depth-induced wave breaking parameterization (*Salmon et al.*, 2013) compared with the default depth-induced wave breaking parameterization in SWAN (*Battjes and Janssen*, 1978).

The effect of the coupling interval was investigated by performing simulations with increasing lengths of the coupling interval, where the shortest coupling interval was 5 minutes and the longest coupling interval was 4 hours. The most important conclusions regarding the coupling interval are itemized:

- The accuracy of the predicted water level was influenced most when varying the coupling interval, while the wave conditions were not affected significantly.
- The wave force appeared to be strongly dependent on the wave boundary conditions, which seems plausible, as the wave boundary conditions are imposed at a relatively small distance from the location where they are dissipated by depth-induced wave breaking.
- This results in an underestimation of the water level before the peak of the storm in terms of wave conditions, and in an over-estimation of the water level after the peak of the storm, where the peak of the storm is defined as the highest wave boundary condition during the storm.
- The difference in computed water level reaches up to values of approximately 10 cm for a 5 minute coupling interval compared with a 240 minute coupling interval. Thereby it was seen that the wave force caused more wave set-up during low water, compared with high water, which is explained by the inertia of the water body.

- The simulation with a 30 minute coupling interval shows good resemblance with the computations made with 5 and 10 minutes coupling intervals, though differences are visible. The advice is not to increase the coupling interval to larger intervals than 30 minutes, though smaller coupling intervals are preferable.

To assess the effect of the *fit* wind drag parameterization [Zijlema et al. \(2012\)](#) in both SWAN and Delft3D-FLOW, numerous simulation are performed at both the Wadden Sea and in an idealized bathymetry. First, the effect of the fit wind drag parameterization in SWAN is investigated, while using the [Charnock \(1955\)](#) in Delft3D-FLOW (Charnock-Fit). Second, the effect of the fit wind drag parameterization is investigated in both SWAN and Delft3D-FLOW (Fit-Fit). The results are compared with simulations that use the wind drag parameterization by [Wu \(1982\)](#) in SWAN and [Charnock \(1955\)](#) in Delft3D-FLOW (Charnock-Wu). In the idealized case the wind speed is gradually increased, while at the Wadden Sea the storm of 9 November 2007 is used to assess the effect. The most important conclusions are:

- The idealized case showed that the difference in water level is mainly caused by the wind drag parameterization in Delft3D-FLOW.
- The wave-induced set-up decreased during higher wind speeds, while the wave forces increased in case the Charnock wind drag parameterization is used in Delft3D-FLOW. An explanation is that the effect of the wave force becomes less, due to the increase volume of the water body.
- The effect on the significant wave height starts to become significant during wind speeds larger than 30 m/s , when the fit wind drag parameterization is applied instead of [Wu \(1982\)](#).
- The Wadden Sea case showed that differences of approximately 8 cm in the Wadden Sea interior occur, when the fit wind drag parameterization is applied in Delft3D-FLOW.
- The Wadden Sea case showed that the wave conditions are hardly affected due to the different wind drag parameterizations.

The influence of the new parameterization of depth-induced wave breaking by [Salmon et al. \(2013\)](#) was investigated at the eastern Wadden Sea, which is called the nkd-scaling model parameterization. The most important conclusions are:

- During storm conditions, the location of depth-induced wave breaking at the ebb-tidal delta near Friesche Zeegat appeared to be influenced by the nkd-scaling model, where waves tended to break at a larger depth, which means that $\gamma_{nkd} < \gamma_{BJ}$ at that location.
- This causes the wave set-up to be lower at the Wadden Sea interior in the area behind the Friesche Zeegat for almost the entire storm. The differences are dependent on the location, but are approximately 15% lower at wave buoys Schiermonnikoog and Lauwersoog when nkd-scaling model is applied.
- During ebb, the nkd-scaling causes a larger set-up, which is caused by the dependence on the normalized wave number. Waves are able to penetrate further towards the Wadden Sea and occasionally even penetrate into the Wadden Sea. This causes that the wave force are closer to the Wadden Sea, which makes the set-up higher in case of applying the nkd-scaling model.
- The comparison with wave measurements did show that the prediction of waves generally is better when [Battjes and Janssen \(1978\)](#) is applied.
- Penetration of non-locally generated waves into the Wadden Sea is observed in the measurements and represented better when nkd-scaling model is applied.

11.4 Conclusions regarding the set goals

The answer on the question whether the understanding of a two-way coupled model is improved is positive. The relative importance of all physical processes that are in the two-way coupled model strongly depend on the location and the schematization of the model. Drawing general conclusions on whether something is, or is not, important are hard to define. The literature survey served as a reference on what is globally available in the field of numerical modeling of wave-current interaction. Discrepancies are appointed and form a set, which was used to decide what to investigate further in this study. The eastern Wadden Sea functioned as a test set-up to investigate the relative importance of some physical aspects in that area.

The choice of the depth-induced wave breaking parameterization had a significant effect on both wave set-up as the prediction of wave conditions, which was in the order of 10 *cm*. The maximum wave set-up is approximately of 45 *cm*. Penetration of low-frequency waves was better represented with the parameterization of *Salmon et al. (2013)*, while the conditions were generally better represented when the parameterization of *Battjes and Janssen (1978)* was used. This shows that the depth-induced wave breaking is a relatively important process and users should be aware of these effects.

The Wadden Sea case showed that the storm surge was approximately a decimeter lower inside the Wadden Sea interior, due to the wind drag parameterization in Delft3D-FLOW. This is similar to the effect of the depth-induced breaker formulation. An important remark is that the boundary conditions for the circulation model are computed with a different wind drag parameterization with higher wind drag coefficients. This will cause that the difference in computed water level would be even lower, when adjusting these boundary conditions. Re-validation of the model will be necessary, as the bottom stress has to decrease to compensate for the decreased wind stress.

The effect will be larger when the wind speed increases, which can be obtained from the idealized case. This causes that the importance of wave-current interaction should not be overestimated at the Wadden Sea.

The change of wind drag parameterization in SWAN does not have an influence for the storm of 9 November 2007. The effect of the wind on wave generation is too small during the storm, to have a significant effect on wave conditions. For higher wind speeds, these effects might become more significant. Especially when the size of the basin is larger and will cause significant differences in significant wave heights. Though the idealized case shows that differences in significant wave height do not cause large differences in wave set-up, it is not blindly expected to be true at the eastern Wadden Sea, as the bathymetry is way more complex.

Chapter 12

Recommendations

The last goal of this study formulated the desire to give advice on what direction further research is needed, with respect to the modeling of wave-current interaction in a two-way coupled model.

- The investigated parameterizations are only tested with the use of one storm: the storm of 9 November 2007. To generate a more reliable result, the use of multiple storms would benefit the reliability of the results.
- As observed when investigating the wind drag parameterization, the wind drag becomes increasingly important during high wind speeds. The fit wind drag parameterization already is an improvement compared with the *Charnock (1955)* and *Wu (1982)*, as the parameterization is based on measurements during high wind speeds. Though the effect of waves on wind stress is incorporated indirectly, the parameterization is only dependent on wind speed, while the sea-state is not necessarily similar in all cases for the same wind speed. Therefore a better understanding of wind stress for high wind speeds is necessary with respect to different sea-states.
- A subject of consideration is the correct representation of the influence of currents on waves under stratified conditions. At this moment, the depth averaged velocity is transferred to the wave model, while this may deviate significantly from the velocity at the surface. The effect this might have, is currently unknown.
- The influence of the different settings and parameterizations was only investigated at the eastern Wadden Sea, which can be considered as a small basin where stationary SWAN computations are admissible. The influence of the parameterizations at larger basins would require instationary SWAN computations. Whether the results obtained in this study would still be valid is unknown and a study at a larger basin is recommended.
- At the eastern Wadden Sea model, the wave boundary conditions are based on the measurements at two wave buoys that lie rather close to each other and do not represent the wave boundary conditions in an appropriate way at the whole domain, as wave boundary conditions had to be modified at the several locations at the ebb-tidal delta. Thereby wave-current interaction induced effect are neglected in the boundary conditions used by Delft3D-FLOW, while effects are likely to be present, as especially at the shallow ebb-tidal deltas wave force is probable to have an influence on boundary condition used by Delft3D-FLOW. It is therefore recommended to find a solution in such a way that all wave-current interaction effects are

incorporated.

- ([Alkyon, 2009](#)) posed three possibilities for the underestimation of low-frequency wave energy. The first possibility is that refraction for low-frequency waves is too strong in areas with steep channel slopes and the wave length of low-frequency wave components compared with the scale of the variation of the channel slopes, which might cause that the action balance does not hold in this situation. The second possibility posed that diffraction effects might reduce the accumulation of low-frequency wave energy on the sides of the channels. The third possibility stated that dissipation effects might be overestimated and a weaker bottom friction formulation or an adapted depth-induced wave breaking may be required.

In this study the nkd-scaling model depth-induced wave breaking parameterization ([Salmon et al., 2013](#)) already showed that it allows low-frequency wave energy to penetrate further in the eastern Wadden Sea. These findings are not based on comparison with measurement though, but on a visual interpretation of the computed and measured wave spectra. The effect of a lowered bottom friction formulation in SWAN was not investigated, while [Zijlema et al. \(2012\)](#) showed that the JONSWAP friction coefficient $C_{bfr} = C_{JONSWAP}$ should be lowered to $0.038m^2s^{-3}$.

As it was shown that the nkd-scaling model had a significant effect on the computed wave set-up, the effect of the reduced bottom friction coefficient is recommended to investigate, as it also might have a significant effect on the prediction of wave set-up.

Chapter 13

Bibliography

- Alkyon (2008), Effects of dumping silt in the eems estuary, 3d model study, hydromorphological study for the eia of eemshaven and eia of fairway to eemshaven, *Tech. Rep. A1836R2R3*, Alkyon.
- Alkyon (2009), Swan hindcast in the eastern wadden sea and eems-dollard estuary, *Tech. rep.*, Alkyon.
- Alves, J., and M. L. Banner (2003), Performance of a saturation-based dissipation-rate source term in modeling the fetch-limited evolution of wind waves, *Journal of Physical Oceanography*, *33*(6), 1274–1298.
- Apotsos, A., B. Raubenheimer, S. Elgar, and R. Guza (2008), Testing and calibrating parametric wave transformation models on natural beaches, *Coastal Engineering*, *55*(3), 224–235.
- Ardhuin, F., A. D. Jenkins, and K. A. Belibassakis (2008a), Comments on the three-dimensional current and surface wave equations., *Journal of Physical Oceanography*, *38*(6).
- Ardhuin, F., N. Raschle, and K. A. Belibassakis (2008b), Explicit wave-averaged primitive equations using a generalized lagrangian mean, *Ocean Modelling*, *20*(1), 35–60.
- Battjes, J., and J. Janssen (1978), Energy loss and set-up due to breaking of random waves, *Coastal Engineering Proceedings*, *1*(16).
- Battjes, J., and M. Stive (1985), Calibration and verification of a dissipation model for random breaking waves, *Journal of Geophysical Research: Oceans (1978–2012)*, *90*(C5), 9159–9167.
- Benetazzo, A., S. Carniel, M. Sclavo, and A. Bergamasco (2013), Wave–current interaction: Effect on the wave field in a semi-enclosed basin, *Ocean Modelling*.
- Bennis, A.-C., and F. Ardhuin (2011), Comments on ‘the depth-dependent current and wave interaction equations: A revision’, *Journal of Physical Oceanography*, *41*(10).
- Bennis, A.-C., F. Ardhuin, and F. Dumas (2011), On the coupling of wave and three-dimensional circulation models: Choice of theoretical framework, practical implementation and adiabatic tests, *Ocean Modelling*, *40*(3), 260–272.
- Bolaños, R., J. Brown, and A. Souza (2011), Three dimensional circulation modeling in the dee estuary, *J Coast Res SI*, *64*, 1457–1461.
- Bolanos, R., P. Osuna, J. Wolf, J. Monbaliu, and A. Sanchez-Arcilla (2011), Development of the polcoms–wam current–wave model, *Ocean Modelling*, *36*(1), 102–115.
- Bolanos-Sanchez, R., J. Wolf, J. Brown, P. Osuna, J. Monbaliu, and A. Sanchez-Arcilla (2009), Comparison of wave-current interaction formulation using polcoms-wam wave-current model, -.
- Booij, N., R. Ris, and L. H. Holthuijsen (1999), A third-generation wave model for coastal regions: 1. model description and validation, *Journal of Geophysical Research: Oceans (1978–2012)*, *104*(C4), 7649–7666.
- Bouws, E., and G. Komen (1983), On the balance between growth and dissipation in an extreme depth-limited wind-sea in the southern north sea, *Journal of physical oceanography*, *13*(9), 1653–1658.
- Brown, J. M., R. Bolaños, and J. Wolf (2011), Impact assessment of advanced coupling features in a tide–surge–wave model, polcoms-wam, in a shallow water application, *Journal of Marine Systems*, *87*(1), 13–24.
- Brown, J. M., R. Bolaños, and J. Wolf (2013), The depth-varying response of coastal circulation and water levels

- to 2d radiation stress when applied in a coupled wave–tide–surge modelling system during an extreme storm, *Coastal Engineering*, 82, 102–113.
- Bye, J. A., M. Ghantous, and J.-O. Wolff (2010), On the variability of the charnock constant and the functional dependence of the drag coefficient on wind speed, *Ocean Dynamics*, 60(4), 851–860.
- Bye, J. A. T., and A. D. Jenkins (2006), Drag coefficient reduction at very high wind speeds, *Journal of Geophysical Research: Oceans (1978–2012)*, 111(C3).
- Cavaleri, L., and P. Malanotte-Rizzoli (1981), Wind wave prediction in shallow water: Theory and applications, *Journal of Geophysical Research: Oceans (1978–2012)*, 86(C11), 10,961–10,973.
- Charnock, H. (1955), Wind stress on a water surface, *Quarterly Journal of the Royal Meteorological Society*, 81(350), 639–640.
- Collins, J. I. (1972), Prediction of shallow-water spectra, *Journal of Geophysical Research*, 77(15), 2693–2707.
- Craig, P. D., and M. L. Banner (1994), Modeling wave-enhanced turbulence in the ocean surface layer, *Journal of Physical Oceanography*, 24(12), 2546–2559.
- Craik, A. D. D., and S. Leibovich (1976), A rational model for langmuir circulations, *Journal of Fluid Mechanics*, 73(03), 401–426.
- Dalrymple, R. A., and R. G. Dean (1991), *Water wave mechanics for engineers and scientists*, Prentice-Hall.
- Davies, A. M., and J. Lawrence (1995), Modeling the effect of wave-current interaction on the three-dimensional wind-driven circulation of the eastern irish sea, *Journal of Physical Oceanography*, 25(1), 29–45.
- Dean, R. G., and C. J. Bender (2006), Static wave setup with emphasis on damping effects by vegetation and bottom friction, *Coastal Engineering*, 53(23), 149 – 156, doi:http://dx.doi.org/10.1016/j.coastaleng.2005.10.005, coastal Hydrodynamics and Morphodynamics Symposium celebrating the academic closing address of Jurjen A. Battjes.
- Deltares (2011), *User Manual Delft3D-FLOW*, Deltares, Rotterdamseweg 185, 2600 MH Delft, The Netherlands, 3.15 ed.
- Dietrich, J., M. Zijlema, J. Westerink, L. Holthuijsen, C. Dawson, R. Luettich Jr, R. Jensen, J. Smith, G. Stelling, and G. Stone (2011a), Modeling hurricane waves and storm surge using integrally-coupled, scalable computations, *Coastal Engineering*, 58(1), 45–65.
- Dietrich, J., S. Tanaka, J. J. Westerink, C. Dawson, R. Luettich Jr, M. Zijlema, L. Holthuijsen, J. Smith, L. Westerink, and H. Westerink (2012), Performance of the unstructured-mesh, swan+ adcirc model in computing hurricane waves and surge, *Journal of Scientific Computing*, 52(2), 468–497.
- Dietrich, J. C., J. J. Westerink, A. B. Kennedy, J. M. Smith, R. E. Jensen, M. Zijlema, L. H. Holthuijsen, C. Dawson, R. A. Luettich Jr, M. D. Powell, et al. (2011b), Hurricane gustav (2008) waves and storm surge: Hindcast, synoptic analysis, and validation in southern louisiana, *Monthly Weather Review*, 139(8), 2488–2522.
- Dingemans, M. W., A. C. Radder, and H. J. De Vriend (1987), Computation of the driving forces of wave-induced currents, *Coastal Engineering*, 11(5), 539–563.
- Donelan, M., B. Haus, N. Reul, W. Plant, M. Stiassnie, H. Graber, O. Brown, and E. Saltzman (2004), On the limiting aerodynamic roughness of the ocean in very strong winds, *Geophysical Research Letters*, 31(18).
- Donelan, M. A., F. W. Dobson, S. D. Smith, and R. J. Anderson (1993), On the dependence of sea surface roughness on wave development, *Journal of Physical Oceanography*, 23(9), 2143–2149.
- Edwards, K. L., J. Veeramony, D. Wang, K. T. Holland, and Y. L. Hsu (2009), *Sensitivity of Delft3D to input conditions*, IEEE.
- Eldeberky, Y., and J. A. Battjes (1995), Parameterization of triad interactions in wave energy models, *Proc. Coastal Dynamics '95 (Gdansk)*.
- Fan, Y., I. Ginis, and T. Hara (2009), The effect of wind-wave-current interaction on air-sea momentum fluxes and ocean response in tropical cyclones, *Journal of Physical Oceanography*, 39(4), 1019–1034.
- Fredsøe, J., and R. Deigaard (1992), *Mechanics of coastal sediment transport*, vol. 3, World Scientific.
- Funakoshi, Y., S. C. Hagen, and P. Bacopoulos (2008), Coupling of hydrodynamic and wave models: Case study for hurricane floyd (1999) hindcast, *Journal of waterway, port, coastal, and ocean engineering*, 134(6), 321–335.
- Garratt, J. (1977), Review of drag coefficients over oceans and continents, *Monthly weather review*, 105(7), 915–929.
- Group, T. W. (1988), The wam model—a third generation ocean wave prediction model, *Journal of Physical Oceanography*, 18(12), 1775–1810.

- Hasselmann, K., T. P. Barnett, E. Bouws, H. Carlson, D. E. Cartwright, K. Enke, J. A. Ewing, H. Gienapp, D. Hasselmann, P. Kruseman, et al. (1973), Measurements of wind-wave growth and swell decay during the joint north sea wave project (jonswap), -.
- Holthuijsen, L. H. (2007), *Waves in oceanic and coastal waters*, Cambridge University Press.
- Janssen, P. A. E. M. (1989), Wave-induced stress and the drag of air flow over sea waves, *Journal of Physical Oceanography*, 19(6), 745–754.
- Janssen, P. A. E. M. (1991), Quasi-linear theory of wind-wave generation applied to wave forecasting, *Journal of Physical Oceanography*, 21(11), 1631–1642.
- Janssen, P. A. E. M., O. Saetra, C. Wettre, H. Hersbach, and J. Bidlot (2004), The impact of the sea state on the atmosphere and oceans, *Annales Hydrographiques* 3, 772, 3.1–3.23.
- Jonsson, I. G. (1966), Wave boundary layers and friction factors, in *Coastal Engineering (1966)*, pp. 127–148, ASCE.
- Jonsson, I. G., and N. A. Carlsen (1976), Experimental and theoretical investigations in an oscillatory turbulent boundary layer, *Journal of Hydraulic Research*, 14(1), 45–60.
- Kaminsky, G. M., and N. C. Kraus (1993), Evaluation of depth-limited wave breaking criteria, in *Ocean Wave Measurement and Analysis (1993)*, pp. 180–193, ASCE.
- Kim, S. Y., T. Yasuda, and H. Mase (2008), Numerical analysis of effects of tidal variations on storm surges and waves, *Applied Ocean Research*, 30(4), 311–322.
- Komen, G. J., K. Hasselmann, and K. Hasselmann (1984), On the existence of a fully developed wind-sea spectrum, *Journal of Physical Oceanography*, 14(8), 1271–1285.
- Lane, E. M., J. M. Restrepo, and J. C. McWilliams (2007), Wave-current interaction: A comparison of radiation-stress and vortex-force representations, *Journal of physical oceanography*, 37(5), 1122–1141.
- Leibovich, S. (1980), On wave-current interaction theories of langmuir circulations, *J. Fluid Mech*, 99(4), 715–724.
- Longuet-Higgins, M. S., and R. Stewart (1960), Changes in the form of short gravity waves on long waves and tidal currents, *J. Fluid Mech*, 8(4), 565–585.
- Longuet-Higgins, M. S., and R. Stewart (1962), Radiation stress and mass transport in gravity waves, with application to surf beats, *Journal of Fluid Mechanics*, 13(04), 481–504.
- Longuet-Higgins, M. S., and R. W. Stewart (1964), Radiation stresses in water waves; a physical discussion, with applications, in *Deep Sea Research and Oceanographic Abstracts*, vol. 11-4, pp. 529–562, Elsevier.
- Luettich, R. A., and J. J. Westerink (2004), *Formulation and numerical implementation of the 2D/3D ADCIRC finite element model version 44. XX*, R. Luettich.
- Luo, W., and J. Monbaliu (1994), Effects of the bottom friction formulation on the energy balance for gravity waves in shallow water, *Journal of Geophysical Research: Oceans (1978–2012)*, 99(C9), 18,501–18,511.
- Madsen, O. S. (1994), Spectral wave-current bottom boundary layer flows, *Coastal Engineering Proceedings*, 1(24).
- Madsen, O. S., Y.-K. Poon, and H. C. Graber (1988), Spectral wave attenuation by bottom friction: Theory, *Coastal Engineering Proceedings*, 1(21).
- McWilliams, J. C., and J. M. Restrepo (1999), The wave-driven ocean circulation, *Journal of physical oceanography*, 29(10), 2523–2540.
- Mellor, G. (2003), The three-dimensional current and surface wave equations, *Journal of Physical Oceanography*, 33(9), 1978–1989.
- Mellor, G. (2005), Some consequences of the three-dimensional current and surface wave equations, *Journal of Physical Oceanography*, 35(11), 2291–2298.
- Mellor, G. (2011a), Wave radiation stress, *Ocean Dynamics*, 61(5), 563–568.
- Mellor, G. (2011b), Corrigendum, *J. Phys. Oceanogr.*, 41(7), 1417–1418.
- Mellor, G. (2011c), Reply, *J. Phys. Oceanogr.*, 41(10), 2013–2015.
- Mellor, G. (2013), Waves, circulation and vertical dependence, *Ocean Dynamics*, pp. 1–11.
- Mellor, G. L., and T. Yamada (1982), Development of a turbulence closure model for geophysical fluid problems, *Reviews of Geophysics*, 20(4), 851–875.
- Mellor, G. L., M. A. Donelan, and L.-Y. Oey (2008), A surface wave model for coupling with numerical ocean circulation models, *Journal of Atmospheric and Oceanic Technology*, 25(10), 1785–1807.
- Moon, I.-J. (2005), Impact of a coupled ocean wave–tide–circulation system on coastal modeling, *Ocean Modelling*, 8(3), 203–236.
- Powell, M. D., P. J. Vickery, and T. A. Reinhold (2003), Reduced drag coefficient for high wind speeds in tropical cyclones, *Nature*, 422(6929), 279–283.

- Rogers, W. E., A. V. Babanin, and D. W. Wang (2012), Observation-consistent input and whitecapping dissipation in a model for wind-generated surface waves: Description and simple calculations, *Journal of Atmospheric and Oceanic Technology*, 29(9), 1329–1346.
- Ruessink, B. G., D. J. R. Walstra, and H. N. Southgate (2003), Calibration and verification of a parametric wave model on barred beaches, *Coastal Engineering*, 48(3), 139–149.
- Salmon, J., and L. Holthuijsen (2010), Re-scaling the battjes-janssen model for depth-induced wave-breaking, -.
- Salmon, J., L. Holthuijsen, M. Zijlema, G. v. Vledder, and J. Pietrzak (2013), Scaling depth-induced wave-breaking in third-generation spectral wave models, -.
- Shchepetkin, A. F., and J. C. McWilliams (2005), The regional oceanic modeling system (roms): a split-explicit, free-surface, topography-following-coordinate oceanic model, *Ocean Modelling*, 9(4), 347–404.
- Signell, R. P., R. C. Beardsley, H. C. Graber, and A. Capotondi (1990), Effect of wave-current interaction on wind-driven circulation in narrow, shallow embayments, *Journal of Geophysical Research: Oceans (1978–2012)*, 95(C6), 9671–9678.
- Soulsby, R., L. Hamm, G. Klopman, D. Myrhaug, R. Simons, and G. Thomas (1993), Wave-current interaction within and outside the bottom boundary layer, *Coastal engineering*, 21(1), 41–69.
- Svendsen, I. A. (1984), Wave heights and set-up in a surf zone, *Coastal Engineering*, 8(4), 303–329.
- Svendsen, I. A., K. Haas, and Q. Zhao (2002), Quasi-3d nearshore circulation model shorecirc, *Center for Appl. Coastal Res., Univ. of Delaware, Internal Rep., CACR-02-01, Newark, DE*.
- Tang, C., W. Perrie, A. Jenkins, B. DeTracey, Y. Hu, B. Toulany, and P. Smith (2007), Observation and modeling of surface currents on the grand banks: A study of the wave effects on surface currents, *Journal of Geophysical Research: Oceans (1978–2012)*, 112(C10).
- Thornton, E. B., and R. T. Guza (1983), Transformation of wave height distribution, *Journal of Geophysical Research: Oceans (1978–2012)*, 88(C10), 5925–5938.
- Tolman, H. L. (1991), A third-generation model for wind waves on slowly varying, unsteady, and inhomogeneous depths and currents, *Journal of Physical Oceanography*, 21(6), 782–797.
- Umlauf, L., and H. Burchard (2003), A generic length-scale equation for geophysical turbulence models, *Journal of Marine Research*, 61(2), 235–265.
- Warner, J. C., N. Perlin, and E. D. Skyllingstad (2008a), Using the model coupling toolkit to couple earth system models, *Environmental Modelling & Software*, 23(10), 1240–1249.
- Warner, J. C., C. R. Sherwood, R. P. Signell, C. K. Harris, and H. G. Arango (2008b), Development of a three-dimensional, regional, coupled wave, current, and sediment-transport model, *Computers & Geosciences*, 34(10), 1284 – 1306.
- Westhuysen, A., A. Dongeren, J. Groeneweg, G. P. Vledder, H. Peters, C. Gautier, and J. C. C. Nieuwkoop (2012), Improvements in spectral wave modeling in tidal inlet seas, *Journal of Geophysical Research: Oceans (1978–2012)*, 117(C8).
- Westhuysen, A. J. v. d. (2010), Modeling of depth-induced wave breaking under finite depth wave growth conditions, *Journal of Geophysical Research: Oceans (1978–2012)*, 115(C1).
- Westhuysen, A. J. v. d., M. Zijlema, and J. A. Battjes (2007), Nonlinear saturation-based whitecapping dissipation in swan for deep and shallow water, *Coastal Engineering*, 54(2), 151–170.
- WL (2006), Storm hindcasts norderneyer seegat and amelande zeegat, *Tech. rep.*, WL — Delft Hydraulics.
- WL (2007a), Storm hincast for wadden sea, *Tech. rep.*, WL — Delft Hydraulics.
- WL (2007b), Sensitivity analysis of swan for the amelande zeegat, *Tech. rep.*, WL — Delft Hydraulics.
- WL (2007c), Evaluation and development of wave-current interaction in swan, *Tech. rep.*, WL — Delft Hydraulics.
- WL (2008), Uncertainty analyses of the hydraulic boundary conditions of the wadden sea, *Tech. rep.*, WL — Delft Hydraulics.
- Wu, J. (1982), Wind-stress coefficients over sea surface from breeze to hurricane, *Journal of Geophysical Research: Oceans (1978–2012)*, 87(C12), 9704–9706.
- Xia, H., Z. Xia, and L. Zhu (2004), Vertical variation in radiation stress and wave-induced current, *Coastal engineering*, 51(4), 309–321.
- Xie, L., K. Wu, L. Pietrafesa, and C. Zhang (2001), A numerical study of wave-current interaction through surface and bottom stresses: Wind-driven circulation in the south atlantic bight under uniform winds, *Journal of Geophysical Research: Oceans (1978–2012)*, 106(C8), 16,841–16,855.

- Xie, L., L. Pietrafesa, and K. Wu (2003), A numerical study of wave-current interaction through surface and bottom stresses: Coastal ocean response to hurricane Fran of 1996, *Journal of Geophysical Research: Oceans (1978–2012)*, 108(C2).
- Xie, L., H. Liu, and M. Peng (2008), The effect of wave-current interactions on the storm surge and inundation in Charleston harbor during hurricane Hugo 1989, *Ocean Modelling*, 20(3), 252–269.
- Xu, F., W. Perrie, and S. Solomon (2013), Shallow water dissipation processes for wind waves off the Mackenzie delta, *Atmosphere-Ocean*, –(ahead-of-print), 1–13.
- Zijlema, M. (2010), Computation of wind-wave spectra in coastal waters with SWAN on unstructured grids, *Coastal Engineering*, 57(3), 267–277.
- Zijlema, M., G. P. van Vledder, and L. H. Holthuijsen (2012), Bottom friction and wind drag for wave models, *Coastal Engineering*, 65, 19–26.

Appendix A

Matlab codes

A.1 Introduction

The matlab scripts in Appendix A are meant to provide better insight in the derivation of the presented solutions.

A.2 Depth-induced wave breaking

To solve the analytical solution of the balance between the water level gradient and radiation stress gradient, an iterative script in Matlab is used. The iterative procedure is stopped when the maximum difference betweenThe iterative procedure is presented beneath:

```
1 %% Analytical solution
2 Hm0=8;
3 T=11;
4 h0=50;
5 h1=0;
6 s=50000;
7 dx=200;
8 depth=linspace(h0,h1,s/dx);
9 set_up_analytical=zeros(1,length(depth));
10 niter=0;
11 h_new=1;
12 h=0;
13 while max(abs(h_new-(depth+set_up_analytical)))>1e-15
14     disp(sprintf('%0.3f',max(abs(depth+set_up_analytical))));
15     niter=niter+1;
16     h=depth+set_up_analytical;
17     h_new=h;
18     [set_up_analytical,y]=wave_energy_model(Hm0,T,h,s);
19 end
```

The matlab function file `wave_energy_model.m` is used to solve the analytical solution of the balance between the water level gradient and radiation stress gradient.

```

1 function [set_up , x , Fx]=wave_energy_model(Hm0,T,h,s)
2 % [set_up]=wave_energy_model(Hm0,T,h0,h1,s)
3 %
4 % Hm0 = Significant wave height at boundary in metres
5 % T = Mean wave period in seconds
6 % h = depth
7 % s = distance between offshore and shore in metres
8 %
9 % see also: dispersion , wave_energy_dissipation
10
11 %% Determine depth profile
12 rho_w=1025;
13 g=9.81;
14 dx=200;
15 x=linspace(0,s,s/dx);
16 %%
17 k=zeros(1,length(h));
18 n=zeros(1,length(h));
19 c=zeros(1,length(h));
20 cg=zeros(1,length(h));
21 E=zeros(1,length(h));
22 Ecg=zeros(1,length(h));
23 Sxx=zeros(1,length(h));
24 Hs=zeros(1,length(h));
25 Dw=zeros(1,length(h));
26
27 Hrms=Hm0/sqrt(2);
28 k(1)=dispersion(h(1),T);
29 n(1)=0.5*(1+(2*k(1)*h(1))/(sinh(2*k(1)*h(1)))));
30 c(1)=sqrt(g/k(1)*tanh(k(1)*h(1)));
31 cg(1)=c(1)*n(1);
32 E(1)=1/16*Hm0^2;
33 Ecg(1)=E(1)*cg(1);
34 Sxx(1)=rho_w*g*(2*n(1)-0.5)*E(1);
35 Hs(1)=4*sqrt(E(1));
36
37 % Determine Sxx
38 for i=2:length(h);
39     k(i)=dispersion(h(i),T);
40     n(i)=0.5*(1+(2*k(i)*h(i))/(sinh(2*k(i)*h(i)))));
41     c(i)=sqrt(g/k(i)*tanh(k(i)*h(i)));
42     cg(i)=c(i)*n(i);
43     [Dw(i),Qb(i)]=wave_energy_dissipation(E(i-1),T,(h(i-1)+h(i))/2);
44     Ecg(i)=Ecg(i-1)-Dw(i)*dx;
45     E(i)=Ecg(i)/cg(i);

```

```

46     Sxx(i)=rho*g*(2*n(i)-0.5)*E(i);
47     Hs(i)=4*sqrt(E(i));
48 end
49
50 % Determine the gradient of Sxx and the setup where the setup is the
    water
51 % level gradient based on Sxx
52 Fx=NaN*ones(1,length(h));
53 set_up=zeros(1,length(h));
54 for i=2:length(h);
55     Fx(i)=-(Sxx(i)-Sxx(i-1))/dx;
56     niter=0;
57     set_up1=set_up(i-1);
58     set_up2=set_up(i-1)-0.1;
59     while abs(set_up1-set_up2)>1e-15
60         set_up2=set_up1;
61         set_up1=Fx(i)*dx/(rho*g*(h(i)+set_up2))+set_up(i-1);
62     end
63     set_up(i)=set_up1;
64 end
65 if isnan(set_up(end))
66     set_up(end)=set_up(end-1);
67 end

```

The matlab function file `wave_energy_dissipation.m` is used to determine the amount of wave energy dissipation at a specific depth. The formulation of energy dissipation due to depth-induced wave breaking is equal to the formulation in SWAN, which is presented in Chapter 4.

```

1 function [Dw,Qb,Hrms,Hmax,beta,sigma]=wave_energy_dissipation(E,T,h);
2 % [Dw]=wave_energy_dissipation(E,T,h);
3 %
4 % The wave energy dissipation Dw is calculated with the use of the bore
5 % model of Battjes & Janssen (1978). The input parameters are defined
    as
6 % follows:
7 %
8 % E      =   Wave energy (variance density)
9 % T      =   mean wave period Tm01
10 % h      =   depth
11 %
12
13 alpha=1;
14 gamma=0.73;
15 Hrms=4/sqrt(2)*sqrt(E);
16 Hmax=gamma*h;
17 beta=Hrms/Hmax;
18 sigma=1/T;
19

```

```
20 if beta <= 0.2
21     Qb=0;
22 elseif beta >0.2 && beta <0.5
23     Q0=0;
24     Qb=Q0-(beta ^ 2) *(Q0-exp ((Q0-1)/(beta ^ 2)))/((beta ^ 2)-exp ((Q0-1)/(beta
    ^ 2)));
25 elseif beta >=0.5 && beta < 1
26     Q0=(2*beta -1) ^ 2;
27     Qb=Q0-(beta ^ 2) *(Q0-exp ((Q0-1)/(beta ^ 2)))/((beta ^ 2)-exp ((Q0-1)/(beta
    ^ 2)));
28 elseif beta >= 1
29     Qb=1;
30 end
31 Dw=alpha*Qb*(Hmax^2)/(8*pi); %The relative frequency is left out so far
```

Appendix B

Input files

B.1 Introduction

For both Delft3D-FLOW and SWAN the input files are presented in this appendix. Section B.2 shows the *.mdf file that is used to specify the commands in Delft3D-FLOW. The wave module Delft3D-WAVE is part of the Delft3D suite and provides the opportunity to couple Delft3D-FLOW to SWAN. Delft3D-WAVE uses a *.mdw file as input file and the program writes an input file used by SWAN, based in the *.mdw file. Section B.3 presents the *.mdw used by Delft3D-WAVE. Section B.4 presents the coupling procedure used. As the Delft3D suite does not provides the opportunity of using varying wave boundary conditions in both time and space, a workaround has been created.


```

Iter = 2
Dryflp = #YES#
Dpsopt = #MAX#
Dpuopt = #MEAN#
Dryflc = 1.0000000e-001
Dco = -9.9900000e+002
Tlfsmo = 0.0000000e+000
ThetQH = 0.0000000e+000
Forfuv = #Y#
Forfw = #Y#
Sigcor = #Y#
Trasol = #Cyclic-method#
Momsol = #Cyclic#
Commnt =
Commnt = no. discharges: 4
Filsrc = #eems2.src#
Fildis = #eems2.dis#
Commnt = no. observation points: 123
Filsta = #eems2.obs#
Commnt = no. drogues: 0
Commnt =
Commnt =
Commnt = no. cross sections: 13
Filcrs = #eems2.crs#
Commnt =
SMhydr = #YYYYYY#
SMderv = #YYYYYY#
SMproc = #YYYYYYYYYYYY#
PMhydr = #YYYYYY#
PMderv = #YYY#
PMproc = #YYYYYYYYYYYY#
SHhydr = #YYYY#
SHderv = #YYYY#
SHproc = #YYYYYYYYYYYY#
SHflux = #YYYY#
PHhydr = #YYYYYY#
PHderv = #YYY#
PHproc = #YYYYYYYYYYYY#
PHflux = #YYYY#
Online = #N#
Waqmod = #N#
WaveOL = #Y#
Flmap = 7.5600000e+003 10 1.0080000e+004
Flhis = 7.5600000e+003 10 1.0080000e+004
Flpp = 7.5600000e+003 10 1.0080000e+004
Flrst = 10
Commnt =
SMVelo = #GLM#
Commnt =

```

B.3 SWAN

```

[WaveFileInformation]
  FileVersion      = 02.00
[General]
  ProjectName      = 2191
  ProjectNr        = w01s
  Description       = definitieve som
  Description       = met fix aantal decimalen hotfile, geen
  setup, wel gebruik hotfile,
  Description       = stationary
  FlowFile          = w01s.mdf
  OnlyInputVerify  = false
  SimMode           = stationary
  DirConvention     = cartesian
  ReferenceDate     = 2007-11-03
  WindSpeed         = 0.0000000e+000
  WindDir           = 0.0000000e+000
[Constants]
  WaterLevelCorrection = 0.0000000e+000
  Gravity             = 9.8100004e+000
  WaterDensity        = 1.0250000e+003
  NorthDir            = 9.0000000e+001
  MinimumDepth        = 5.0000001e-002
[Processes]
  GenModePhys        = 3
  Breaking            = true
  BreakAlpha         = 1.0000000e+000
  BreakGamma         = 7.3000002e-001
  Triads              = true
  TriadsAlpha        = 1.0000000e-001
  TriadsBeta         = 2.5000000e+000
  BedFriction        = jonswap
  BedFricCoef        = 6.7000002e-002
  Diffraction        = false
  DiffracCoef        = 2.0000000e-001
  DiffracSteps       = 5
  DiffracProp        = true
  WindGrowth         = true
  WhiteCapping       = Komen
  Quadruplets        = true
  Refraction          = true
  FreqShift          = true
  WaveForces         = radiation stresses
[Numerics]
  DirSpaceCDD        = 5.0000000e-001
  FreqSpaceCSS       = 5.0000000e-001
  RChsTm01           = 2.0000000e-002
  RChMeanHs          = 2.0000000e-002
  RChMeanTm01        = 2.0000000e-002
  PercWet             = 9.9000000e+001
  MaxIter            = 25
[Output]
  TestOutputLevel    = 0
  TraceCalls          = false
  UseHotFile         = false

```

```

MapWriteInterval      = 0.0000000e+000
WriteCOM              = true
COMWriteInterval     = 5.0000000e+000
LocationFile         = swan_uit.loc
WriteTable           = true
WriteSpec1D          = true
WriteSpec2D          = true
[Domain]
Grid                 = eems-gvv.grd
FlowBedLevel         = 1
FlowWaterLevel       = 1
FlowVelocity         = 1
FlowWind             = 1
BedLevel             = bodem_nw.dep
DirSpace            = circle
NDir                 = 36
StartDir             = 0.0000000e+000
EndDir              = 0.0000000e+000
FreqMin             = 2.9999999e-002
FreqMax            = 8.0000001e-001
NFreq               = 35
Output              = true
[Boundary]
Name                 = eastboundary
Definition           = grid-coordinates
StartCoordM         = 0
EndCoordM           = 0
StartCoordN         = 0
EndCoordN           = 37
SpectrumSpec        = from file
Spectrum            = WEW.BND
[Boundary]
Name                 = westboundary
Definition           = grid-coordinates
StartCoordM         = 303
EndCoordM           = 303
StartCoordN         = 0
EndCoordN           = 53
SpectrumSpec        = from file
Spectrum            = SON.BND
[Boundary]
Name                 = northboundary
Definition           = grid-coordinates
StartCoordM         = 0
EndCoordM           = 303
StartCoordN         = 0
EndCoordN           = 0
SpectrumSpec        = from file
CondSpecAtDist      = 0.0000000e+000
Spectrum            = WEW1.BND
CondSpecAtDist      = 1.3199000e+004
Spectrum            = WEW2.BND
CondSpecAtDist      = 3.5000000e+004
Spectrum            = OND.BND

```

CondSpecAtDist	=	5.5000000e+004
Spectrum	=	OND1.BND
CondSpecAtDist	=	6.2710000e+004
Spectrum	=	WEW3.BND
CondSpecAtDist	=	7.6611000e+004
Spectrum	=	SON1.BND
CondSpecAtDist	=	1.0290900e+005
Spectrum	=	SON2.BND

B.4 Coupling procedure

The Delft3D suite provides the opportunity to couple Delft3D-FLOW and Delft3D-WAVE. The Delft3D-WAVE module uses the wave model SWAN to perform the computations. Figure B.1 shows the coupling procedure of the two-way coupled model existing of Delft3D-FLOW and SWAN. Both Delft3D-FLOW and SWAN are forced by boundary conditions. Delft3D-FLOW uses Riemann boundary conditions, derived with the use of the Kuststrook grof and Kuststrook Fijn model, as specified by Rijkswaterstaat, The Netherlands. SWAN uses boundary conditions based on measurements at the wave buoys Schiermonnikoog Noord and Westereems West. As the Delft3D suite does not provide the opportunity to force SWAN with non-uniform wave boundary conditions in both space and time, a workaround is created. The Delft3D suite creates after Delft3D-FLOW is finished with its computations files that are used by SWAN: BOTNOW (water level), CURNOW (current field), WNDNOW (Wind field) and the computational grid. After the SWAN run, new wave boundary conditions are set with the use of a combination of the command prompt environment and (small) FORTRAN based routines.

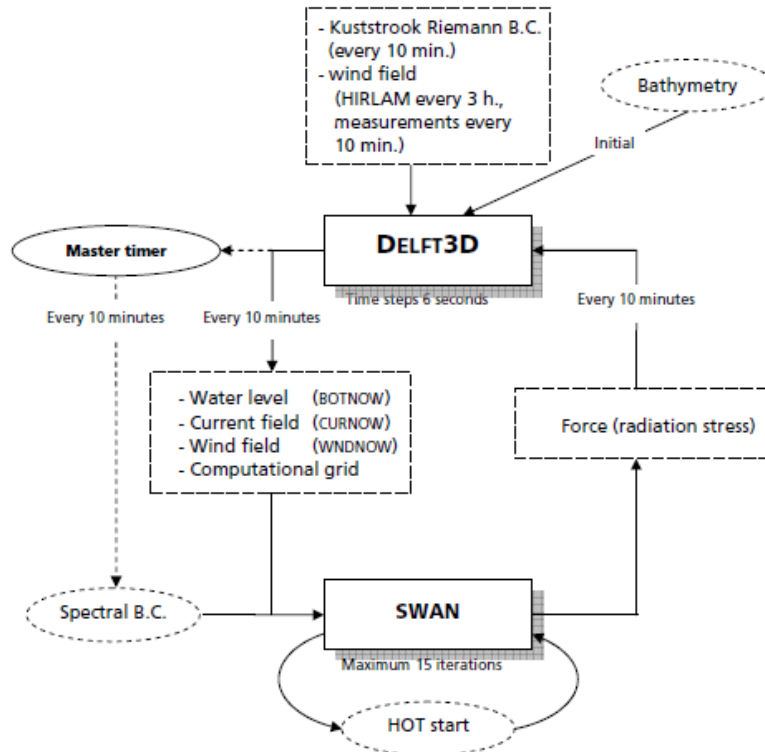


Figure B.1: Schematization of coupling procedure